1-1-2012

Identifying sm22 as a key player in arterial diseases

Jianbin Shen
Wayne State University,

IDENTIFYING SM22 AS A KEY PLAYER IN ARTERIAL DISEASES

by

JIANBIN SHEN

DISSERTATION

Submitted to the Graduate School

of Wayne State University,

Detroit, Michigan

in partial fulfillment of the requirements

for the degree of

DOCTOR OF PHILOSOPHY

2012

MAJOR: MOLECULAR BIOLOGY AND GENETICS

Approved by:

_____

Advisor Date

_____

_____

_____

ACKNOWLEDGMENTS

The research training toward my PhD's degree has been closely supervised by my mentor Dr. Li Li, Ph.D.. I am grateful to Dr. Li for her being always open-minded, encouraging and great help in my career decision. I am also grateful to my committee members S. Helena Kuivaniemi, M.D., Ph.D., Jeffrey A. Loeb, M.D., Ph.D., and Maozhou Yang, Ph.D. for their practical critiques, inspiring advice and consistent support throughout my research training.

I am thankful to our lab colleagues Ms. Hong Jiang, Ms. Donghong Ju, Jianpu Zheng, Ph.D., Zhonghui Xu, M.S., and Raquel P. Ritchie, Ph.D. for their daily help and assistance. I am also thankful to Alexander Gow, Ph.D., Cherie M. Southwood and Zhenzhong Ma, Ph.D. for their advice and discussion.

I appreciate the academic guidance and help from CMMG faculty members Lawrence I. Grossman, Ph.D., Gregory Kapatos, Ph.D., and David D. Womble, Ph.D.; I also appreciate the administrative support from Ms. Suzanne Shaw and Ms. Mary Anne Housey.

PREFACE

Vascular smooth muscle cells (VSMCs) are the major type of cell content in the media of vasculature and are essential for maintaining vascular homeostasis. One distinct feature of VSMCs is phenotypic plasticity or phenotypic modulation: VSMCs can bear a spectrum of phenotypes from contractile form to synthetic form or to pro-inflammatory form or to osteochondrogenic form. The phenotypic modulation of VSMCs is associated with a diversity of vascular disorders and participates in the arterial pathogenesis.

One characteristic of VSMC phenotypic modulation is the downregulation of contractile cytoskeletal proteins such as smooth muscle α actin, myosin heavy chain and SM22. This phenomenon is conventionally viewed as a passive outcome of arterial diseases until recently. In this project, we focused research on SM22, one of the contractile cytoskeletal proteins, and used *Sm22* disruption *in vivo* and *in vitro* as a probe attempting to answer the question whether downregulation of contractile cytoskeletal proteins plays active roles in arterial pathogenesis such as inflammation and osteochondrogenesis.

TABLE OF CONTENTS

LIST OF TABLES

LIST OF FIGURES

BACKGROUND

B1. Phenotypic modulation of vascular smooth muscle cells (VSMCs) and pathogenesis of vascular disorders

VSMCs are the major cell type residing in the medial layer of arteries and veins. Interweaved with the medial extracellular matrix (ECM), VSMCs are essential for medial structure by synthesizing and organizing ECM proteins such as elastin and collagen; meanwhile, VSMCs control contraction/dilation of vessels to regulate blood pressure and tissue blood flow. VSMCs are classically known to bear two phenotypes: contractile form and synthetic form [1-3]. The contractile phenotype, also known as differentiated phenotype, is characterized by the presence of distinct contractile and motile apparatus in subcellular domains such as abundant stress fibers and high expression of contractile apparatus proteins such as smooth muscle α actin (ACTA2), myosin and calponin, and this is the typical physiological phenotype of VSMCs. The synthetic phenotype, also known as "dedifferentiated phenotype", on the other hand, is featured by low expression of contractile proteins, increased expression of other cytoskeletal proteins such as vimentin and loss of subcellular organization of contractile apparatus, and this phenotype of VSMCs is mostly present in vascular diseases [1-4]. A variety of stimuli including platelet-derived growth factor can drive VSMCs from the differentiated contractile phenotype to the dedifferentiated synthetic phenotype [2, 4]. Accumulating research based on clinical samples and animal models of vascular diseases further characterizes the dedifferentiated phenotypes of VSMCs under various pathological conditions such as arterial atherosclerosis [5, 6], arteriopathy of diabetes and chronic kidney diseases [3, 7, 8]. These phenotypes include but are not limited to pro-inflammatory [6, 9], osteogenic [3, 10], osteochondrogenic [3, 10] and adipogenic phenotypes [3]. The

diversity of VSMC phenotypes in vascular diseases highlighted the plasticity of VSMCs and its potential active contribution to pathogenesis of vascular disorders.

Current studies on phenotypic modulation of VSMCs focus on extracellular stimuli such as cytokines [2, 11], lipids [12, 13], advanced glycation end products [14, 15] and hemodynamic alterations [6, 9], while the loss of contractile phenotype and corresponding proteins such as ACTA2 and SM22 is generally considered as a passive outcome instead of an active driving force in phenotypic modulation hence pathogenesis. However, research from independent groups revealed that downregulation of contractile proteins is an early event of pathogenesis of vascular disorders and phenotypic modulation [16, 17], which suggests that loss of contractile proteins may actively drive the overall phenotypic modulation. To further explore the putative active role of contractile proteins in VSMC phenotypic modulation during vascular pathogenesis, we used SM22, a VSMC marker contractile protein, as a probe by investigating the distinct responses of *Sm22* knockout mice (*Sm22*$^{-/-}$) to carotid artery denudation, an arterial injury model [18].

B2. Expression of *Sm22* is downregulated in arterial diseases

SM22, also known as SM22α or transgelin, is a 22 kDa protein abundant in smooth muscle cells (SMCs) of vertebrates [19, 20]. It belongs to calponin family since it contains an N-terminal calponin homology domain and a C-terminal calponin-like domain [21, 22]. The C-terminal calponin-like domain is necessary for actin affinity and the actin-binding activity of SM22 is independent of calcium [22]. The basic molecular function of SM22 is to bind actin and participate in formation of cytoskeletal structure such as stress fiber [21, 22] and podosome [23]. SM22 has been widely used as an SMC marker during embryogenesis and in adulthood [24]. SM22 transcription

denotes the onset of cardiovascular system and SMC formation during embryogenesis [25, 26]. Evidence from *Sm22* knockout mice indicates that Sm22 is required in modulating contractility of SMCs [27, 28]. Recent studies reveal that Sm22 also participate in regulation of cell proliferation [29] and apoptosis [30].

SM22 may play a role in the pathogenesis of a variety of human diseases. Expression of SM22 is decreased in several cancers including breast cancer [31], prostate cancer [32] and colon carcinoma [31, 33], indicating SM22's role in cancer progression. More interestingly, expression of SM22 is also down-regulated in atherosclerotic coronary arteries [34], thoracic[16] aortic aneurysms and abdominal aortic aneurysms [35]. In mouse atherosclerosis model, transcription of *Sm22* decreased in atherosclerotic plaques of apolipoprotein E knockout (*ApoE* $^{-/-}$) mice [36]. These data strongly suggest that SM22 may be involved in pathogenesis of such arterial diseases as atherosclerosis. However, *Sm22* $^{-/-}$ mice are fertile with uncompromised vasculature development and morphology, normal blood pressure and heart rate [26]. This suggests that Sm22 may be functionally compensated during vasculature development and that it may be required in arterial stress response instead of homeostasis [26]. Indeed, disruption of *Sm22* in *ApoE* $^{-/-}$ mice lead to enlarged atherosclerotic lesions [37].

These results indicate that loss of Sm22 might independently promote arterial pathogenesis. Arterial inflammation and osteochondrogenesis are two common features of arterial diseases; meanwhile, pro-inflammatory VSMCs and osteochondrogenic VSMCs have emerged as two key phenotypes of VSMC phenotypic modulation. Therefore, it is reasonable to link SM22, as a VSMC marker, to these two VSMC phenotypes and arterial inflammation and

osteochondrogenesis in arterial disorders. To test the hypothesis that SM22 actively participate in arterial pathogenesis, inflammation and osteochondrogenesis in particular, we generated *Sm22* $^{-/-}$ mice [38] and performed carotid artery denudation, an arterial injury model [18], followed by histological and molecular analyses of carotid artery samples. We also conducted corresponding investigation on primary *Sm22*$^{-/-}$ VSMCs as well as in PAC1 cell, a VSMC cell line [39], after *Sm22* knockdown.

PART I

Disruption Of *Sm22* Promotes Arterial Inflammation

1. Introduction

Loss of *Sm22* in *ApoE* $^{-/-}$ mice led to enlarged atherosclerotic lesions with prominent macrophage infiltration, a sign of enhanced inflammation [37]. It is well documented that inflammation is involved in development of atherosclerosis [40-43]. However, what are the mechanisms underlying the augmented inflammatory response in *Sm22*$^{-/-}$*ApoE*$^{-/-}$ mice? Inflammation is also involved in other arterial diseases such as hypertension [44, 45], abdominal aortic aneurysms [46], diabetic arteriopathy [44, 45] and chronic kidney disease (CKD) [47]. Is pro-inflammation an intrinsic feature after loss of *Sm22*? To answer these questions in arterial injury responses, we challenged *Sm22* knockout mice using an arterial injury model, carotid artery denudation [18].

2. Materials and Methods

2.1. Artery injury by carotid artery denudation.

The mouse carotid artery denudation protocol was approved by the Animal Investigation Committee at Wayne State University. *Sm22*$^{-/-}$ mice and their *Sm22*$^{+/+}$ littermates on a mixed C57BL6 x SV129 genetic background were used. Carotid artery denudation was carried out on male *Sm22*$^{-/-}$ mice and their wild type littermates of 18–20 weeks of age, as described [18]. Briefly, *Sm22*$^{-/-}$ mice and their *Sm22*$^{+/+}$ littermates were subjected to surgery. After anesthesia of mice using 2% avertin intraperitoneally (0.25 mg/g body weight), a curved guide wire of 0.35 mm in

diameter was introduced into the left common carotid and passed in and out of the left common carotid with constant rotation for three passages. Two weeks after surgery, the mice were sacrificed and both carotid arteries were harvested. Five *Sm22*$^{-/-}$ mice and their *Sm22*$^{+/+}$ littermates were used for histological and immunohistochemical analyses. The carotid segments of 3 mm in length covering the part from 2 mm to 5 mm proximal to the carotid bifurcation were harvested and embedded in OCT medium (Tissue-Tek), and around 100 frozen slides were made for each mouse with triplicate sections on each slide at 8 μm thickness. Five *Sm22*$^{-/-}$ mice and their *Sm22*$^{+/+}$ littermates were used for real-time RT-PCR: the carotid arteries of these mice were stored separately in RNAlater reagent (Ambion) at 4°C for no more than 1 week before RNA extraction.

2.2. Immunohistochemical (IHC) analyses.

Six slides, in the order of one every 15 consecutive slides, from each mouse were used for Hematoxylin and eosin (H&E) staining to screen sections with most prominent inflammatory responses. IHC was performed on the properly selected consecutive frozen slides using VECTASTAIN Elite ABC Kit (Vectorlabs). Briefly, air-dried slides were fixed in methanol containing 0.3% H_2O_2 for 10 minutes and blocked with serum for 20 minutes. The following incubation steps of primary antibody, secondary antibody, ABC reagent and DAB substrate were performed according to the manufacturer's protocol. The slides were counterstained with hematoxylin. The primary antibodies (1:50 dilution) were against F4/80 (Abcam, ab6640), CD3 (Abcam, ab5690), PTGS2 (Santa Cruz, sc-1747), CX3CL1 (Abcam, ab25088), CCL2 (Abcam, ab7202), VCAM1 (Santa Cruz, sc-1504), ICAM1 (Santa Cruz, sc-1511), SPP1 (Santa Cruz, sc-10593).

2.3. Morphometric analysis

For each antibody, both 100X and 400X images were taken using a Leica DM4000B microscope (Leica). Images of adventitia and media were separated using Photoshop 7.0 software. Semi-quantitative analyses of positive signals in adventitia and media were performed on all 100X images using color segmentation and integrative optical density function in the Image-Pro software (Media Cybernetics).

2.4. Primary VSMC culture.

VSMCs were isolated from aortas of six *Sm22*$^{-/-}$ mice and six *Sm22*$^{+/+}$ mice as described [48]. Primary VSMCs were kept in the DMEM medium (Invitrogen) containing 10% fetal bovine serum (FBS) (Invitrogen) and passed upon confluency at a 1:2 dilution ratio. Primary VSMCs in passage 2 to passage 4 were used for experiments.

2.5. Transfection of primary VSMCs

Primary *Sm22*$^{-/-}$ VSMCs at 80% confluency in a 12-well plate were transfected with the pcDNA3_*Sm22* expression plasmids or the pcDNA3 vectors using the Lipofectamine and Plus reagents (Invitrogen). Cells were harvested for mRNA extraction two days after transfection when confluency was reached.

2.6. *Sm22* knockdown in PAC1 cells with siRNA.

Sm22 knockdown was achieved using Dicer-Substrate siRNA duplexes (IDT, MMC.RNAI.N011526.5.1, siA in Table 1). PAC1 cells [39] (a pulmonary arterial SMC cell line) were seeded at 30% confluency 24 hours before transfection. Transfection was performed using

DharmaFECT3 (Dharmacon) with siRNA duplex or scrambled RNA duplex at 100 nM, and the FBS was diluted to 2% with media 24 hours after transfection for optimal cell density. In parallel experiments, the following small molecules were added respectively 24 hours after transfection: NF-κB inhibitors, Bay-11-7082 (10 μM) and IMD-0354 (200 nM); ROS scavengers, Tiron (5 mM), Tempol (1 mM) and NAC (5 mM); NADPH oxidase and mitochondria complex I inhibitor, DPI (5 μM). Cells were used for experiments 72 hours after transfection unless otherwise specified. Two other siRNA duplexes (IDT, MMC.RNAI.N011526.5.2, designated as siC and IDT, MMC.RNAI.N011526.5.3, designated as siB in Table 1) were also used independently at 200 nM concentration to rule out off-target effects of the siRNAs.

siA	**nt**	**sequence**
MMC.RNAI.N011526.5.1-S1	25	rGrCrArGrArUrCrArUrCrArGrUrUrArGrArArArGrGrGrAAG
MMC.RNAI.N011526.5.1-A1	27	rCrUrUrCrCrCrUrUrUrCrUrArArCrUrGrArUrGrArUrCrUrGrCrCrG
siB		
MMC.RNAI.N011526.5.3-S1	25	rGrGrArGrCrArUrArArGrArGrGrGrArCrUrUrCrArCrArGAC
MMC.RNAI.N011526.5.3-A1	27	rGrUrCrUrGrUrGrArArGrUrCrCrCrUrCrUrUrArUrGrCrUrCrCrUrG
siC		
MMC.RNAI.N011526.5.2-S1	25	rCrCrArGrUrCrCrArCrArArArCrGrArCrCrArArGrCrCrUTC
MMC.RNAI.N011526.5.2-A1	27	rGrArArGrGrCrUrUrGrGrUrCrGrUrUrUrGrUrGrGrArCrUrGrGrArA

Table 1. *Sm22* siRNA sequences.

2.7. Real-time RT-PCR (rtRT-PCR).

Total RNA from carotid arteries was extracted and purified using RNeasy Fibrous Tissue Kit (Qiagen), and total RNA from primary VSMCs or PAC1 cells was extracted and purified using RNeasy Kit (Qiagen). The cDNA was synthesized using the Superscript II reverse transcriptase (Invitrogen). Real-time PCR was performed using SYBR Green on a StepOnePlus system (Applied Biosystems). Gapdh and snRNA U6 were used as internal controls in ΔΔCt method. All PCR primers were designed to cover at least 2 exons (Table 2).

Gene	Forward (5' - 3')	Reverse (5' - 3')	Size (bp)
Ccl2			
Mouse	CAGTTAACGCCCCACTCAC	GGTTCTGATCTCATTTGGTTCC	217
Rat	CAGTTAATGCCCCACTCAC	GTTTCTGATCTCACTTGGTTCT	217
Cx3cl1			
Mouse	CCTCGGCATGACGAAATGCGAAAT	TTTCTCCTTCGGGTCAGCACAGAA	163
Rat	CCTCGGCATGACGAAATGCAACAT	TCTCCTTTGGGTCAGCACAGAAGT	161
Gapdh			
Mouse	TGAATACGGCTACAGCAACAGGGT	TTGTGAGGGAGATGCTCAGTGTTG	151
Rat	same as mouse	same as mouse	151
Icam1			
Mouse	AGTCCGCTGTGCTTTGAGAACTGT	ACTCTCCGGAAACGAATACACGGT	60
Rat	ACAGCAGACCACTGTGCTTTGAGA	ACTCGCTCTGGGAACGAATACACA	60
Ptgs2			
Mouse	GGCCATGGAGTGGACTTAAATC	AAGGCGCAGTTTATGTTGTCTGT	66
Rat	same as mouse	same as mouse	66
Sm22			
Mouse	TCCTTCCAGTCCACAAACGACCAA	TTTGGACTGCACTTCTCGGCTCAT	92
Rat	TCCTTCCAGCCCACAAACGACCAA	CTTGGACTGCACTTCACGGCTCAT	92
Vcam1			
Mouse	TGTGAAGGGATTAACGAGGCTGGA	GCACATTTCCACAAGTGCAGGAGA	151
Rat	TGTGAAGGGATTAACGAGGCTGGA	GCACACTTCCACAAGTACAGGAGA	151

Table 2. List of primer sequence for rtRT-PCR in inflammation. Tm = 60°C for all primers.

2.8. Immunofluorescence (IF).

PAC1 cells on chamber slides were fixed in methanol for 10 minutes at -20°C and blocked with 10% chicken serum for 30 minutes. Then, cells were incubated with primary antibodies at 1:100 dilution for 2 hours followed by incubation with Alexa Fluor chicken secondary antibodies at 1:200 dilution (Invitrogen) for 1 hour. Slides were mounted with Vectashield with DAPI (Vectorlabs) and examined on a Leica DM4000B microscope (Leica). Quantification was performed using Image-Pro software (Media Cybernetics). Primary antibodies were against SM22 (Abcam, ab14106), CCL2 (Santa Cruz, sc-1785).

2.9. Preparation of cell lysates.

M-PER Mammalian Protein Extraction Reagent (Pierce) with Halt Protease Inhibitor Cocktail (Pierce) was used to prepare whole cell lysates from primary VSMCs and PAC1 cells. Cell lysates were stored at -20 °C.

2.10. Western blotting.

Equal amount of whole cell lysates, the nuclear fraction or cytoplasmic fraction from primary VSMCs or PAC1 cell samples were loaded on a 4-12% Bis-Tris NuPAGE Mini-gel (Invitrogen) for electrophoresis, followed by transfer onto an Immobilon-P membrane (Millipore). The membrane was blocked with 5% milk for 30 minutes, followed by primary antibody incubation overnight at 4 °C. After incubation with biotinlyated secondary antibody for 30 minutes, the membrane was subject to enhanced chemiluminescence detection using SuperSignal West Pico Chemiluminescent Substrate (Pierce). The primary antibodies were against SM22 (1:1000, Abcam, ab14106), VCAM1 (1:100, Santa Cruz, sc-1504), and GAPDH (1:2500, Abcam, ab9485).

2.11. Statistics.

Five *Sm22*$^{-/-}$ mice and five *Sm22*$^{+/+}$ littermates were used in histology, IHC and rtRT-PCR analyses. Primary VSMCs from four *Sm22*$^{-/-}$ mice and four *Sm22*$^{+/+}$ mice were used for rtRT-PCR analyses. Three independent experiments were performed in *Sm22* knockdown research in PAC1 cells. Values are means ± SE. Statistical analyses were performed using SPSS13.0 software (IBM). Student t-test was applied to evaluate differences in all experiments and differences were considered significant at $p < 0.05$.

3. Results

3.1. *Sm22*$^{-/-}$ mice developed higher inflammatory responses upon artery injury

To determine the roles of Sm22 under pathological conditions, we performed carotid artery denudation using the *Sm22*$^{-/-}$ mice and their *Sm22*$^{+/+}$ littermates. Before injury, the size of the media and adventitia for their carotid arteries are similar (Fig. 1A, B). 2 weeks after injury, we found that the injured carotid arteries from *Sm22*$^{-/-}$ mice swelled significantly more than those from *Sm22*$^{+/+}$ mice. In addition, the response was similar between *Sm22*$^{+/+}$ and *Sm22*$^{+/-}$ littermates (Fig. 1C). These carotid arteries adhered tightly to the surrounding tissues and were difficult to isolate. H&E staining showed thicker and fibrotic artery walls (Fig. 2A) with remarkable cell infiltration in the media and adventitia of the carotid arteries in *Sm22*$^{-/-}$ mice (Fig. 2A). IHC using F4/80 (a macrophage specific marker) (Fig. 2B) and CD3 (a T lymphocyte marker) (Fig. 2C) revealed greater macrophage and T lymphocyte infiltration in the injured carotid arteries of *Sm22*$^{-/-}$ mice. These findings demonstrate enhanced inflammatory response of *Sm22*$^{-/-}$ mice upon artery injury.

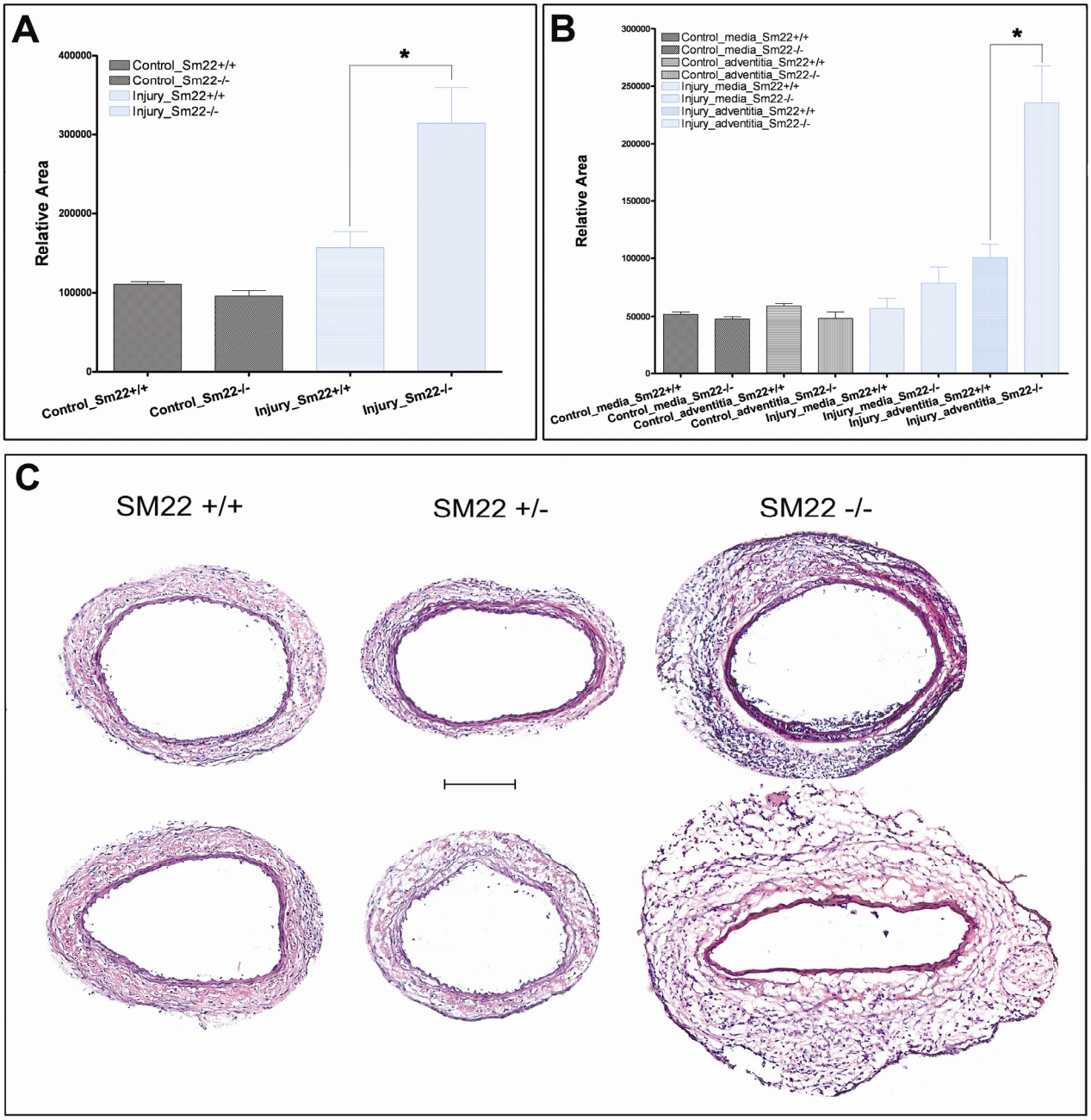

Figure 1. Enhanced inflammatory responses in *Sm22*$^{-/-}$ mice 2 weeks after carotid artery denudation. (**A**) Quantitative analysis of carotid artery areas without and with injury. (**B**) Quantitative analysis of medial and adventitial areas of carotid arteries respectively. (**C**) H&E staining showed similar inflammatory responses of carotid arteries to denudation between *Sm22*$^{+/+}$ mice and *Sm22*$^{+/-}$ littermates. Bar, 100 μm. Values (**A**, **B**) were means ± SE from five pairs of mice. The asterisk, *, indicates $p < 0.05$.

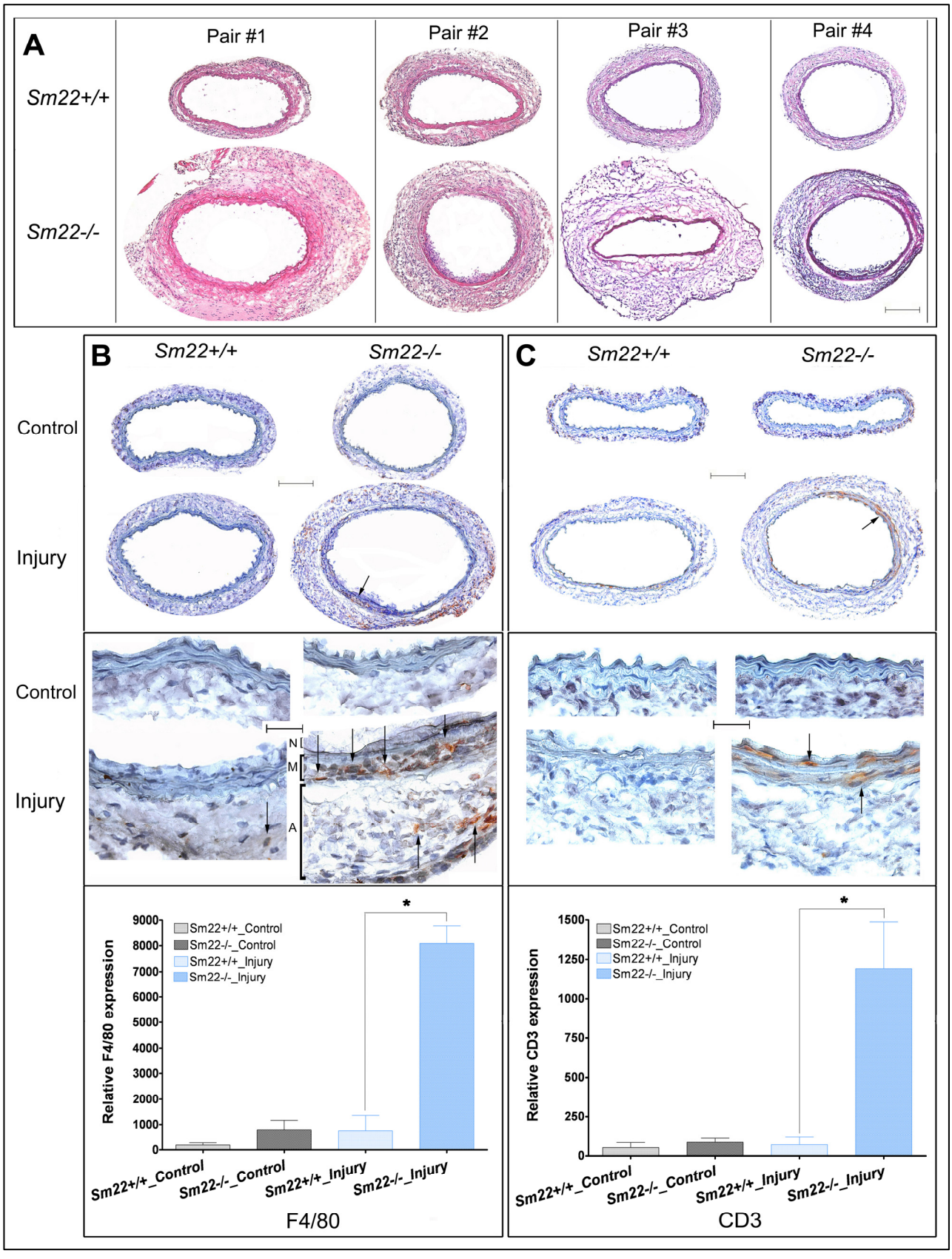

Figure 2. Prominent inflammatory cell infiltration in *Sm22*$^{-/-}$ mice 2 weeks after carotid artery denudation. (**A**) H&E staining showed pronounced carotid swelling, edema, prominent fibrotic adhesion and cell infiltration in denuded carotid arteries of *Sm22*$^{-/-}$ mice. Bar, 100 μm. (**B, C**) IHC using a macrophage marker, F4/80 (**B**) and a T cell marker, CD3 (**C**). Top panels, 100X; middle panels, 400X; bottom panels: quantification of positive signals from images at 100X magnification of carotid arteries from five *Sm22*$^{-/-}$ and their littermates *Sm22*$^{+/+}$ mice. Values are means ± SE. The asterisk, *, indicates $p < 0.05$. Representative positive signals (brown) are indicated by arrows. Bars: upper panels, 100 μm; middle panels, 20 μm. Abbreviations: N, neointima; M, media; A, adventitia.

3.2. The pro-inflammatory environment in injured carotid arteries of *Sm22*$^{-/-}$ mice

To reveal the molecular mechanisms underlying the inflammation prone scenario in carotid arteries of *Sm22*$^{-/-}$ mice after injury, we investigated the expression of several major pro-inflammatory molecules using rtRT-PCR in whole carotid arteries and IHC in the VSMC-rich media of carotid arteries. Cell adhesion molecules, including vascular cell adhesion molecule 1 (VCAM1) and intercellular adhesion molecule 1 (ICAM1), contribute to arterial inflammation via retention of inflammatory cells such as macrophages and T lymphocytes in the inflammation sites [49]. There was no significant difference between the two groups in mRNA expression of either adhesion molecule without injury (Fig. 3A, left panel); however, the injury induced change of *Vcam1* mRNA expression was two times higher in *Sm22*$^{-/-}$ mice (Fig. 3A, right panel). IHC showed that expression of both Vcam1 (Fig. 3B) and Icam1 (Fig. 3C) in the media was five times higher in *Sm22*$^{-/-}$ mice.

Chemokine (C-X3-C motif) ligand 1 (CX3CL1) and monocyte chemotactic protein-1 (CCL2), two chemokines that potently recruit monocytes and T lymphocytes, participate in various arteriopathies [49]. Both the basal level and injury induced change of *Cx3cl1* mRNA appear to be higher in *Sm22*$^{-/-}$ mice (Fig. 4A, left panels), while no obvious difference was observed for *Ccl2* (Fig. 4A, right panels). Protein expression of Cx3cl1 (Fig. 4B) in the media

was three times higher in *Sm22*$^{-/-}$ mice while the difference in Ccl2 (Fig. 4C) was not significant. Prostaglandin-endoperoxide synthase 2 (PTGS2), also known as cycloxygenase 2, is a characteristic inflammation marker since it mediates the synthesis of the vessel-active prostaglandin during inflammation [50]. Despite similar transcriptional levels in the whole carotid arteries (Fig. 5A), Ptgs2 expression was two times higher in carotid media of *Sm22*$^{-/-}$ mice than in those of their *Sm22*$^{+/+}$ littermates (Fig. 5B). These findings highlight a pro-inflammatory environment in injured carotid arteries of *Sm22*$^{-/-}$ mice where inflammatory cells were recruited, retained and activated.

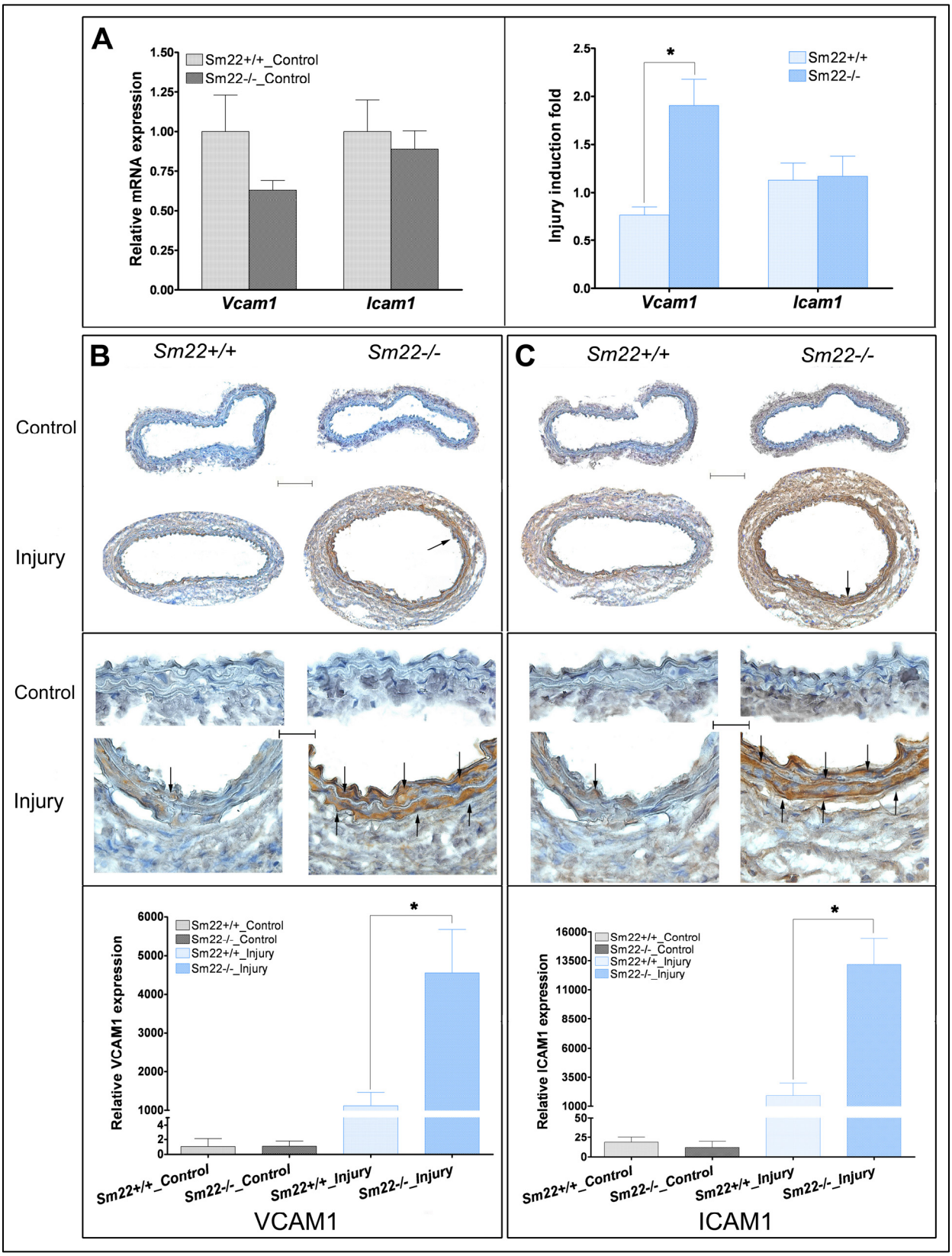

Figure 3. Expression of cell adhesion molecules is higher in *Sm22*$^{-/-}$ mice 2 weeks after carotid artery denudation. (**A**) Relative mRNA level of *Vcam1* and *Icam1* in carotid arteries without injury (left panel) and expression level induced by injury (right panel) was evaluated using rtRT-PCR. (**B, C**) IHC analyses of Vcam1 (**B**) and Icam1 (**C**). Top panels, 100X; middle panels, 400X; bottom panels, quantification of positive signals at 100X magnification in the media of carotid arteries from five *Sm22*$^{-/-}$ and their littermates *Sm22*$^{+/+}$ mice. Values (**A**, **B** and **C**) are means ± SE from five pairs of mice. The asterisk, *, indicates $p < 0.05$. Representative positive signals (brown) are indicated by arrows. Bars: top panels, 100 μm; middle panels, 20 μm.

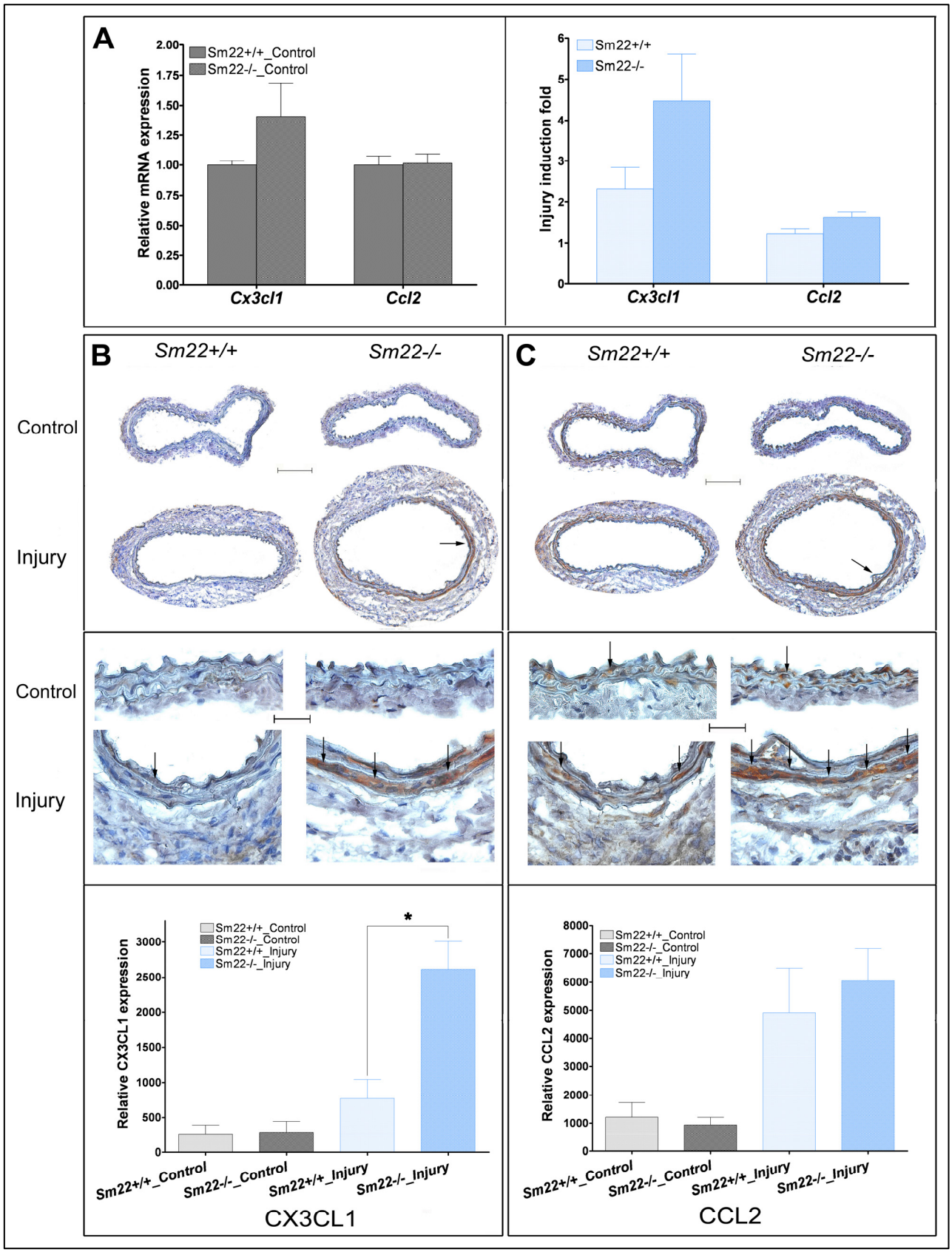

Figure 4. Higher expression of chemokines in *Sm22*$^{-/-}$ mice 2 weeks after carotid artery denudation. (**A**) Left panel: relative mRNA expression of *Cx3cl1* and *Ccl2* in carotid arteries of mice without injury evaluated using rtRT-PCR. Right panel: "Injury induction fold": the ratio between *Cx3cl1* and *Ccl2* mRNA expression in the injured carotid artery and the corresponding expression in the uninjured carotid artery of each mouse using rtRT-PCR. (**B, C**) IHC analyses of Cx3cl1 (**B**) and Ccl2 (**C**). Top panels, 100X; middle panels, 400X; bottom panels, quantification of positive signals in images at 100X magnification in the media of carotid arteries from five *Sm22*$^{-/-}$ and their littermates *Sm22*$^{+/+}$ mice. Values (**A**, **B** and **C**) are means ± SE from five pairs of mice. The asterisk, *, indicates $p < 0.05$. Representative positive signals (brown) are indicated by the arrows. Bars: top panels, 100 μm; middle panels, 20 μm.

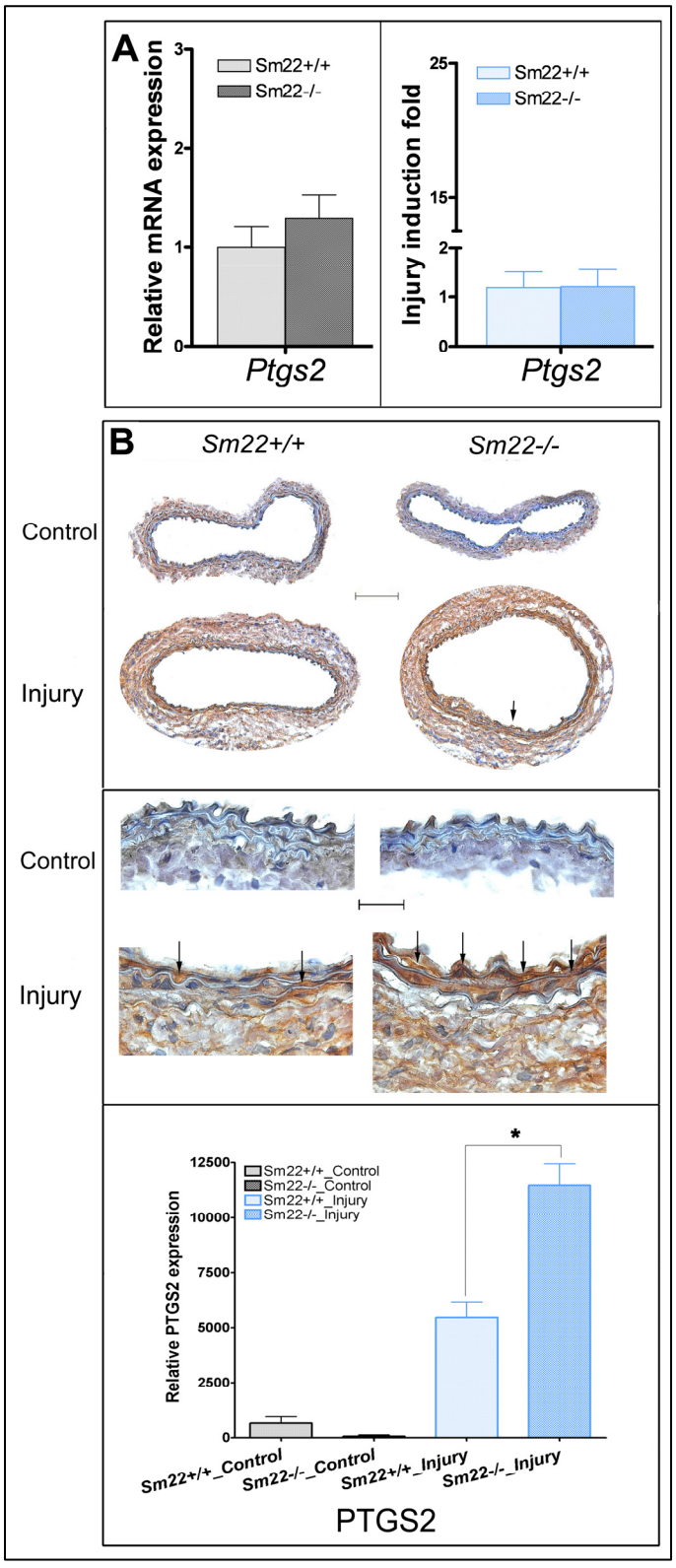

Figure 5. High induction of Ptgs2 in *Sm22*$^{-/-}$ mice 2 weeks after carotid artery denudation. (**A**) Relative mRNA expression of *Ptgs2* in carotid arteries without injury (left panel) and injury induction level (right panel) was evaluated using rtRT-PCR. (**B**) IHC analyses of Ptgs2 in the media. Upper panels, 100X; middle panels, 400X; lower panels, quantification of positive signals at 100X magnification in the media of carotid arteries from five *Sm22*$^{-/-}$ and their littermates *Sm22*$^{+/+}$ mice. Values (**A**, **B**) were means ± SE from five pairs of mice. The asterisk, *, indicates $p < 0.05$ versus *Sm22*$^{+/+}$ mice. Representative positive signals (brown) are indicated by the arrows. Bars: upper panels, 100 μm; middle panels, 20 μm.

3.3 The contributions of VSMCs to arterial inflammation after disruption of *Sm22*

Since the expression of the pro-inflammatory molecules was mainly located in the VSMC-rich artery media, we focused our efforts on analyzing VSMCs. We isolated VSMCs from aortas of both *Sm22*$^{-/-}$ and *Sm22*$^{+/+}$ mice for primary culture. VSMCs from *Sm22*$^{-/-}$ mice expressed higher levels of *Vcam1*, *Icam1*, *and Ccl2* (Fig. 6A). We also knocked down *Sm22* in a VSMC line, PAC1 cells, using siRNA (Fig. 6B). As the *Sm22* knockdown efficiency increased over time (Fig. 6B), the expression of the aforementioned pro-inflammatory molecules was gradually induced (Fig. 6B). Similarly, the extent of induction of *Vcam1*, *Cx3cl1* and *Ccl2* appeared to correlate with *Sm22* knockdown efficiency using three different siRNAs (Fig. 7A). Furthermore, to investigate if recapitulation of *Sm22* could reverse the pro-inflammatory traits of VSMCs in the absence of *Sm22*, we re-introduced *Sm22* into primary *Sm22*$^{-/-}$ VSMCs via plasmid transfection and observed 40-60% decrease in expression of *Vcam1*, *Icam1*, *Cx3cl1* and *Ccl2* (Fig. 7B).

These observations highlight the intrinsic pro-inflammatory character of VSMCs after disruption of *Sm22* expression and underscore the contributions of medial VSMCs to the enhanced arterial inflammatory responses upon injury in *Sm22*$^{-/-}$ mice.

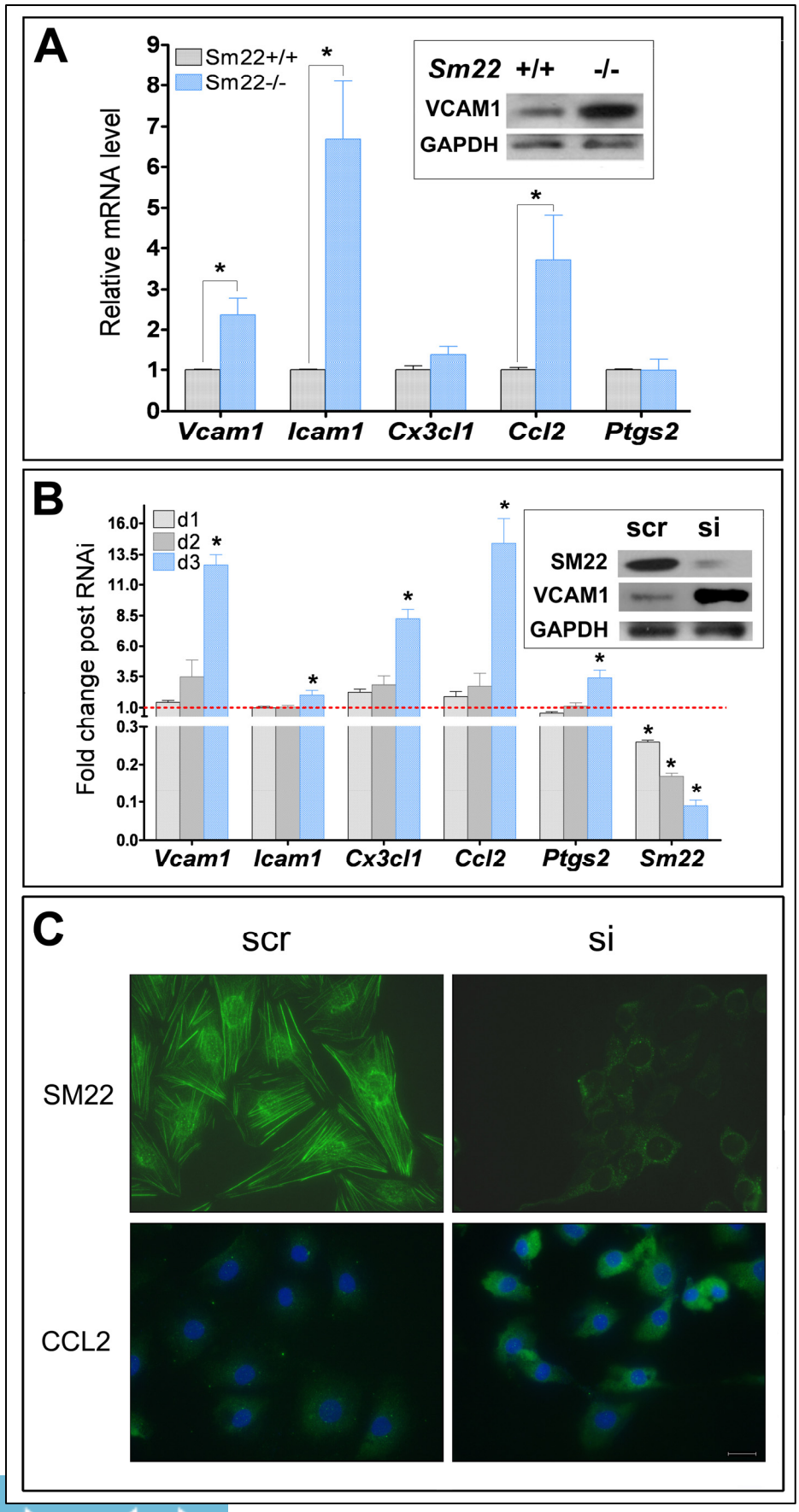

Figure 6. Transcriptional upregulation of pro-inflammatory genes in primary *Sm22*$^{-/-}$ VSMCs and in PAC1 cells after *Sm22* knockdown. (**A**) In primary *Sm22*$^{-/-}$ and *Sm22*$^{+/+}$ VSMCs, relative mRNA expression of *Vcam1*, *Icam1*, *Cx3cl1*, *Ccl2* and *Ptgs2* was examined using rtRT-PCR and WB (inserted panel). Values are means ± SE from primary VSMCs of four pairs of mice. The asterisk, *, indicates $p < 0.05$. (**B - C**) In PAC1 cells, *Sm22* knockdown efficiency and the expression of pro-inflammatory genes were determined by rtRT-PCR 1 day, 2 days and 3 days after transfection and by WB (**B**, inserted panel) and IF (**C**) 3 days after transfection. Green: Sm22 and Ccl2; blue: DAPI**.** Values in (**B**) are means ± SE from three independent experiments. The asterisk, *, indicates $p < 0.05$. Bar in (**C**): 20 µm. Abbreviations: scr, scrambled siRNA; si, *Sm22* siRNA; d1/2/3, 1/2/3 days after transfection into PAC1 cells.

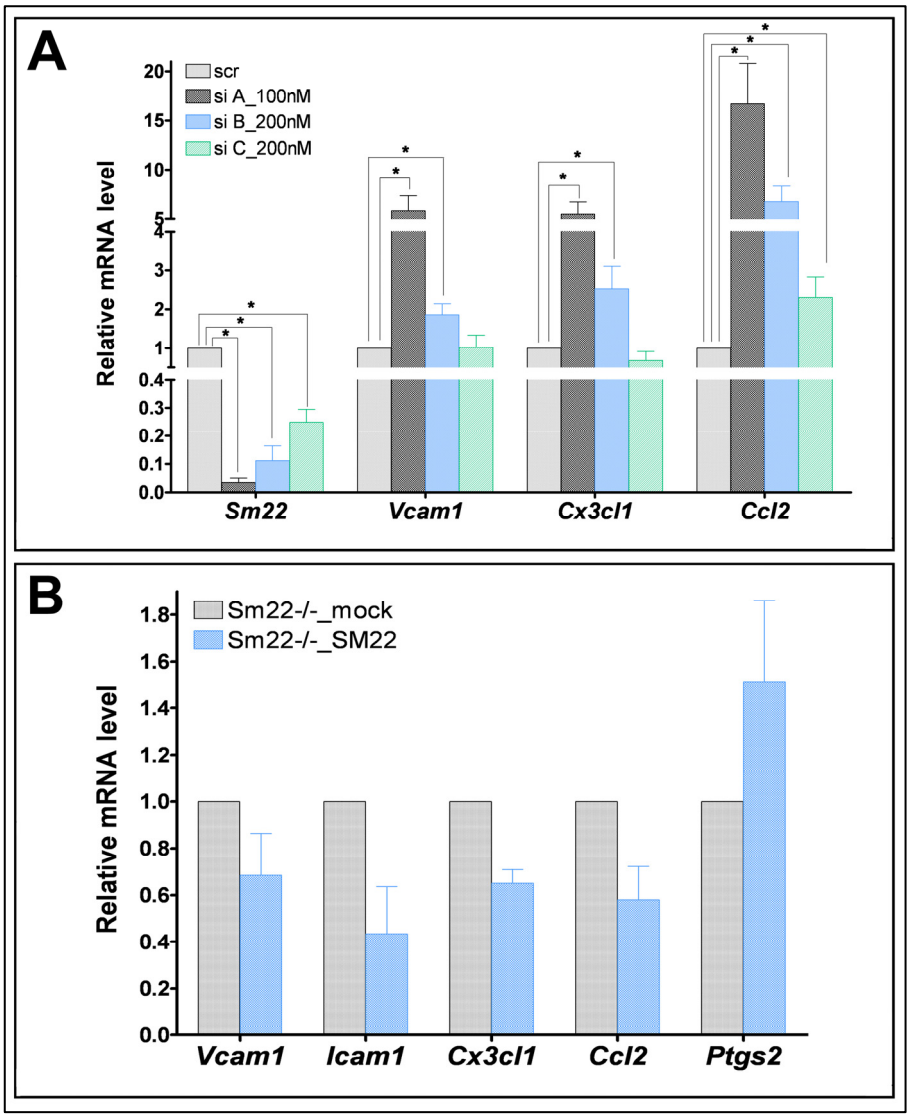

Figure 7. Induction of pro-inflammatory genes by *Sm22* siRNAs in PAC1 cells and inhibition of pro-inflammatory gene expression in primary *Sm22*$^{-/-}$ VSMCs by *Sm22* overexpression. (**A**) Relative mRNA expression of *Vcam1*, *Icam1*, *Cx3cl1* and *Ccl2* by three different *Sm22* siRNAs (siA, siB, and siC) was evaluated using rtRT-PCR. Values were means ± SE from three independent experiments. The asterisk, *, indicates $p < 0.05$. (**B**) Relative mRNA expression of *Vcam1*, *Icam1*, *Cx3cl1*, *Ccl2* and *Ptgs2* was evaluated using rtRT-PCR in primary *Sm22*$^{-/-}$ VSMCs after transfection with pcDNA3-*Sm22* plasmids (SM22) or the control vector pcDNA3 (mock). Values were means ± SE. Abbreviations: scr, scrambled RNA; si, *Sm22* siRNA; *Sm22*$^{-/-}$_mock, *Sm22*$^{-/-}$ primary VSMCS transfected with pcDNA3 plasmids; *Sm22*$^{-/-}$_SM22, *Sm22*$^{-/-}$ primary VSMCS transfected with pcDNA3-*Sm22* plasmids.

4. Discussion

Highly expressed in SMCs [19, 20], SM22 has been viewed as a SMC marker, especially in VSMCs. Several *Sm22* Cre mice were generated and used in SMC specific conditional gene knockout [51, 52]. Lack of vascular phenotypes in *Sm22*$^{-/-}$ mice implied that Sm22 might be required under stressed conditions of arteries [26]. Studies show that SM22 may participate in pathogenesis of arterial diseases including atherosclerosis [34, 36, 37] and abdominal aortic aneurysm [35]. In particular, the findings that *Sm22*$^{-/-}$*ApoE*$^{-/-}$ mice exhibited more macrophage infiltration than *Sm22*$^{+/+}$*ApoE*$^{-/-}$ mice in atherosclerotic plaques implying that Sm22 might be involved in inflammation of injured arteries [37]. Inflammation is involved in multiple arteriopathies including atherosclerosis [40-43], hypertension [44, 45] and chronic kidney disease (CKD) [47]. Therefore, it is worthwhile to look into the role of Sm22 in inflammation upon artery injury.

The loss of functional compensation of Sm22 in diseased arteries highlights the molecular differences between the embryonic VSMC differentiation, artery homeostasis and phenotypic modulation of VSMCs [2, 10, 53-55] under arterial stresses. Proliferation and re-differentiation is one of the features during VSMC phenotypic modulation in injured arteries, and this feature is common in cell culture system. So, we investigated events after *Sm22* disruption using both *in vivo* injury model and *in vitro* VSMC culture system.

Chronic arterial inflammation features infiltration of macrophages and T lymphocytes along with fibrosis in the artery wall [40, 43, 44, 56, 57]. Several pro-inflammatory molecules are involved in the inflammatory status: chemokines such as CCL2 [40, 43, 44, 49, 56] and CX3CL1 [13, 49], adhesion molecules such as VCAM1 and ICAM1 [13, 40, 43, 44, 56, 57]. In addition, PTGS2 is also a

well known pro-inflammatory molecule in arterial diseases [50]. Inflammation is one major event along with neointima formation in artery injury models such as carotid artery denudation, femoral denudation [58-62], and the inflammatory responses cover the whole artery wall from lumen to adventitia [58-61]. Expression of Sm22 in artery adventitia after injury implied involvement of Sm22 in adventitial inflammatory responses [63]. More macrophage and T lymphocyte infiltration in media and adventitia, excessive adventitial fibrosis and prominent thickening of denuded carotid arteries depicted higher inflammatory responses of arteries of *Sm22*$^{-/-}$ mice upon injury. The elevated expression of Ptgs2, Ccl2, Cx3cl1, Vcam1, and icam1 uncovered the existence of an injury-inducible pro-inflammatory molecular environment in arteries of *Sm22*$^{-/-}$ mice, and the discrepancy of induction between mRNA level and protein level might be due to post-transcriptional modifications or increased stability of proteins. Since expression of pro-inflammatory genes is finely regulated during inflammation [49], it is not surprising that changes in some pro-inflammatory genes such as *Cxcl12* were not detected under the same conditions.

In our system we only observed marginal neointima formation in injured carotid arteries: this might be due to the C57BL6 mice having mixed genetic background that may be resistant to injury-induced neointima formation [64-67]. The dominant distribution of pro-inflammatory proteins in the VSMC-rich media suggests VSMCs as the cell sources for inflammation. Consistent with this notion, primary VSMCs from *Sm22*$^{-/-}$ mice and PAC1 after *Sm22* knockdown also show upregulated expression of these pro-inflammatory genes. These results imply that disruption of *Sm22* in VSMCs may independently establish a pro-inflammatory environment in the arteries under stressed conditions.

PART II

Disruption Of *Sm22* Promotes Arterial Chondrogenesis

1. Introduction

VSMCs have the capacity to undergo drastic phenotypic modulation from contractile and differentiated state to proliferative, dedifferentiated, chondrocytic and osteoblastic phenotypes in arterial diseases such as atherosclerosis and in vascular complications due to diabetes and CKD [7, 8]. Arterial chondrogenesis and osteogenesis lead to increased artery stiffness and compromised blood pressure regulation capacity, thus contributing to chronic heart failure [7, 8]. Medial VSMCs play essential roles in this process, as evidenced by the trans-differentiation of VSMCs to osteochondrocytic cells [8, 52, 68, 69]. VSMC chondrogenic transdifferentiation features high expression of the key transcription factor SRY-box containing gene 9 (SOX9), syntheses and deposition of distinct extracellular matrix (ECM) proteins in the arterial media, such as type II collagen, aggrecan and osteopontin [7, 8, 52, 68]. Expression of VSMC cytoskeleton proteins, including SM22, is down-regulated in the pathogenesis of arterial diseases and VSMCs exhibit distinct morphological changes [8, 34, 52, 68]. In order to address the question of whether this downregulation of SM22 is just a passive outcome or an active pro-chondrogenic driving force, we analyzed the carotid arteries of *Sm22* knockout mice after carotid artery denudation as wells as primary *Sm22*$^{-/-}$ VSMCs and PAC1 cells after *Sm22* knockdown.

2. Materials and Methods

2.1. Artery injury by carotid artery denudation.

The mouse carotid artery denudation protocol was approved by the Animal Investigation Committee at Wayne State University. *Sm22*$^{-/-}$ mice on mixed C57BL6 and SV129 genetic background and their *Sm22*$^{+/+}$ littermates were used. Carotid artery denudation was carried out on male *Sm22*$^{-/-}$ mice and their wild type littermates of 18–20 weeks of age, as described [18]. Briefly, *Sm22*$^{-/-}$ mice and their *Sm22*$^{+/+}$ littermates were subjected to surgery. After anesthesia of mice using 2% avertin intraperitoneally (0.25 mg/g body weight), a curved guide wire of 0.35 mm in diameter was introduced into the left common carotid artery and passed in and out of the left common carotid artery with constant rotation for three passages. Two weeks after surgery, the mice were sacrificed and both carotid arteries were harvested. Five *Sm22*$^{-/-}$ mice and their *Sm22*$^{+/+}$ littermates were used for histological and immunohistochemical analyses. The carotid segments of 3 mm in length covering the part from 2 mm to 5 mm proximal to the carotid bifurcation were harvested and embedded in OCT medium (Tissue-Tek), and around 100 frozen slides were made for each mouse with triplicate sections on each slide at 8 μm thickness. Five *Sm22*$^{-/-}$ mice and their *Sm22*$^{+/+}$ littermates were used for rtRT-PCR: the carotid arteries of these mice were stored separately in RNAlater reagent (Ambion) at 4°C for no more than 1 week before RNA extraction.

2.2. Immunohistochemical (IHC) analyses.

Six slides, in the order of one every 15 consecutive slides, from each mouse were used for H&E staining to screen sections with most prominent inflammatory responses. IHC was performed on the properly selected consecutive frozen slides using VECTASTAIN Elite ABC Kit (Vectorlabs). Briefly, air-dried slides were fixed in methanol containing 0.3% H_2O_2 for 10 minutes and blocked with serum for 20 minutes. The following incubation steps of primary

antibody, secondary antibody, ABC reagent and DAB substrate were performed according to the manufacturer's protocol. The slides were counterstained with hematoxylin. The primary antibodies (1:50 dilution) were rabbit anti-type II collagen IgG (Abcam, ab53047), rabbit anti-aggrecan (Santa Cruz, sc-25674), goat anti-SPP1 (Santa Cruz, sc-10593), rabbit anti-BMP2 (Abcam, ab14933), rabbit anti-SOX9 (Abcam, ab3697) and rabbit anti-matrix GLA protein (MGP) (Santa Cruz, sc-66965). Semi-quantitative analyses were performed using the Image-Pro software (Media Cybernetics).

2.3. Alcian blue staining.

Alcian blue staining was performed using the Alcian blue, pH 2.5 kit (VWR), and nucleus was counter-stained with Fast Red (VWR).

2.4. Primary VSMC culture.

VSMCs were isolated from aortas of six *Sm22*$^{-/-}$ mice and six *Sm22*$^{+/+}$ mice as described [48]. Primary VSMCs were kept in the DMEM medium (Invitrogen) containing 10% FBS (Invitrogen) and passed upon confluency at a 1:2 dilution ratio. Primary VSMCs in passage 2 to passage 4 were used for experiments.

2.5. *Sm22* knockdown in PAC1 cells with siRNA.

Sm22 knockdown was achieved using Dicer-Substrate siRNA duplexes (IDT, MMC.RNAI.N011526.5.1, siA). PAC1 cells [39] (a pulmonary arterial SMC cell line) were seeded at 30% confluency 24 hours before transfection. Transfection was performed using DharmaFECT3 (Dharmacon) with siRNA duplex or scrambled RNA duplex at 100 nM, and the

FBS was diluted to 2% with media 24 hours after transfection for optimal cell density. Cells were used for experiments 72 hours after transfection unless otherwise specified.

2.6. RtRT-PCR

Total RNA from carotid arteries was extracted and purified using RNeasy Fibrous Tissue Kit (Qiagen), and total RNA from primary VSMCs or PAC1 cells was extracted and purified using RNeasy Kit (Qiagen). The cDNA was synthesized using the Superscript II reverse transcriptase (Invitrogen). Real-time PCR was performed using SYBR Green on a StepOnePlus system (Applied Biosystems). Gapdh and snRNA U6 were used as internal controls in ΔΔCt method. All PCR primers were designed to cover at least 2 exons.

Gene	Forward (5' - 3')	Reverse (5' - 3')	Size (bp)
Acan			
Mouse/Rat	AGAACCCTCGGGCAGAAGAAAGAT	TCTGTAGCCTGTGCTTGTAGGTGT	175
Acta2			
Mouse/Rat	GAGAAGCCCAGCCAGTCG	ATCTTTTCCATGTCGTCCCAGTTG	309
Bmp2			
Mouse	TGCGCAGCTTCCATCACGA	CTGTGTGGTCCACCGCATCA	329
Rat	TGCTCAGCTTCCATCACGA	CTGTGCTGTCCATCGCATCA	329
Col2a1			
Mouse/Rat	TGGAAAGCAAGGTGACCAGGGTAT	TTTGGGACCATCAGTACCAGGAGT	163
Gapdh			
Mouse/Rat	TGAATACGGCTACAGCAACAGGGT	TTGTGAGGGAGATGCTCAGTGTTG	151
Myh11			
Mouse/Rat	AACGCCCTCAAGAGCAAACTCAGA	TCCCGAGCGTCCATTTCTTCTTCA	161
Myocd			
Mouse/Rat	CAGTGAAGCAGCAAATGACTCGG	GTCGTTGGCGTAGTGATCGAAGG	230
Sm22			
Mouse	TCCTTCCAGTCCACAAACGACCAA	TTTGGACTGCACTTCTCGGCTCAT	92
Rat	TCCTTCCAGCCCACAAACGACCAA	CTTGGACTGCACTTCACGGCTCAT	92
Sox9			
Mouse/Rat	GGCGGAGGAAGTCGGTGAAGAA	CACGTCGGTTTTGGGAGTGGTG	206

Table 3. List of primer sequence for rtRT-PCR in chondrogenesis. Tm = 60°C for all primers.

2.7. Immunofluorescence (IF) analyses.

PAC1 cells on chamber slides were fixed in methanol for 10 minutes at -20°C and blocked with 10% chicken serum for 30 minutes. Then, cells were incubated with primary antibodies at 1:100 dilution for 2 hours followed by incubation with Alexa Fluor chicken secondary antibodies at 1:200 dilution (Invitrogen) for 1 hour. Slides were mounted with Vectashield with DAPI (Vectorlabs) and examined on a Leica DM4000B microscope. Quantification was performed using Image-Pro software (Media Cybernetics). Primary antibodies were rabbit anti-SM22 IgG (Abcam, ab14106), mouse anti-smooth muscle alpha actin (SMA) IgG2a (Santa Cruz, sc-58669) and rabbit anti-SMA antibody (Abcam, ab5694).

2.8. Preparation of cell lysate.

M-PER Mammalian Protein Extraction Reagent (Pierce) with Halt Protease Inhibitor Cocktail (Pierce) was used to prepare whole cell lysates from primary VSMCs and PAC1 cells. Cell extracts were stored at -20°C.

2.9. Western blotting (WB).

Equal amount of whole cell lysates, the nuclear fraction or cytoplasmic fraction from primary VSMCs or PAC1 cell samples were loaded on a 4-12% Bis-Tris NuPAGE Mini-gel (Invitrogen) for electrophoresis, followed by transfer onto an Immobilon-P membrane (Millipore). The membrane was blocked with 5% milk for 30 minutes, followed by primary antibody incubation overnight at 4 °C. After incubation with biotinylated secondary antibody for 30 minutes, the membrane was subjected to enhanced chemiluminescence detection using SuperSignal West Pico Chemiluminescent Substrate (Pierce). The primary antibodies were rabbit

anti-SM22 IgG (1:1000, Abcam, ab14106), rabbit anti-SMA IgG (1:500, Abcam, ab5694), rabbit anti-SOX9 (1:100, Santa Cruz, sc-20095), goat anti-myocardin (1:100, Santa Cruz, sc-21561) and rabbit anti-GAPDH (1:2500, Abcam, ab9485).

2.10. Measurement of F/G-actin ratio.

F/G-actin ratio in PAC1 cells was determined using the G-actin/F-actin *in vivo* assay kit (Cytoskeleton Inc.) according to manufacturer's protocol. Briefly, PAC1 cells were homogenized in cell lysis and F-actin stabilization buffer (50 mmol/L PIPES, 50 mmol/L NaCl, 5 mmol/L $MgCl_2$, 5 mmol/L EGTA, 5% (v/v) lyceral, 0.1% (v/v) Nonidet P-40, 0.1% (v/v) Triton X-100, 0.1% (v/v) Tween 20, 0.1% (v/v) 2-mercaptoethanol and 0.001% (v/v) antifoam)and the protease inhibitor cocktail. Centrifugation was performed for 2 hours at 70 000 g at 37°C to separate the F-actin from G-actin pool and supernatants (G-actin) were collected after centrifugation. The pellets (F-actin) were resuspended in ice-cold ddH_2O containing 1 μmol/L cytochalasin D followed by incubation and mixing on ice for 1 h to dissociate F-actin. Equal amount of the supernatant (G-actin) and the resuspended pellet (F-actin) were subjected to analysis by WB using the rabbit anti-actin antibody in the kit. The quantification was performed using the Image-Pro software (Media Cybernetics).

2.11. Statistics.

Five $Sm22^{-/-}$ mice and five $Sm22^{+/+}$ littermates were used in histology, IHC and rtRT-PCR analyses. Primary VSMCs from four $Sm22^{-/-}$ mice and four $Sm22^{+/+}$ mice were used for rtRT-PCR analyses. Three independent experiments were performed in *Sm22* knockdown research in PAC1 cells. Values are means ± SE. Statistical analyses were performed using

SPSS13.0 software (IBM). Student t-test was applied to evaluate differences in all experiments and differences were considered significant at $p < 0.05$.

3. Results

3.1. Enhanced medial chondrogenesis with compromised myogenesis in *Sm22*$^{-/-}$ mice after carotid injury

Carotid arteries were harvested 2 weeks after carotid artery denudation. IHC analysis showed remarkable expression of a chondrocyte marker, type II collagen (Col2a1), in the media of *Sm22*$^{-/-}$ mice (Fig. 8A, B) with morphology of chondrocytic cells (Fig. 9). Alcian blue staining revealed marked expression of mucopolysaccharides and glycosaminoglycans in the media of *Sm22*$^{-/-}$ mice (Fig.8Da, Db). A variety of ECM proteins, such as aggrecan (ACAN) and osteopontin (SPP1) [70, 71], are required during normal chondrogenesis. IHC analysis indicated that expression of both Acan (Fig. 10A) and Spp1 (Fig. 11) in the media was significantly higher in *Sm22*$^{-/-}$ mice compared to their *Sm22*$^{+/+}$ littermates. These data support a pro-chondrogenic ECM environment in injured arteries of *Sm22*$^{-/-}$ mice. Furthermore, bone morphogenetic protein 2 (Bmp2), one of the major cytokines with pivotal roles in every step of chondrogenesis [71], was intensely expressed in injured carotid artery media of *Sm22*$^{-/-}$ mice (Fig. 10B).

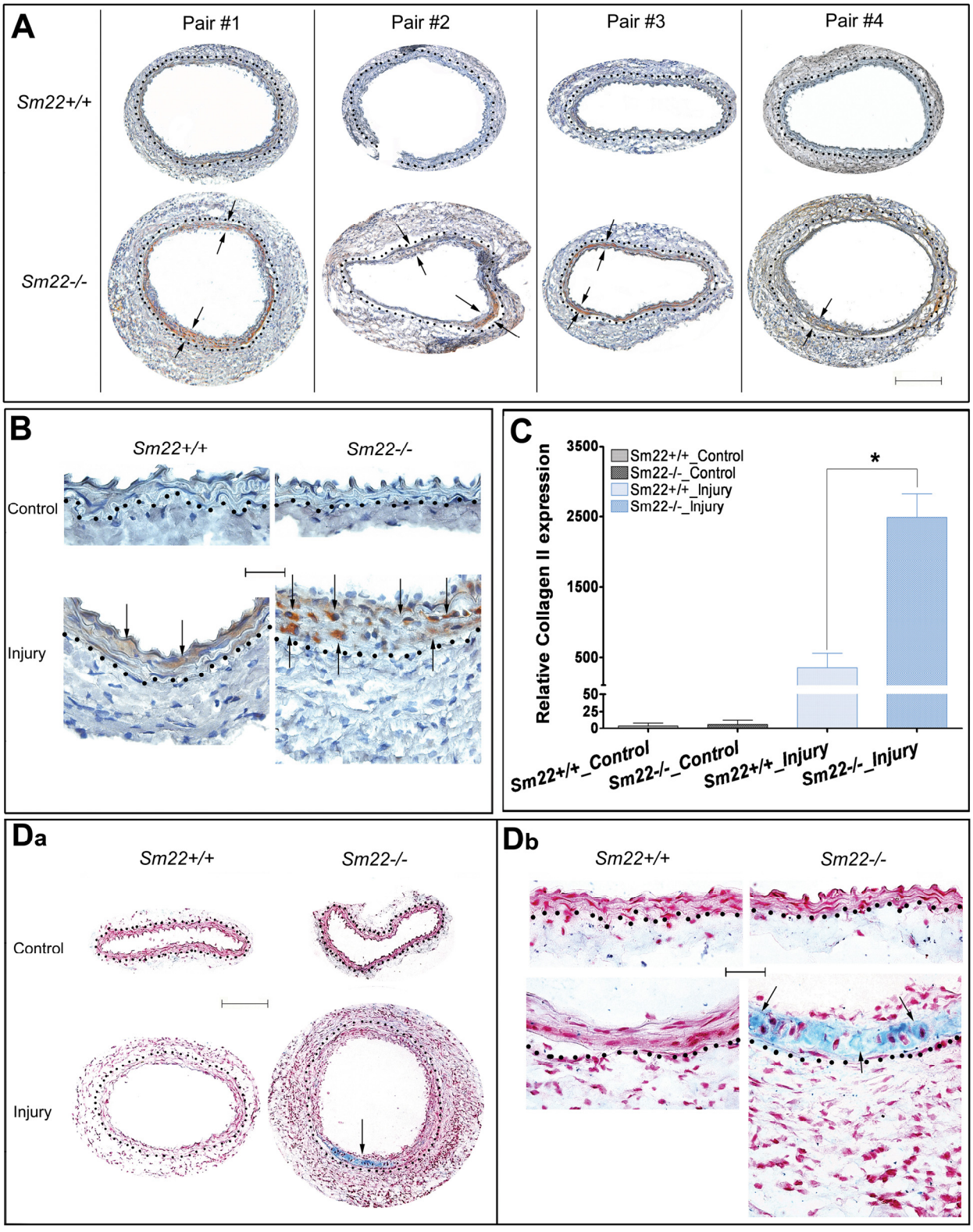

Figure 8. Enhanced expression of type II collagen in *Sm22*$^{-/-}$ mice 2 weeks after carotid artery denudation. Expression of type II collagen was evaluated by IHC. (**A**) Injured carotid arteries from four *Sm22*$^{-/-}$ mice and their wild-type littermates at 100X magnification. (**B**) Both injured carotid arteries and non-injured controls at 400X magnification. Representative brown signals were indicated by the arrows. (**C**) Quantification of positive signals from images at 100X magnification in the media of carotid arteries from five *Sm22*$^{-/-}$ and their littermates *Sm22*$^{+/+}$ mice. (**D**) Alcian blue staining of carotid arteries at 100X (Da) and at 400X magnification (Db). Blue signals, Alcian blue; red signals, nuclear fast red. Bar in (**A, Da**), 100 μm; bar in (**B, Db**), 20 μm. Dashed lines demarcated the border between media and adventitia. Values are means ± SE. The asterisk, *, indicates $p < 0.05$.

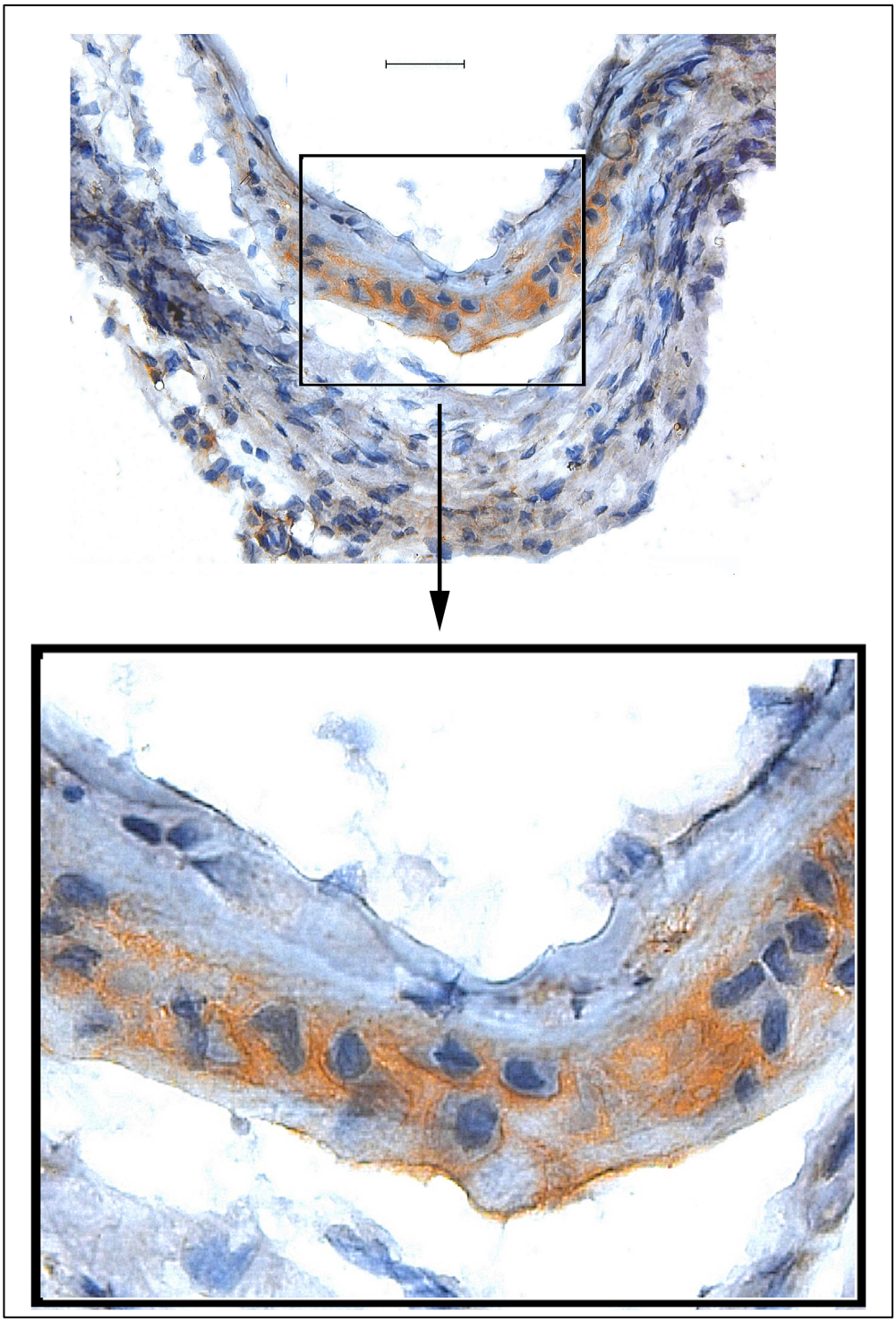

Figure 9. Chondrocytic morphology of medial layers in *Sm22*$^{-/-}$ mice 2 weeks after carotid artery denudation. The IHC (type II collagen) image of carotid artery from *Sm22*$^{-/-}$ mouse of pair # 2 in Figure 8 was enlarged to highlight the cell morphology in media layer. Bar, 100 µm.

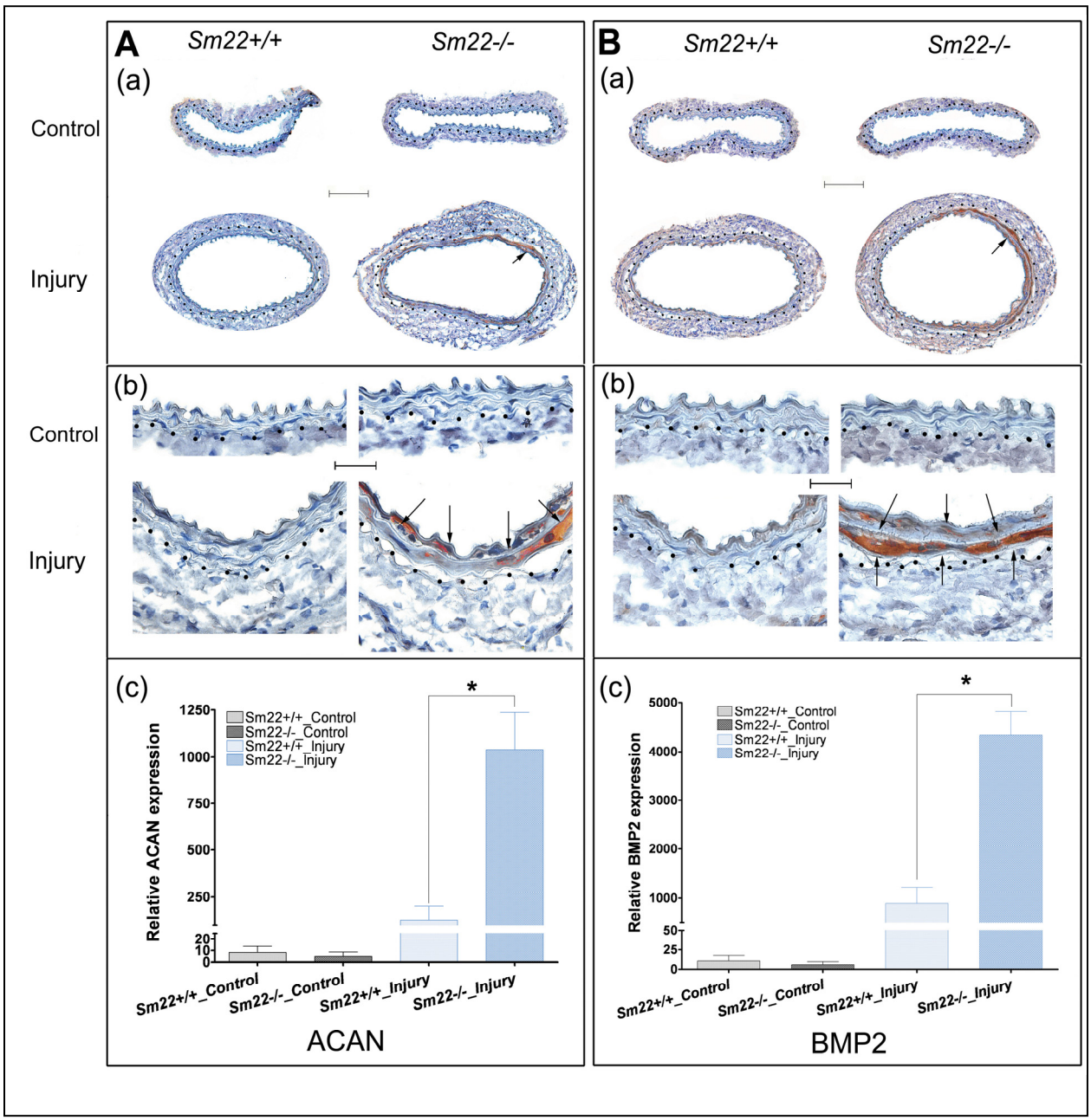

Figure 10. Augmented expression of aggrecan and Bmp2 in *Sm22*$^{-/-}$ mice 2 weeks after carotid artery denudation. (**A**) IHC analyses of Acan (a) at 100X magnification, (b) at 400X magnification and (c) quantification of positive signals from images at 100X magnification in the media of carotid arteries from five *Sm22*$^{-/-}$ and their littermates *Sm22*$^{+/+}$ mice. (**B**) IHC analyses of Bmp2 (a) at 100X magnification, (b) at 400X magnification and (c) quantification of positive signals from images at 100X magnification in the media of carotid arteries from five *Sm22*$^{-/-}$ and their littermates *Sm22*$^{+/+}$ mice. Representative brown signals are indicated by the arrows. Bars in (**A**a and **B**a), 100 μm; Bars in (**A**b and **B**b), 20 μm. Dashed lines demarcated the border between media and adventitia. Values in (**A**c and **B**c) are means ± SE. The asterisk, *, indicates $p < 0.05$.

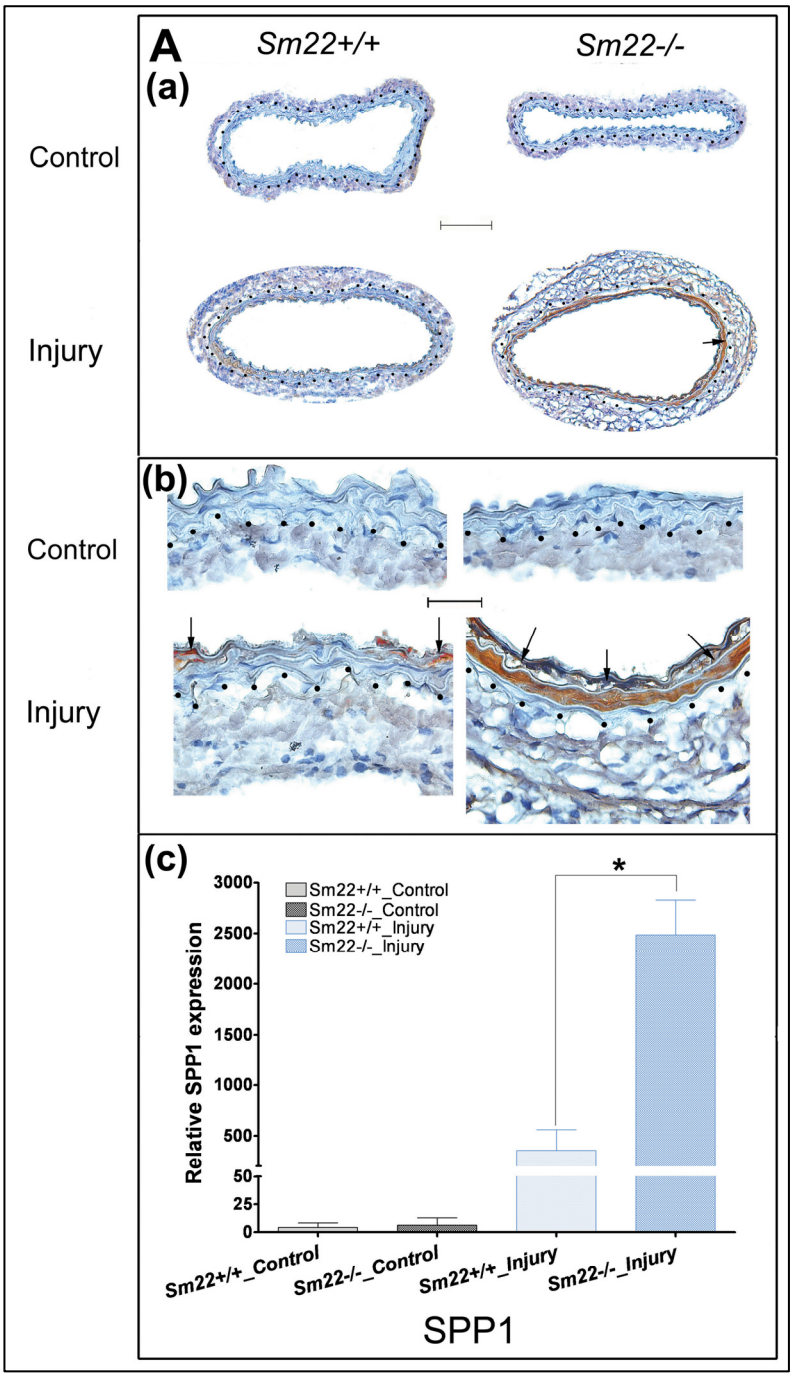

Figure 11. Augmented expression of osteopontin in *Sm22*$^{-/-}$ mice 2 weeks after carotid artery denudation. (**A**) IHC analyses of osteopontin (Spp1) (a) at 100X magnification, (b) at 400X magnification and (c) quantification of positive signals from images at 100X magnification in the media of carotid arteries from five *Sm22*$^{-/-}$ and their littermates *Sm22*$^{+/+}$ mice. Representative brown signals are indicated by the arrows. Bar in (**A**a), 100 μm; Bar in (**A**b), 20 μm. Dashed lines demarcated the border between media and adventitia. Values in (**A**c) are means ± SE. The asterisk, *, indicates $p < 0.05$.

In order to explore the transcriptional basis underlying the ectopic chondrogenesis, we examined expression of a master transcription factor regulating chondrogenesis, SOX9 [71, 72]. IHC results showed marked Sox9 expression in the media of the injured carotid arteries from *Sm22*$^{-/-}$ mice in contrast to the scant Sox9 induction from *Sm22*$^{+/+}$ littermates (Fig. 12A). We also examined the mRNA level of myocardin in the media of the injured carotid arteries. The expression of myocardin decreased significantly in injured carotid arteries of *Sm22*$^{-/-}$ mice compared to that of their *Sm22*$^{+/+}$ littermates (60% vs. 20%, Fig.12B), suggesting a lower pro-myogenic tendency in the VSMCs of *Sm22*$^{-/-}$ mice after injury. The expression of smooth muscle myosin heavy chain (*Myh11*) was reduced, although this reduction was not statistically significant (Fig. 12B). However, the expression of smooth muscle alpha actin (*Acta2*) mRNA was not affected much (Fig. 12B); this could be due to the fact that Acta2 is also expressed in adventitial cells after injury in addition to medial VSMCs. This speculation is supported by IHC analysis of Acta2 (Fig. 13).

On the other hand, we did not find calcium deposition in carotid arteries from either *Sm22*$^{-/-}$ mice or their *Sm22*$^{+/+}$ littermates based on the negative results of Alizarin Red staining. Meanwhile, we analyzed expression of osteocalcin (Bglap), alkaline phosphatase (Alp) and Runx2 using IHC and found little difference between these two groups. These results indicated the lack of medial calcification at this time point.

These *in vivo* findings illustrate a transcriptional shift from pro-myogenesis to pro-chondrogenesis in the arteries of *Sm22*$^{-/-}$ mice upon stress; this suggests that loss of *Sm22* in VSMCs might promote the ectopic medial chondrogenesis via transcriptional switch.

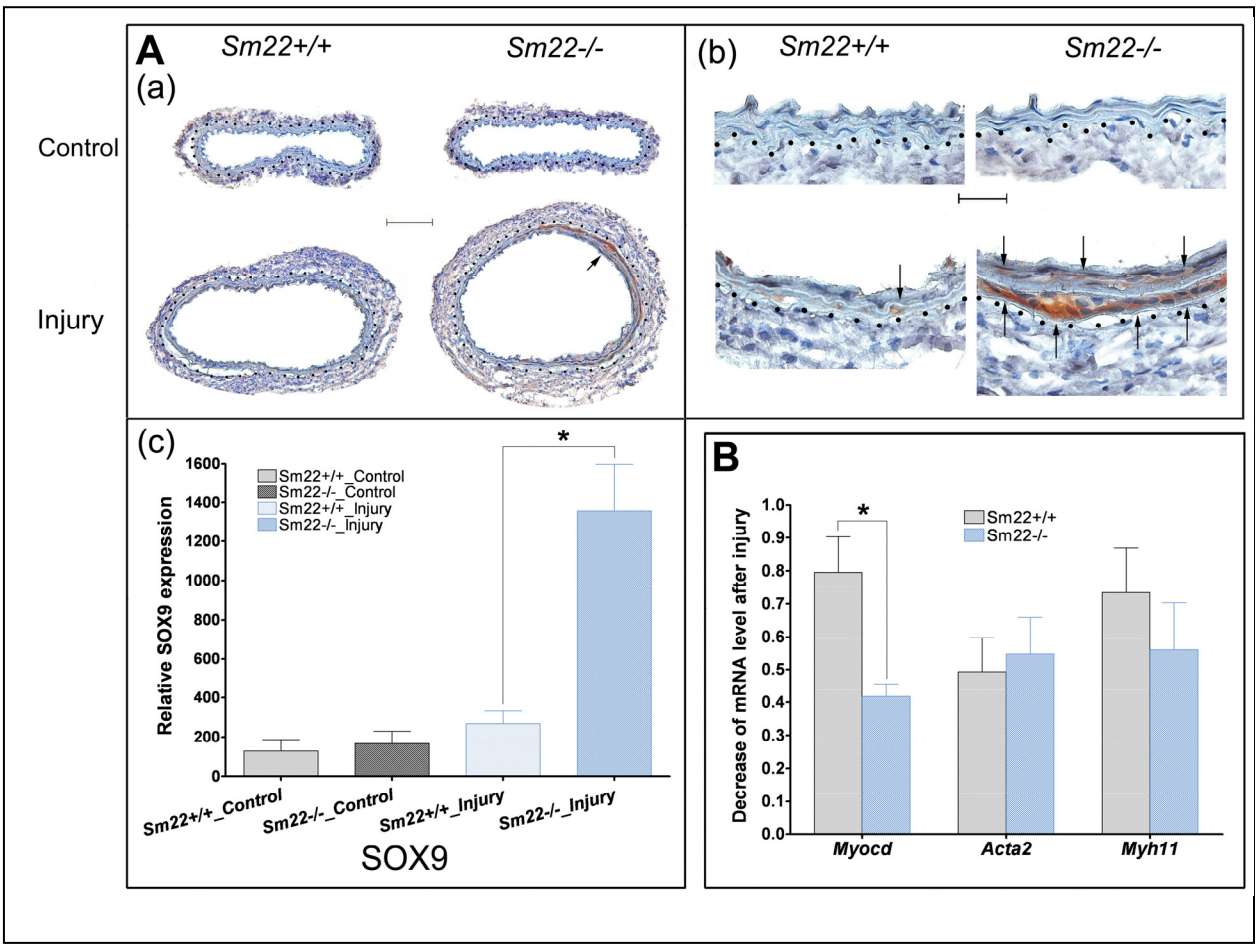

Figure 12. Augmented expression of Sox9 in *Sm22*$^{-/-}$ mice 2 weeks after carotid artery denudation. (**A**) IHC analyses of Sox9 (**a**) at 100X magnification, (**b**) at 400X magnification and (**c**) quantification of positive signals from images at 100X magnification in the media of carotids from five *Sm22*$^{-/-}$ and their littermates *Sm22*$^{+/+}$ mice. Representative brown signals were indicated by the arrows. Bar in (**Aa**, 100 μm; Bar in (**Ab**), 20 μm. (**B**) Relative mRNA level of *Myocd*, *Acta2* and *Myh11* in injured carotids was evaluated using rtRT-PCR. Dashed lines demarcated the border between media and adventitia. Values in (**Ac** and **B**) are means ± SE. The asterisk, *, indicates $p < 0.05$ versus *Sm22*$^{+/+}$ mice.

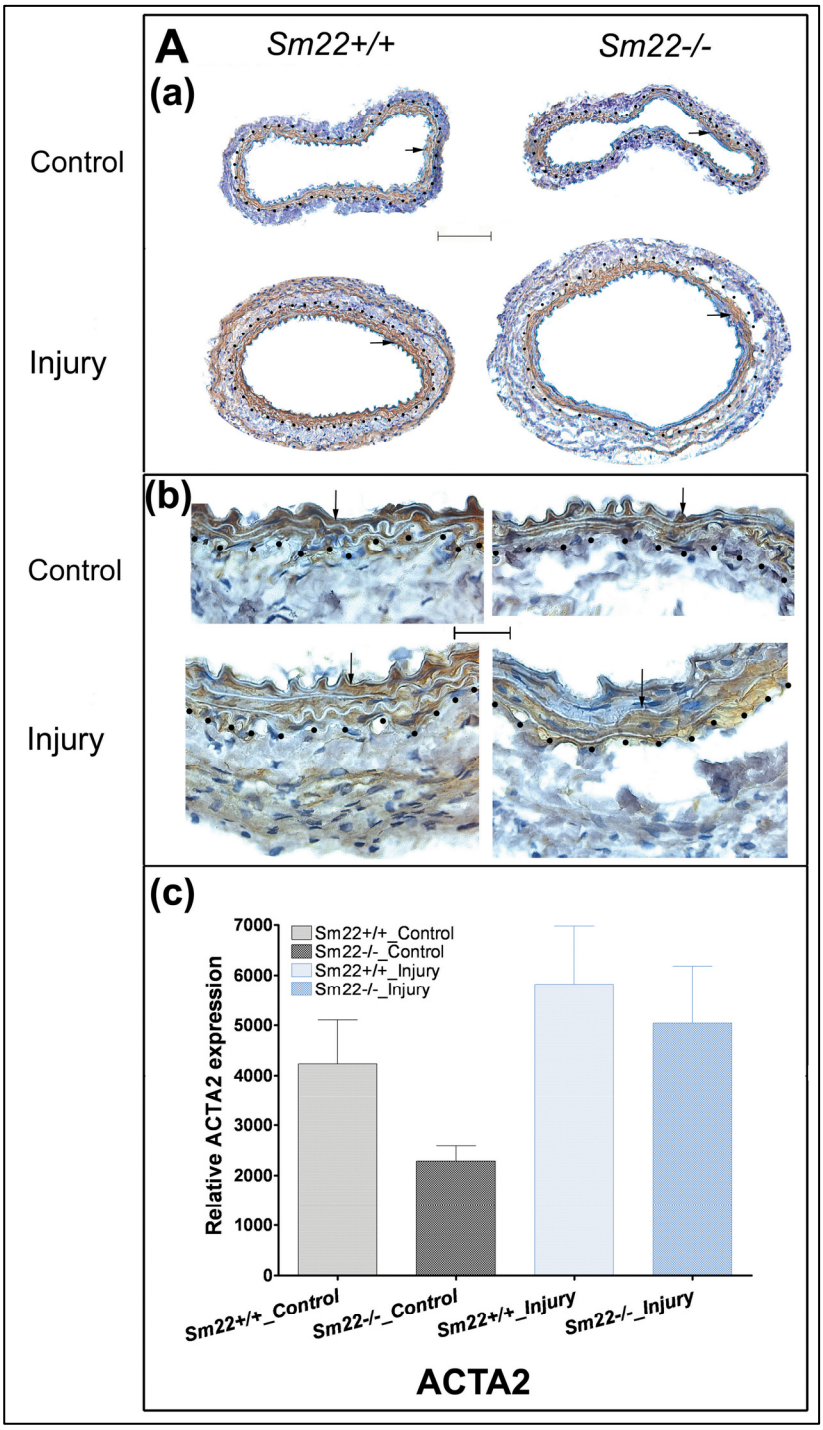

Figure 13. Lower expression of Acta2 in *Sm22*$^{-/-}$ mice 2 weeks after carotid artery denudation. (**A**) IHC analyses of Acta2 (**a**) at 100X magnification, (**b**) at 400X magnification and (**c**) quantification of positive signals from images at 100X magnification in the media of carotid arteries from five *Sm22*$^{-/-}$ and their littermates *Sm22*$^{+/+}$ mice. Representative brown signals are indicated by the arrows. Bar in (**Aa**), 100 μm; Bar in (**Ab**), 20 μm. Dashed lines demarcated the border between media and adventitia. Values in (**Ac**) are means ± SE.

3.2. A transcriptional shift from myogenic to chondrogenic pattern in primary *Sm22*$^{-/-}$ VSMCs and after *Sm22* knockdown in a VSMC line

To explore the transcriptional changes after *Sm22* disruption in VSMCs, we investigated expression of several marker genes in primary VSMCs from *Sm22*$^{-/-}$ mice and their *Sm22*$^{+/+}$ littermates and in PAC1 cells after *Sm22* knockdown. The mRNA levels of *Myocd, Smtn, Acta2* and *Myh11* in *Sm22*$^{-/-}$ VSMCs were lower than those in *Sm22*$^{+/+}$ VSMCs (Fig. 14A), while the mRNA levels of *Sox9*, *Bmp2* and *Col2a1* were higher in *Sm22*$^{-/-}$ VSMCs (Fig. 14A). The expressions of Act2 and Sox9 proteins were also decreased and increased respectively in *Sm22*$^{-/-}$ VSMCs by WB (Fig. 14A, inserted panel). We tried to detect Myocd protein in primary VSMCs using WB but failed after several attempts. In PAC1 cells, the decrease of *Myocd, Smtn, Acta2* and *Myh11* mRNA correlated with the increased *Sm22* knockdown efficiency over time after siRNA treatment (Fig. 14B). In contrast, the expression of *Sox9* mRNA gradually increased (Fig. 14B), although the mRNA levels of *Col2a1* and *Acan* were not upregulated in the VSMC culture conditions (data not shown). Accordingly, WB revealed decreased expression of Myocd and Acta2 and increased expression of Sox9 in PAC1 three days after *Sm22* siRNA treatment (Fig. 14B, inserted panel). These data suggest a switch from myogenesis to chondrogenesis in VSMCs after *Sm22* disruption: this led us to ask how disruption of an actin cytoskeletal protein alters VSMC fate.

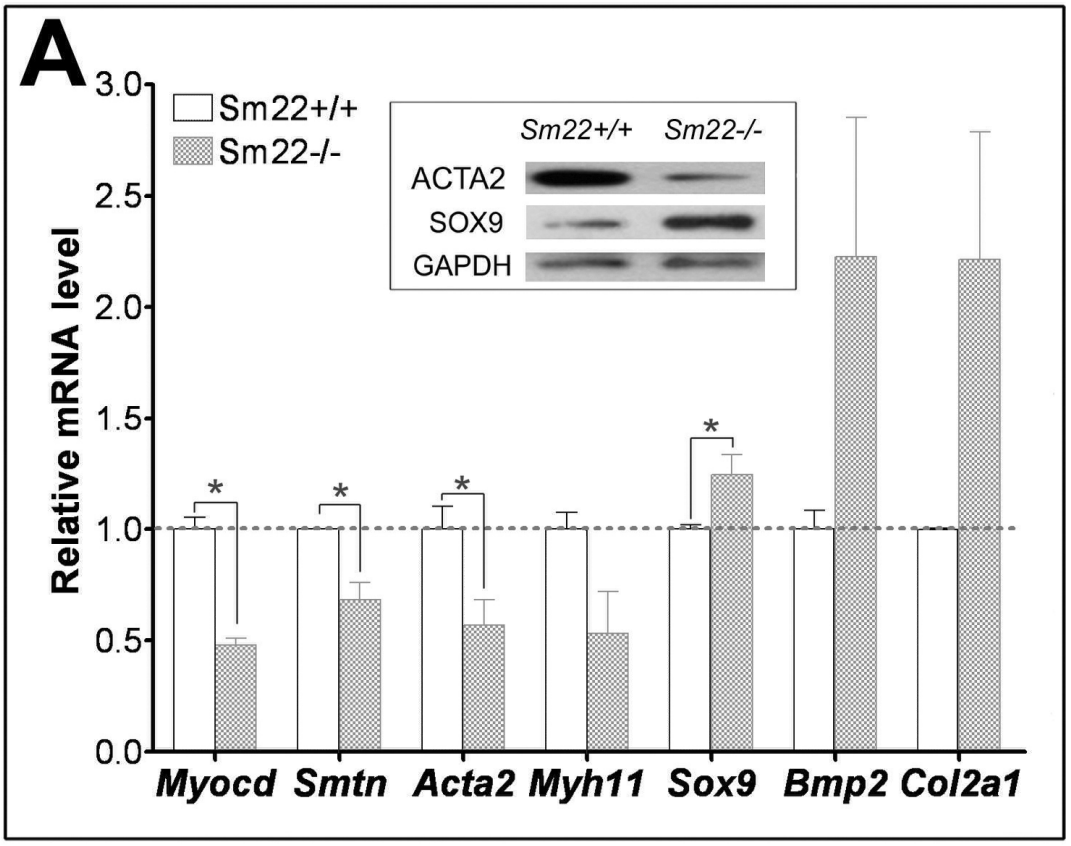

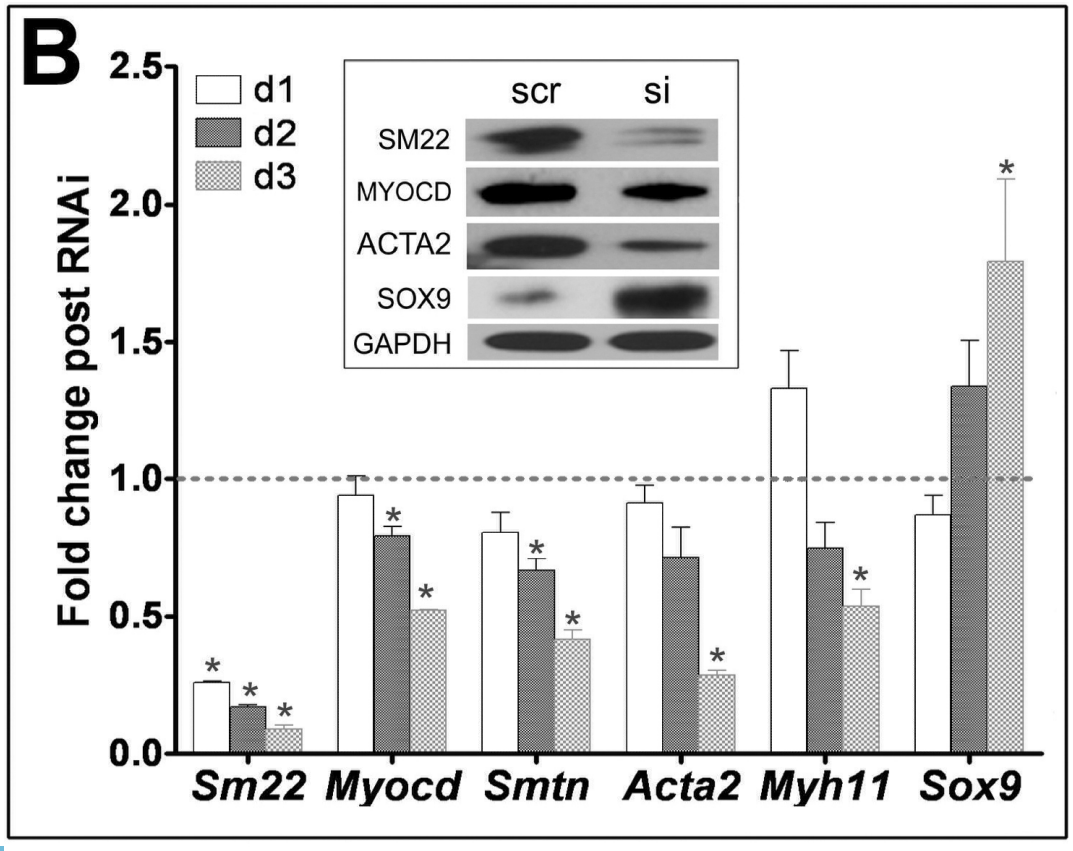

Figure 14. Chondrogenic switch of VSMCs in primary *Sm22*$^{-/-}$ VSMCs and in PAC1 cells after *Sm22* knockdown. (**A**) In primary *Sm22*$^{-/-}$ and *Sm22*$^{+/+}$ VSMCs, relative mRNA expression of *Myocd*, *Smtn*, *Acta2*, *Myh11*, *Sox9*, *Bmp2* and *Col2a1* was examined using rtRT-PCR and WB (inserted panel). Values are means ± SE from primary VSMCs of four pairs of mice. (**B**) In PAC1 cells, *Sm22* knockdown efficiency and the expression of *Myocd*, *Smtn*, *Acta2*, *Myh11* and *Sox9* were determined by rtRT-PCR 1 day, 2 days and 3 days after transfection, and by WB (inserted panel) 3 days after transfection. Values are means ± SE from three independent experiments. The asterisk, *, indicates $p < 0.05$. Abbreviations: scr, scrambled siRNA; si, *Sm22* siRNA; d1/2/3, 1/2/3 days after transfection into PAC1 cells.

3.3 Altered morphology in primary *Sm22*$^{-/-}$ VSMCs and in PAC1 cells after *Sm22* knockdown

Disruption of actin cytoskeleton and increased actin dynamics in mesenchymal cells are known to lead to chondrogenesis [73]. Since SM22 is an actin binding protein, we propose that disruption of *Sm22* might affect actin cytoskeleton and actin dynamic. After passage 2, the primary *Sm22*$^{-/-}$ VSMCs displayed remarkable morphological changes, in which they lost their spindle-shaped appearance and became spherical (Fig. 5A). We observed a similar morphological change after *Sm22* knockdown in PAC1 cells (Fig. 5B). We then used IF to visualize the actin cytoskeleton in PAC1 cells. Abundant actin stress fibers co-localized with Sm22 in control PAC1 cells (Fig. 5C, upper panel). However, there was scant actin stress fiber formation after *Sm22* knockdown (Fig. 5C, lower panel). We further evaluated actin dynamics by G/F-actin ratio and found significant increase (ca. 3-fold) of G/F-actin ratio after *Sm22* knockdown (Fig. 5D). These alterations in cell morphology and actin dynamics could be indications of chondrogenic shift of VSMCs.

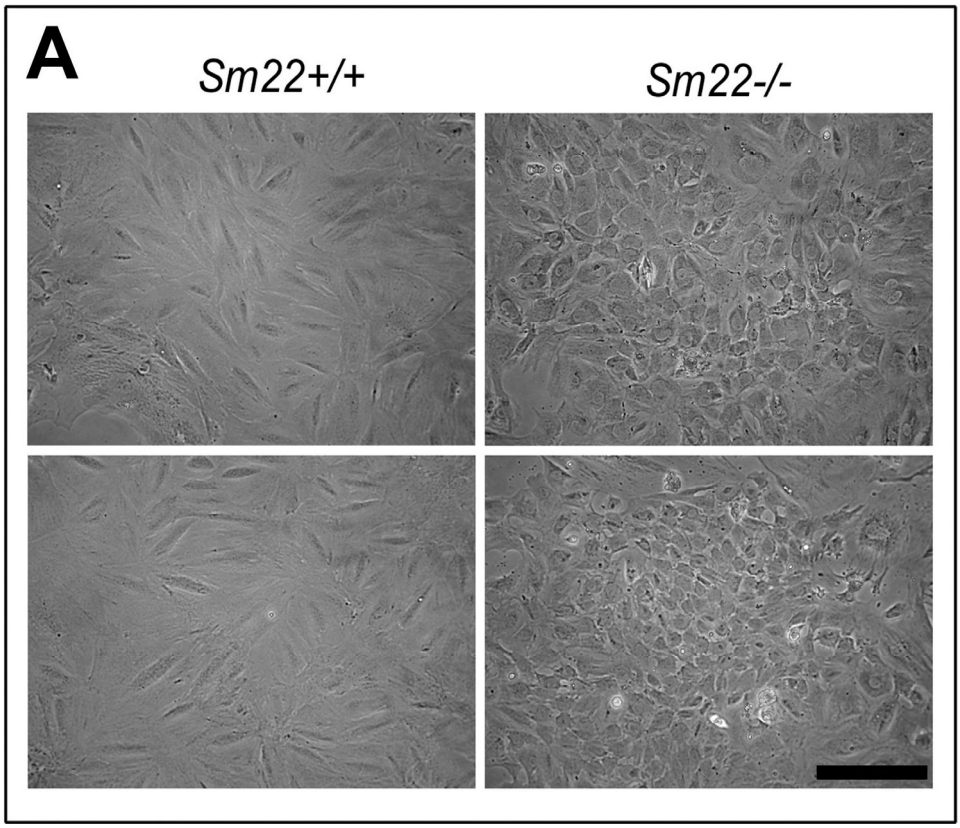

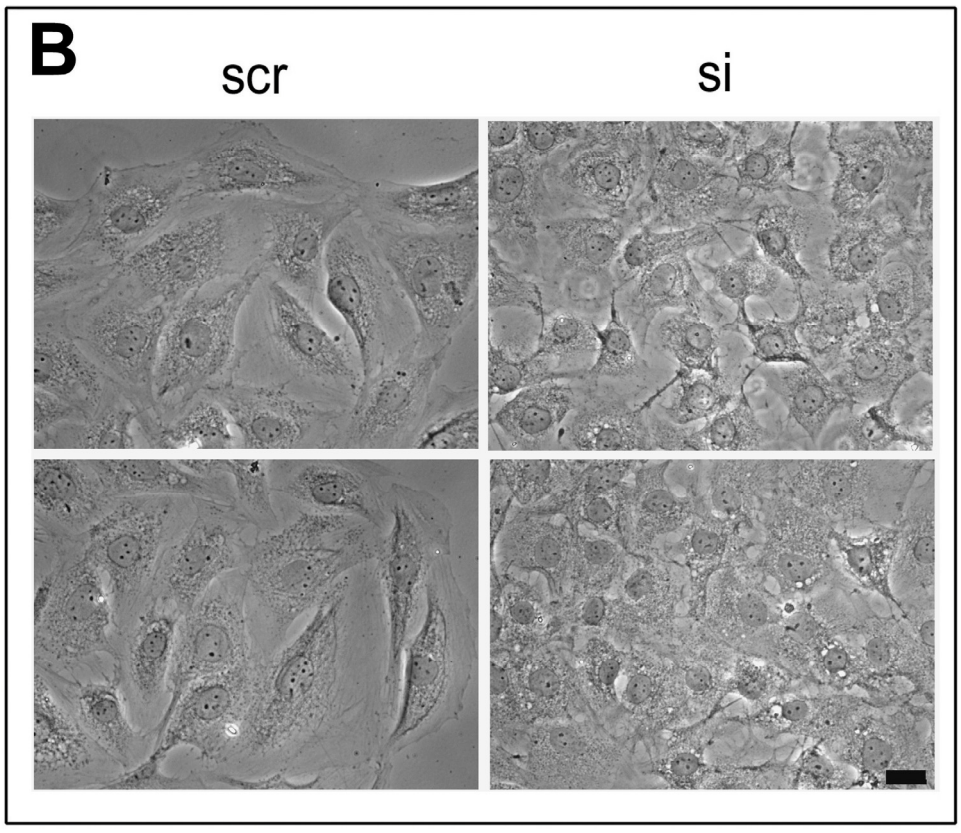

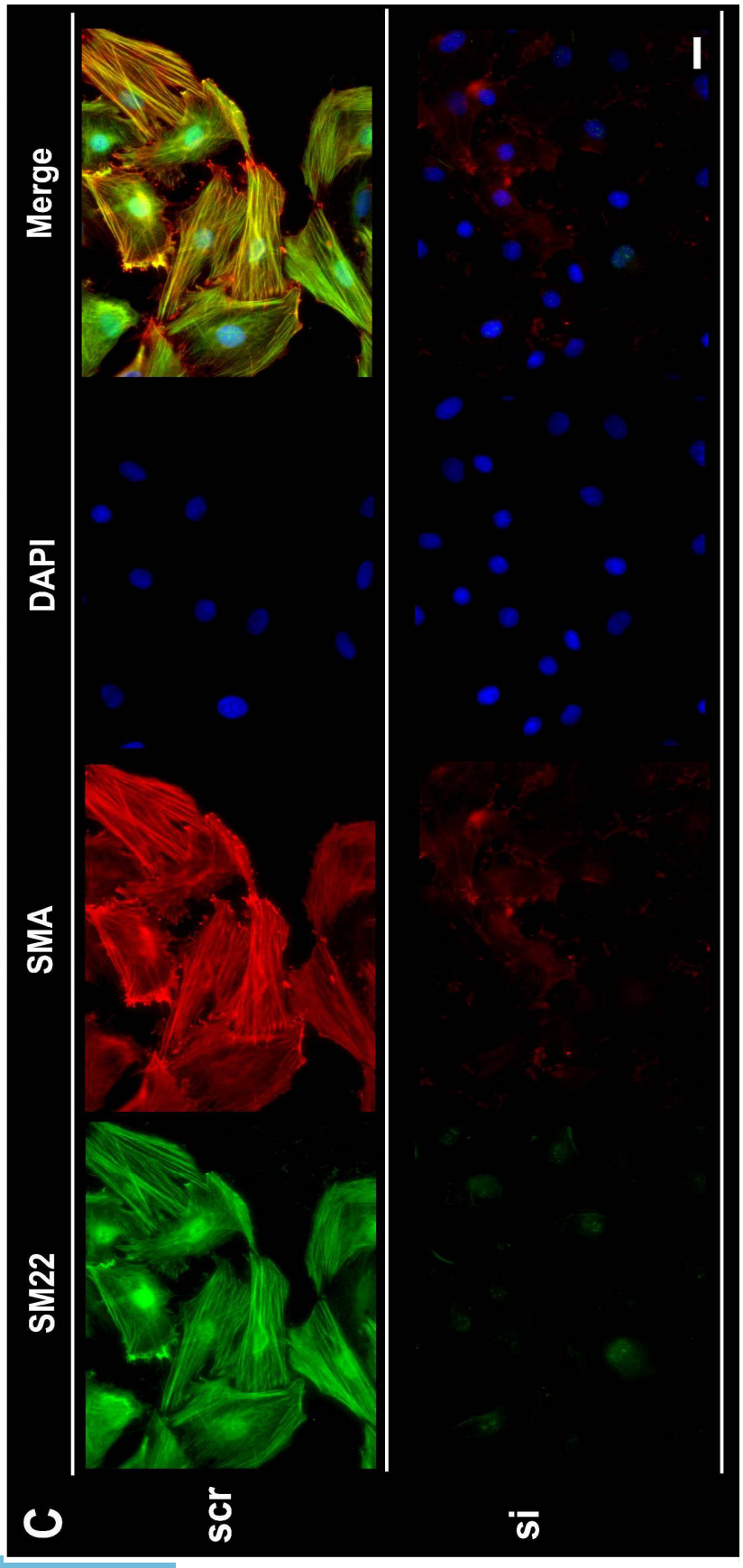

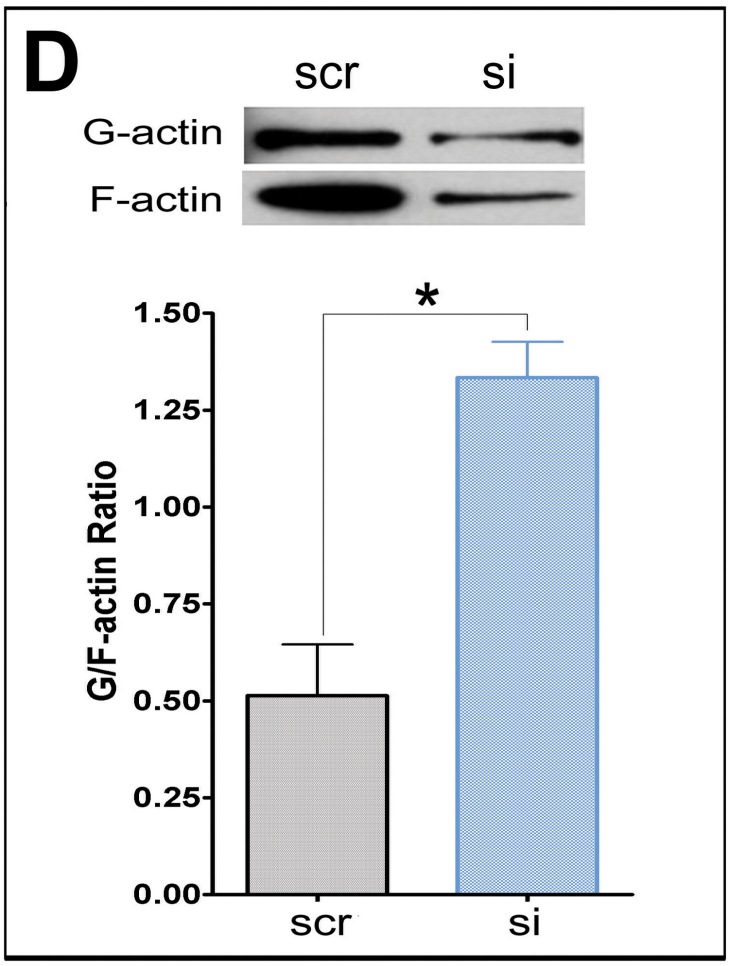

Figure 15. Altered morphology in primary *Sm22*$^{-/-}$ VSMCs and in PAC1 cells after *Sm22* knockdown. (**A**) Two views of phase contrast images from primary *Sm22*$^{-/-}$ and *Sm22*$^{+/+}$ VSMCs at passage 4. Bar, 50 µm. (**B**) The phase contrast images from PAC1 cells in the absence or presence of *Sm22* siRNA. Bar, 20 µm. (**C**) Expression of Sm22 and Sma was investigated using IF. Bars, 20 µm. (**D**) Actin dynamics was determined by G/F-actin ratio in PAC1 cells without or with *Sm22* siRNA. Values are means ± SE from three independent experiments. The asterisk, *, indicates $p < 0.05$.

4. Discussion

The results presented above show that disruption of *Sm22* in VSMC promoted conversion of medial VSMC into chondrogenic cells in response to artery injury. This notion is further supported by *in vitro* experiments using primary VSMCs from *Sm22*$^{-/-}$ mice and PAC1 after *Sm22* knockdown.

4.1. Arterial chondrogenesis and limitations of current *in vivo* model

Although arterial chondrogenesis occurs in the diseased vessel wall, it may share certain common cellular and molecular events and signaling pathways with chondrogenesis during normal development [7, 8, 71]. First, a variety of ECM proteins are expressed distinctly in different stages of chondrogenesis. Proliferation and differentiation of chondroprogenitors are maintained by the ECM structure composed of type II collagen, a hallmark of chondrogenesis, and aggrecan, a major chondrogenic proteoglycan [71]. Chondrocyte terminal differentiation hypotrophy and calcification correlate with the expression of such ECM proteins as osteopontin and osteocalcin [52, 68, 70, 71]. In the media of injured carotid arteries of *Sm22*$^{-/-}$ mice, we observed high expression of ECM proteins including type II collagen, aggrecan and osteopontin. This suggests the existence of a pro-chondrogenic ECM environment in the injured carotid arteries of *Sm22*$^{-/-}$ mice. Second, BMP2 is a cytokine with multifaceted functions required for almost every stage of chondrogenesis [71]: we did find that Bmp2 is highly induced in the media of injured carotid arteries of *Sm22*$^{-/-}$ mice. Finally, the key transcriptional regulator of chondrogenesis, Sox9 [71, 72], is also highly expressed, reflecting the activation of pro-chondrogenic transcription in the media of the injured *Sm22*$^{-/-}$carotid arteries.

Our *in vivo* results suggest that downregulation of *Sm22* may expedite arterial chondrogenesis. This may, at least in part, explain why downregulation of VSMC markers including SM22 is found in arterial calcification [8, 34, 52, 68]. Nevertheless, it is still unclear whether this pro-chondrogenic property of the injured arteries in *Sm22*$^{-/-}$ mice derives from the VSMCs or from other types of cells in the artery wall. Besides, we only observed marginal neointima formation in injured carotid arteries: this might be due to the C57BL6 mice having mixed genetic background that may be resistant to injury-induced neointima formation [66]. It is also noteworthy that we did not gain evidence of arterial calcification. There are at least two possibilities: either that the terminal stage of endochondral calcification requires an extended process beyond the 2-week period in current injury model, or that arterial chondrogenesis could exist as an independent state free of calcification. To answer this question, prolonged post-injury time in the carotid artery denudation model or other injury models such as carotid ligation could be used in further studies.

4.2. Chondrogenic phenotypic modulation of VSMC and limitations of the *in vitro* model

VSMCs are highly plastic and undergo multifaceted phenotypic changes during the pathogenesis of arterial diseases. Under physiological condition, VSMCs express an array of VSMC contractile and cytoskeleton proteins. In response to injury, VSMCs lose their contractile phenotype, increase actin dynamics and acquire the phenotypes of other cell types including chondrocytic cells [3, 17, 52, 69]. The cell fate is determined by the interplay of key transcription factors and signaling pathways, which downregulates VSMC markers and upregulates markers of other lineages.

It is known that VSMCs derive from mesenchymal cells and that disruption of actin cytoskeleton with increased actin dynamics in mesenchymal cells leads to chondrogenesis [73]. Therefore, disrupted actin stress fibers and loss of VSMC morphology may be indicative of chondrogenic conversion. We observed similar morphologic alteration from the spindle-shaped appearance typical of differentiated VSMCs to the spherical appearance of chondrocytes in primary *Sm22*$^{-/-}$ VSMCs and PAC1 cells after *Sm22* knockdown. Furthermore, knockdown of *Sm22* resulted in compromised actin stress fiber formation and increased actin dynamics: this agrees with the findings in a VSMC primary culture system treated with antisense *Sm22* [74].

Structural changes in cells are often associated with transcriptional reprogramming, and morphologic changes in early endochondral bone formation correlate with the activation of chondrogenic transcription [71, 75]. Among others, SOX9 is one key transcription factor that controls the expression of chondrogenic ECM proteins including type II collagen and aggrecan [71, 72]. On the other hand, myocardin is a master transcription factor of VSMCs since it is necessary and sufficient to transactivate SMC markers including SMA and SM22 [76, 77]. In our *in vitro* investigation, along with the cell morphologic transformation after *Sm22* knockdown, the suppressed myocardin expression and augmented expression of *Sox9* was consistent with such a transcriptional shift favoring chondrogenesis over myogenesis.

PART III

Reactive Oxygen Species (ROS) Mediated NF-κB Activation After *Sm22* disruption Couples Pro-inflammatory And Chondrogenic Phenotypes Of VSMCs

1. Introduction

A body of reports linked inflammation with arterial osteochondrogenesis in a variety of arterial diseases [78], so it is interesting that we observed prominent inflammation and medial chondrogenesis simultaneously in the *Sm22*$^{-/-}$ mice. Meanwhile, results from experiments in primary *Sm22*$^{-/-}$ VSMCs and PAC1 cells support the coupling of both pro-inflammatory phenotype and chondrogenic phenotype of VSMCs after *Sm22* disruption. Nevertheless, it is elusive whether these two phenotypes of VSMCs share common molecular signaling pathways and transcriptional regulation network. Among other signaling pathways of inflammation, NF-κB pathway is relatively well characterized. However, NF-κB pathway is conventionally deemed as anti-chondrogenic due to the fact that Sox9, the key transcription factor during chondrogenesis, is downregulated in response to inflammatory stimuli [79-81]. This concept has been challenged by several recent studies demonstrating that NF-κB pathway participates in early chondrogenesis [82-84]. Therefore, we hypothesized that NF-κB activation may underlie the coupling of pro-inflammatory and chondrogenic phenotypes of VSMCs after *Sm22* disruption.

2. Materials and Methods

2.1. Immunohistochemical (IHC) analyses.

Six slides, in the order of one every 15 consecutive slides, from each mouse were subject to H&E staining to screen sections with most prominent inflammatory responses. IHC was performed on the properly selected consecutive frozen slides using VECTASTAIN Elite ABC Kit (Vectorlabs). Briefly, air-dried slides were fixed in methanol containing 0.3% H_2O_2 for 10 minutes and serum blocked for 20 minutes. The following incubation steps of primary antibody, secondary antibody, ABC reagent and DAB substrate were performed according to the manufacturer's protocol. The slides were counterstained with hematoxylin. The primary antibodies (1:50 dilution) were against RELA (Santa Cruz, sc-109) and NFKB2 (Abcam ab31409).

2.2. Morphometric analysis

For each antibody, both 100X and 400X images were taken using a Leica DM4000B microscope (Leica). Images of adventitia and media were separated using Photoshop 7.0 software. Semi-quantitative analyses of positive signals in adventitia and media were performed on all 100X images using color segmentation and integrative optical density function in the Image-Pro software (Media Cybernetics).

2.3. *Sm22* knockdown in PAC1 cells with siRNA.

Sm22 knockdown was achieved using Dicer-Substrate siRNA duplexes (IDT, MMC.RNAI.N011526.5.1, siA). PAC1 cells [39] (a pulmonary arterial SMC cell line) were seeded at 30% confluency 24 hours before transfection. Transfection was performed using DharmaFECT3 (Dharmacon) with siRNA duplex or scrambled RNA duplex at 100 nM, and the FBS was diluted to 2% with media 24 hours after transfection for optimal cell density. In parallel

experiments, the following small molecules were added respectively 24 hours after transfection: NF-κB inhibitors, Bay-11-7082 (10 μM) and IMD-0354 (200 nM); ROS scavengers, Tiron (5 mM), Tempol (1 mM) and NAC (5 mM); NADPH oxidase and mitochondria complex I inhibitor, DPI (5 μM). Cells were used for experiments 72 hours after transfection unless otherwise specified. Two other siRNA duplexes (IDT, MMC.RNAI.N011526.5.2, designated as siC and IDT, MMC.RNAI.N011526.5.3, designated as siB) were also used independently at 200 nM concentration to rule out off-target effects of the siRNAs.

2.4. Immunofluorescence (IF).

PAC1 cells on chamber slides were fixed in methanol for 10 minutes at -20°C and blocked with 10% chicken serum for 30 minutes. Then, cells were incubated with primary antibodies at 1:100 dilution for 2 hours followed by incubation with Alexa Fluor chicken secondary antibodies at 1:200 dilution (Invitrogen) for 1 hour. Slides were mounted with Vectashield with DAPI (Vectorlabs) and examined on a Leica DM4000B microscope (Leica). Quantification was performed using Image-Pro software (Media Cybernetics). Primary antibodies were against SOD2 (Abcam, ab13533), p47phox (Santa Cruz, sc-14015), and α-tubulin (Cellsignaling, 2125S).

2.5. Preparation of cell lysate and nuclear extracts.

M-PER Mammalian Protein Extraction Reagent (Pierce) with Halt Protease Inhibitor Cocktail (Pierce) was used to prepare whole cell lysates from primary VSMCs and PAC1 cells, and NE-PER Nuclear and Cytoplasmic Extraction Reagents (Pierce) with Halt Protease Inhibitor

Cocktail (Pierce) were used to prepare the nuclear fraction and cytoplasmic fraction from primary VSMCs and PAC1 cells. Nuclear extracts were stored at -70°C.

2.6. Western blotting.

Equal amount of whole cell lysates, the nuclear fraction or cytoplasmic fraction from primary VSMCs or PAC1 cell samples were loaded on a 4-12% Bis-Tris NuPAGE Mini-gel (Invitrogen) for electrophoresis, followed by transfer onto an Immobilon-P membrane (Millipore). The membrane was blocked with 5% milk for 30 minutes, followed by primary antibody incubation overnight at 4°C. After incubation with biotinlyated secondary antibody for 30 minutes, the membrane was subject to enhanced chemiluminescence detection using SuperSignal West Pico Chemiluminescent Substrate (Pierce). The primary antibodies were against RELA (1:1000, Santa Cruz, sc-109X), NFKB2 (1:1000, Abcam ab31409), IKB (1:1000, Abcam, ab32518), SOD2 (Abcam, ab13533) and GAPDH (1:2500, Abcam, ab9485).

2.7. *In vitro* NF-κB binding activity.

Equal amount of nuclear extracts (5 μg) from PAC1 samples were incubated with an IRDye 700 labeled NF-κB probe (LI_COR) in the binding buffer for 30 minutes. The binding mixtures were loaded on a 6% DNA retarding gel (Invitrogen) for electrophoresis. The gel was then examined on an Odyssey Infrared Imaging System (LI-COR) for visualization of NF-κB bound probes.

2.8. ROS detection.

ROS in live primary VSMCs or PAC1 cells was detected using dihydroethidium (DHE, Invitrogen) for superoxide and the Image-iT™ LIVE Green ROS detection kit (Invitrogen) for peroxide. Cells on chamber slides were incubated at 37°C with 10 μM of DHE for 10 minutes or 25 μM of carboxy-H2DCFDA for 30 minutes and the fluorescent signals were examined immediately on a Leica DM4000B microscope (Leica) and the fluorescence signals were captured at 2-second exposure time for each 400X field by the Leica DFC350 digital monochrome camera. Semi-quantitative analyses were performed on 30 images (15 - 30 cells/image) of each group from the same batch of experiments using integrative optical density function in the Image-Pro software (Media Cybernetics).

2.9. Statistics.

Five *Sm22*$^{-/-}$ mice and five *Sm22*$^{+/+}$ littermates were used in histology and IHC analyses. Three independent experiments were performed to knockdown *Sm22* in PAC1 cells. Values are means ± SE. Statistical analyses were performed using SPSS13.0 software (IBM). Student t-test was applied to evaluate differences in all experiments and differences were considered significant at $p < 0.05$.

3. Results

3.1. NF-κB pathways were highly activated in injured carotid arteries of *Sm22*$^{-/-}$ mice

The activation of multiple pro-inflammatory genes in injured carotid arteries of *Sm22*$^{-/-}$ mice suggested their transcriptional co-regulation. The NF-κB pathways are key pro-inflammation pathways, and the aforementioned pro-inflammatory molecules are targets of activated NF-κB. Thus, we examined whether NF-κB activation was higher in injured carotid

arteries of *Sm22*$^{-/-}$ mice than in those of their *Sm22*$^{+/+}$ littermates. The activation of NF-κB pathways was shown by the ratio of number of RELA or NFKB2 positive nuclei to the number of all nuclei in the media from five *Sm22*$^{-/-}$ mice and *Sm22*$^{+/+}$ littermates (Fig. 16A, B, the bottom panel). As a canonical NF-κB pathway activation marker, the nuclear RELA (also known as p65) appeared to be higher (about 1.5 times) in *Sm22*$^{-/-}$ mice (Fig. 16A, bottom panel). However, the nuclear NFKB2 (also known as p52), a non-canonical NF-κB pathway activation marker, was significantly higher (more than 2 times) in *Sm22*$^{-/-}$ mice (Fig. 16B, bottom panel). Consistent with this observation, we detected more nuclear NFKB2 protein in primary *Sm22*$^{-/-}$ VSMCs (Fig. 17) by WB using nuclear extracts, while we failed to detect nuclear RELA in either *Sm22*$^{+/+}$ or *Sm22*$^{-/-}$ primary VSMCs (Fig. 17). The difference in nucleus distribution pattern between RELA and NFKB2 suggested that the non-canonical NF-κB pathway may be involved in transactivating NF-κB target genes under this condition.

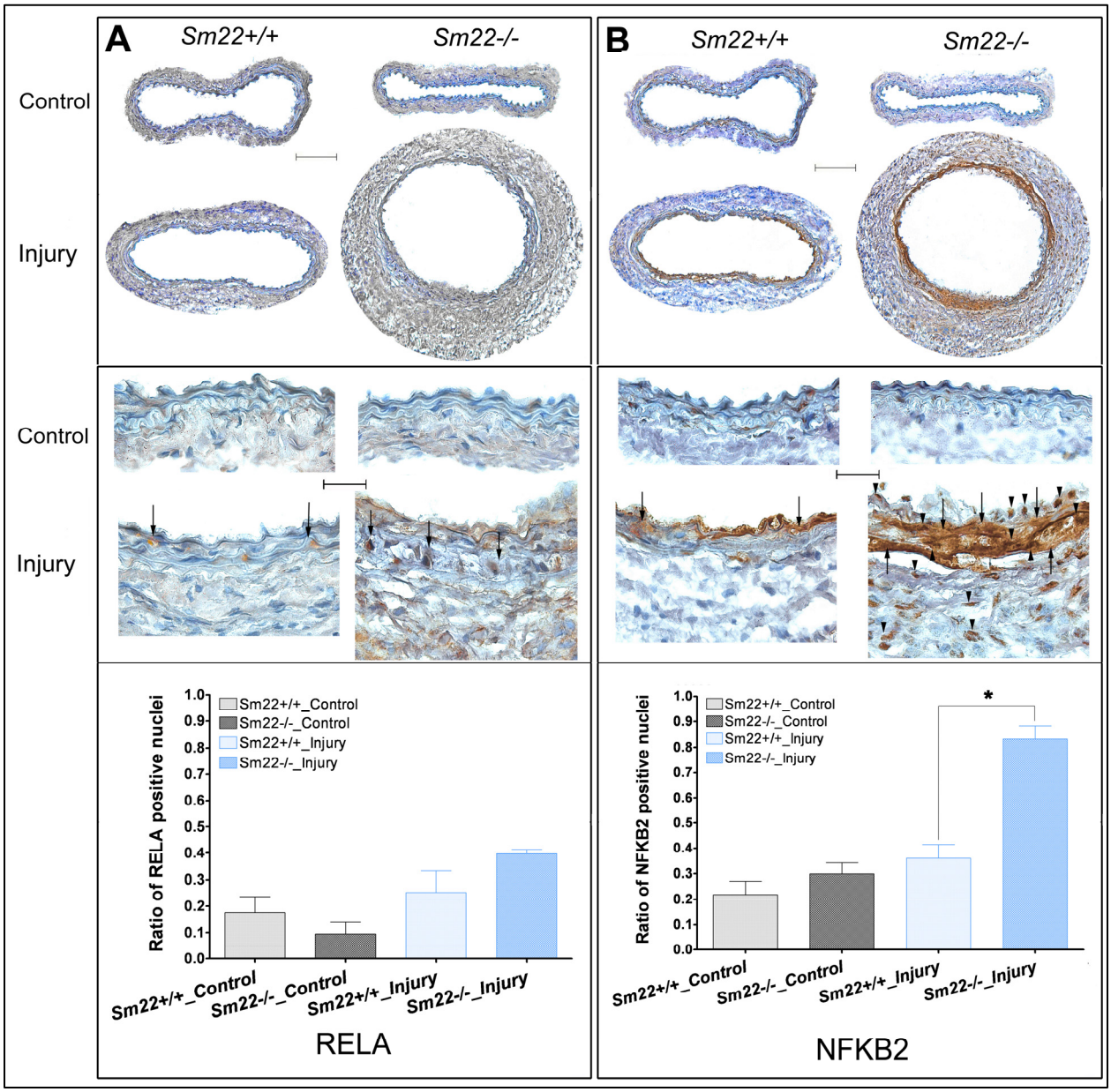

Figure 16. Activation of NF-κB pathway in *Sm22*$^{-/-}$ mice 2 weeks after carotid artery denudation. Activation of both canonical NF-κB RELA **(A),** and non-canonical NF-κB NFKB2 (**B**) was evaluated by IHC. Top panels, 100X; middle panels, 400X. In the middle panel representative positive signals (brown) are indicated by arrows, and nuclear NFKB2 is indicated by arrow heads. Bottom panels: the ratio of signal positive nuclei versus all nuclei in the same area of the media of carotid arteries from five *Sm22*$^{-/-}$ and their littermates *Sm22*$^{+/+}$ mice as quantified using Image-Pro software. Values are means ± SE. The asterisk, *, indicates $p < 0.05$. Bars: top panels, 100 μm; middle panels, 20 μm.

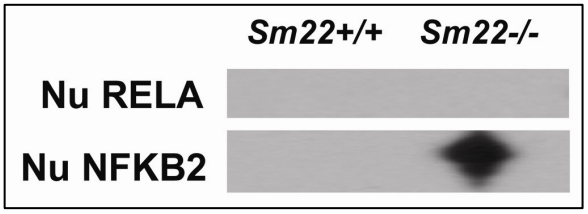

Figure 17. Nuclear expression of NF-κB subunits in primary *Sm22*$^{-/-}$ VSMCs. Nuclear lysates from *Sm22*$^{-/-}$ and *Sm22*$^{+/+}$ VSMCs were investigated using WB for RELA (upper panel) and NFKB2 expression (lower panel).

3.2. NF-κB pathways were activated after *Sm22* knockdown and contributed to upregulation of inflammatory gene expression

To test whether NF-κB was also activated after *Sm22* knockdown, we performed WB using cytoplasmic and nuclear fractions from PAC1 cells. After *Sm22* knockdown, the cytoplasmic IκB level decreased, while the nuclear RELA level increased drastically; this effect was diminished by Bay-11-7082 (a NF-κB pathway inhibitor) (Fig. 18A). Since degradation of cytoplasmic IκB and nuclear translocalization of RELA reflect activation of the canonical NF-κB pathway[85], we concluded that *Sm22* knockdown in PAC1 cells activated the canonical NF-κB pathway. *Sm22* knockdown increased NFKB2 protein level (Fig. 18B); Bay-11-7082 inhibited the processing of p100, the NFKB2 precursor, into NFKB2 and prevented NFKB2 from nuclear translocation upon *Sm22* knockdown (Fig. 18B). These findings indicated that *Sm22* disruption activated NF-κB pathways, consistent with the above *in vivo* observation. We further tested alteration of nuclear NF-κB binding activity in PAC1 cells after *Sm22* knockdown using a consensus NF-κB probe. The NF-κB binding activity was increased after *Sm22* knockdown (Fig. 18C), and Bay-11-7082 reduced this increase (Fig. 18C). We then investigated whether NF-κB activation participates in the induction of the aforementioned pro-inflammatory genes. As shown in Fig. 6, NF-κB inhibitor Bay-11-7082 significantly reduced the transcriptional increase of these

five genes (Fig. 19) and of Vcam1 protein in PAC1 cells after *Sm22* knockdown (Fig. 19 inset). A similar effect was also observed using another NF-κB pathway (IKKbeta) inhibitor, IMD-0354 (Fig. 20).

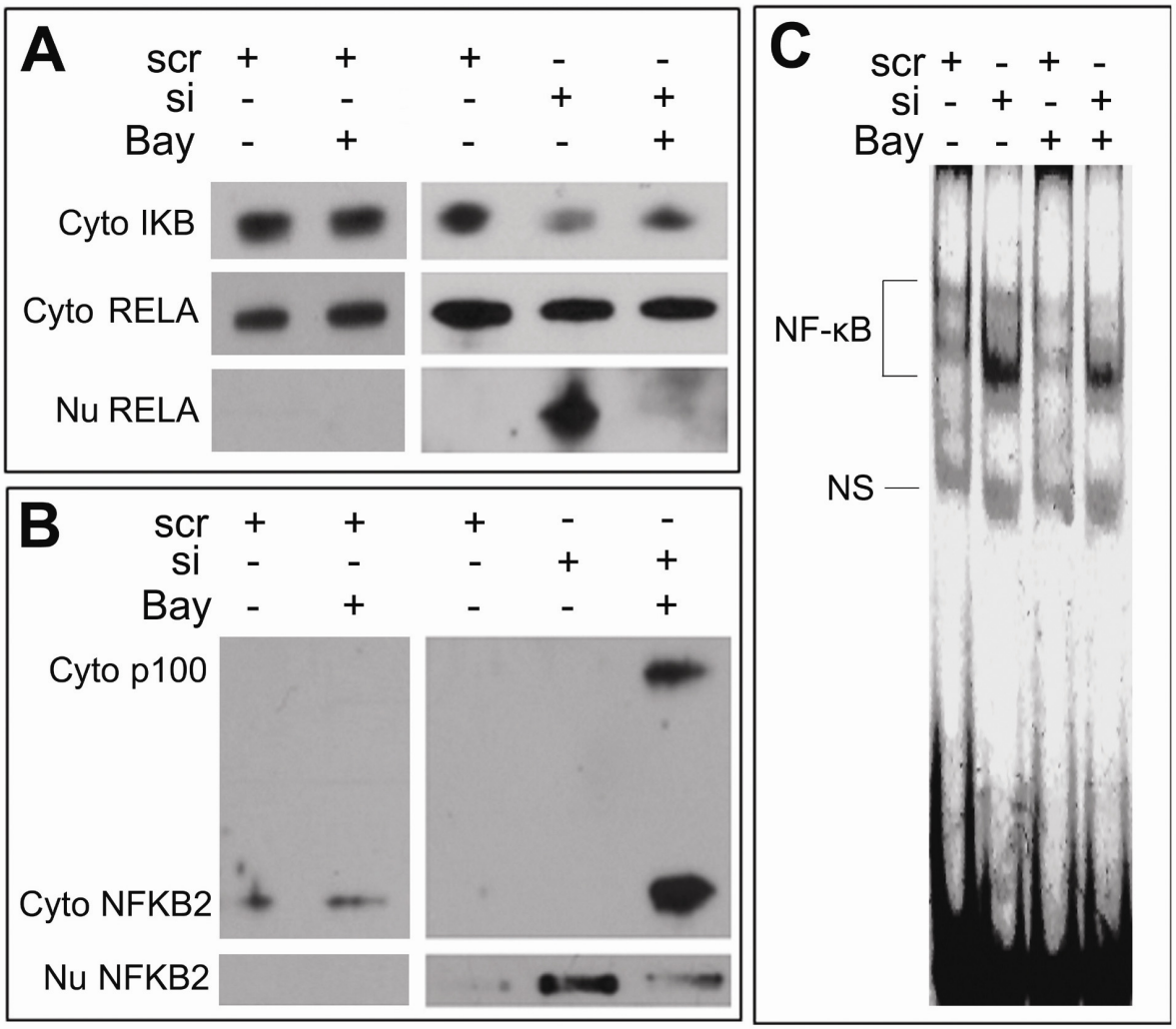

Figure 18. *Sm22* knockdown activated NF-κB pathways. Cytoplasmic and nuclear lysates were isolated from PAC1 cells transfected with scrambled RNA (scr) or *Sm22* siRNA (si). Activation of both canonical NF-κB pathway (**A**) and non-canonical NF-κB pathway (**B**) was investigated by WB using antibodies against RELA, IKB and NFKB2 as indicated. P100 is the precursor of NFKB2. NF-κB binding activitiy of nuclear extracts was investigated using a NF-κB consensus binding site as the probe **(C),** showing increased NF-κB binding activities after *Sm22* knockdown. Data are from three independent experiments. scr, scrambled siRNA; si, *Sm22* siRNA, NS: nonspecific.

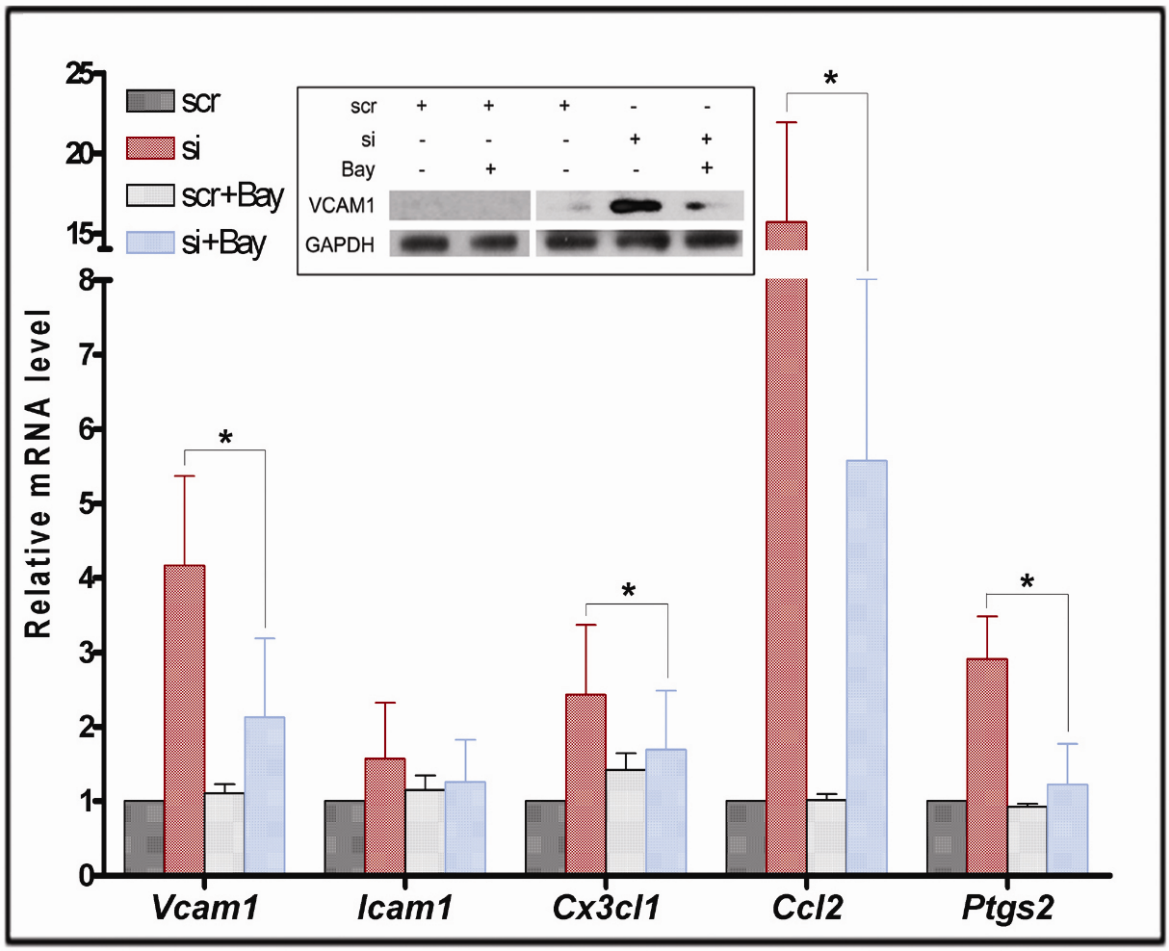

Figure 19. NF-κB inhibitor Bay-11-7082 blocked induction of pro-inflammatory genes after *Sm22* knockdown. PAC1 cells transfected with scrambled RNA (scr) or *Sm22* siRNA (si) in the absence or presence of Bay-11-7082 (Bay), an NF-κB pathway inhibitor. Effect of Bay-11-7082 on induction of inflammatory genes was investigated using rtRT-PCR and WB (inserted panel)**.** Values are means ± SE. The asterisk, *, indicates $p < 0.05$. Data are from three independent experiments.

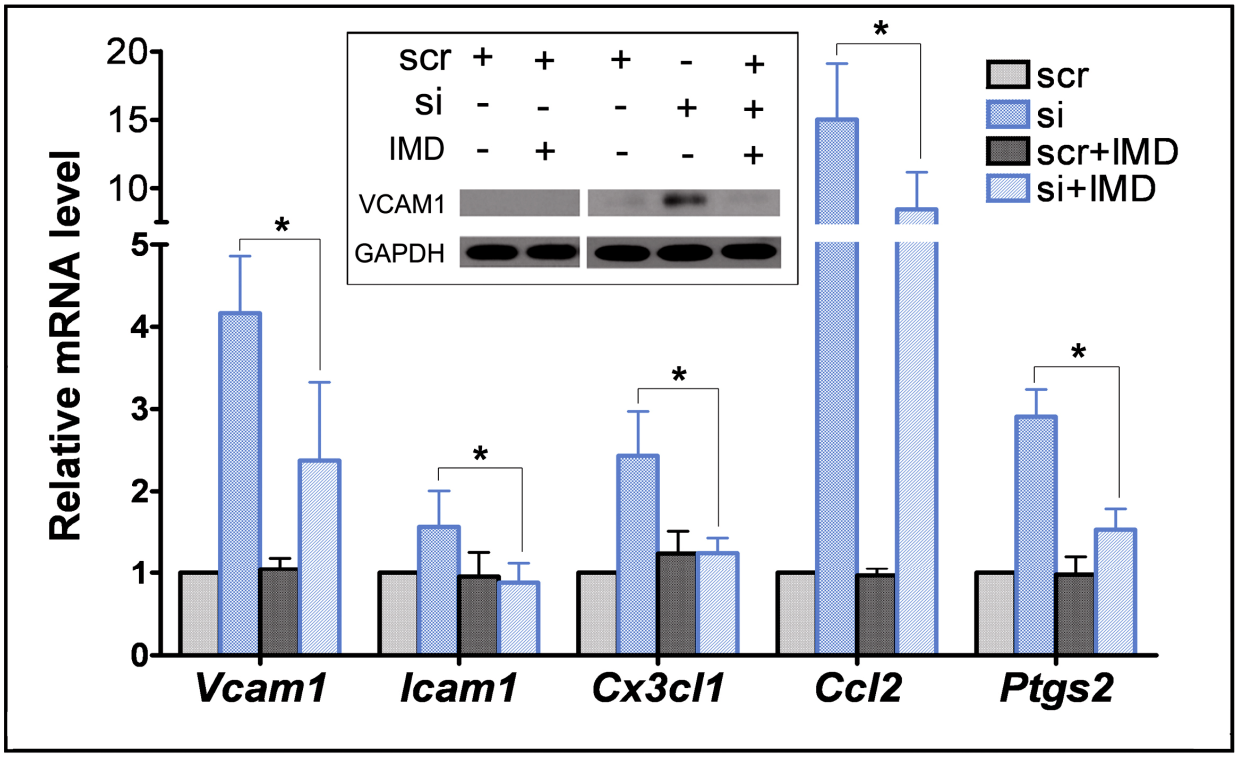

Figure 20. NF-κB inhibitor IMD-0354 blocked induction of pro-inflammatory genes after *Sm22* knockdown. PAC1 cells transfected with scrambled RNA (scr) or *Sm22* siRNA (si) in the absence or presence of IMD-0354 (IMD), an NF-κB pathway inhibitor. Effect of IMD-0354 on induction of inflammatory genes was investigated using rtRT-PCR and WB (inserted panel)**.** Values are means ± SE. The asterisk, *, indicates $p < 0.05$. Data are from three independent experiments.

3.3. NF-κB pathways activation after *Sm22* knockdown contributed to induction of Sox9

NF-κB signaling pathway was recently shown to participate in Sox9 expression and chondrogenesis [82, 84]. We showed that NF-κB pathway is activated after *Sm22* knockdown in PAC1 cells. Thus, we tested whether NF-κB activation contributed to the up-regulation of Sox9 after *Sm22* knockdown. After inhibition of the NF-κB pathway during *Sm22* knockdown in PAC1 cells using NF-κB inhibitors, Bay-11-7082 or IMD-0354, transcriptional activation of *Sox9* was significantly reduced (Fig. 21). Consistently, WB results showed that increased Sox9 protein was suppressed by Bay-11-7082 (Fig. 21, inserted panel). These results suggest that NF-κB pathway activation mediates the transcriptional activation of *Sox9* after *Sm22* knockdown.

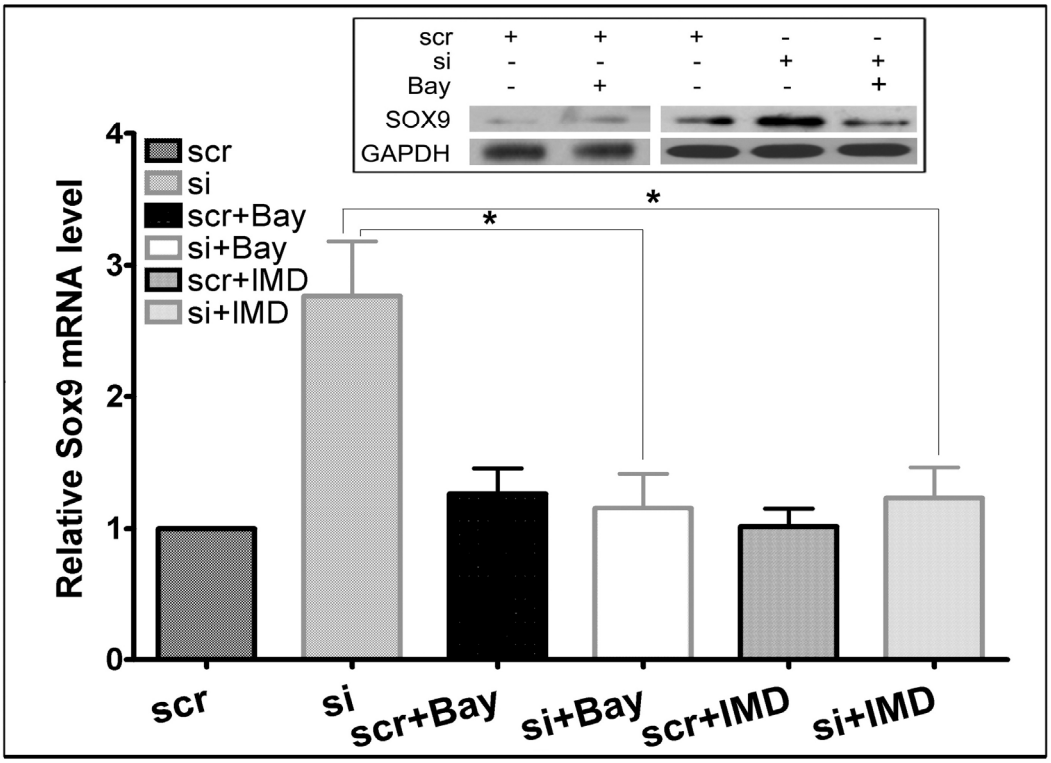

Figure 21. NF-κB inhibitors blocked induction of *Sox9* after *Sm22* knockdown. PAC1 cells transfected with scrambled RNA (scr) or *Sm22* siRNA (si) in the absence or presence of either of the two NF-κB pathway inhibitors, Bay-11-7082 (Bay) or IMD-0354 (IMD). Expression of *Sox9* was evaluated using rtRT-PCR and WB (inserted panel). Values are means ± SE from three independent experiments. The asterisk, *, indicates $p < 0.05$.

These data demonstrate that NF-κB pathway was activated upon *Sm22* disruption in PAC1 cells and promoted the transactivation of both pro-inflammatory genes and the key chondrogenic transcription factor Sox9. However, the issue of how NF-κB activation occurs after disruption of an actin cytoskeleton protein remains to be addressed. NF-κB is a redox-sensitive transcription factor [86], and expression of Sox9 can be activated by ROS dependent transcription factors during developmental chondrogenesis [75]. Thus we hypothesized that NF-κB activation after *Sm22* knockdown might be initiated by ROS increase after *Sm22* knockdown in PAC1 cells.

3.4. Boosted ROS production after *Sm22* knockdown in PAC1 cells contributed to NF-κB activation and induction of pro-inflammatory genes

We investigated ROS production based on fluorescence microscopy using DHE for superoxide and DCFDA for peroxide. Levels of both superoxide (Fig. 22A, E) and peroxide (Fig. 22B, E) were about 30% higher in *Sm22*$^{-/-}$ primary VSMCs, and 50% higher after *Sm22* knockdown in PAC1 cells (Fig. 22C, D, F). To test whether the boosted ROS level contributed to NF-κB activation after *Sm22* knockdown, we used Tiron (a ROS scavenger) or Tempol (a superoxide scavenger), to neutralize the ROS (Fig. 22C, D, F). Tiron decreased the expression of both nuclear RELA (Fig. 23A) and nuclear NFKB2 (Fig. 23B), indicating inhibition of NF-κB pathways. These data indicate that ROS might act upstream of the NF-κB activation. Interestingly, it appears that superoxide rather than peroxide mediated most of these effects since Tempol lowered superoxide without significantly decreasing the elevated peroxide level and Tiron also reduced the production of superoxide more than that of peroxide (Fig. 22F).

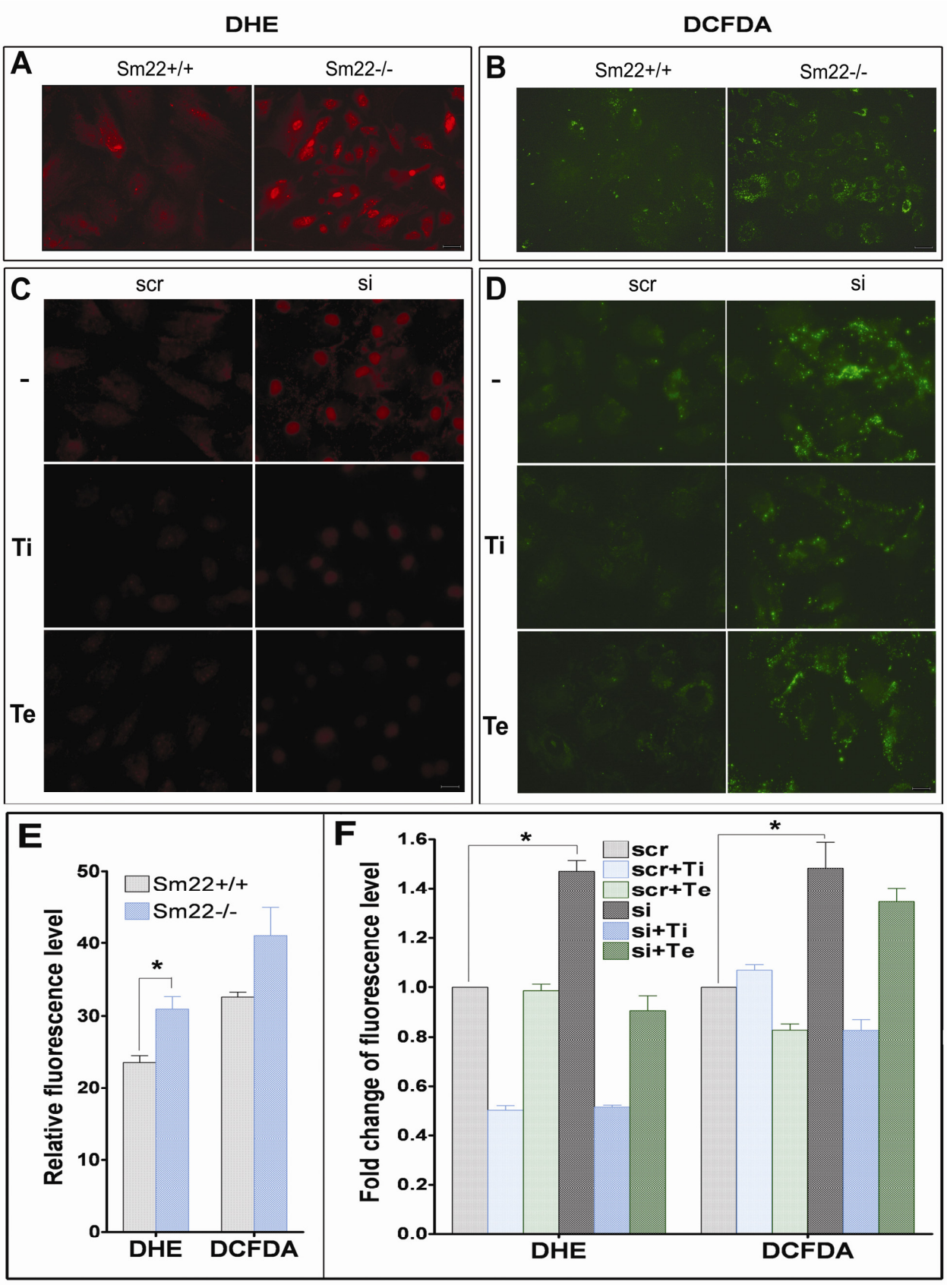

Figure 22. Elevated ROS production after *Sm22* disruption.
(A-B) Primary VSMCs were subjected to fluorescence microscopy after DHE staining for superoxide detection (A) or DCFDA for peroxide (B). **(C-D)** PAC1 cells with *Sm22* siRNA transfection were also subjected to fluorescence microscopy after DHE (C) or DCFDA (D) staining with or without Tiron or Tempol. **(E)** Quantification of images in (A) and (B). **(F)** Quantification of images in (C) and (D). Abbreviations: scr, scrambled RNA; si, *Sm22* siRNA; Ti, Tiron; Te, Tempol. Data were from three independent experiments.

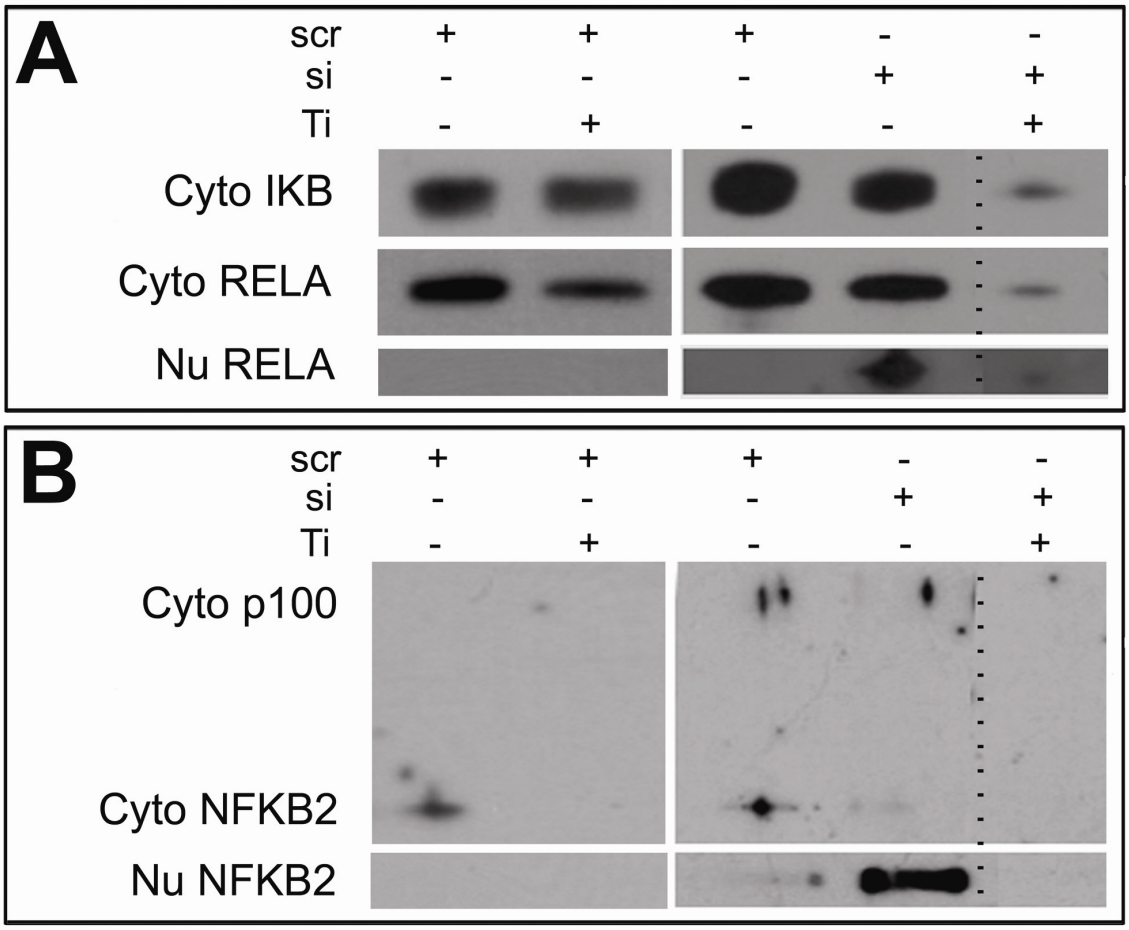

Figure 23. Elevated ROS production after *Sm22* disruption contributed to NF-κB activation. In PAC1 cells, activation of both canonical NF-κB pathway **(A)** and non-canonical NF-κB pathway **(B)** was investigated respectively by WB using antibodies against RELA, IKB and NFKB2 as indicated. P100 is the precursor of NFKB2. Dashed line, images of non-adjacent lanes on the same gel. Abbreviations: scr, scrambled RNA; si, *Sm22* siRNA; Ti, Tiron; Te, Tempol.

3.5. Boosted ROS production after *Sm22* knockdown induced pro-inflammatory genes

To test if the elevated ROS contributes to induction of pro-inflammatory genes after *Sm22* knockdown, we neutralized ROS with Tiron (Fig. 24A) or Tempol (Fig. 24B) or N-acetyl-cysteine (NAC, a ROS scavenger) (Fig. 24C) respectively. Any of the three reagents blocked the upregulation of NF-κB inducible pro-inflammatory genes after *Sm22* knockdown.

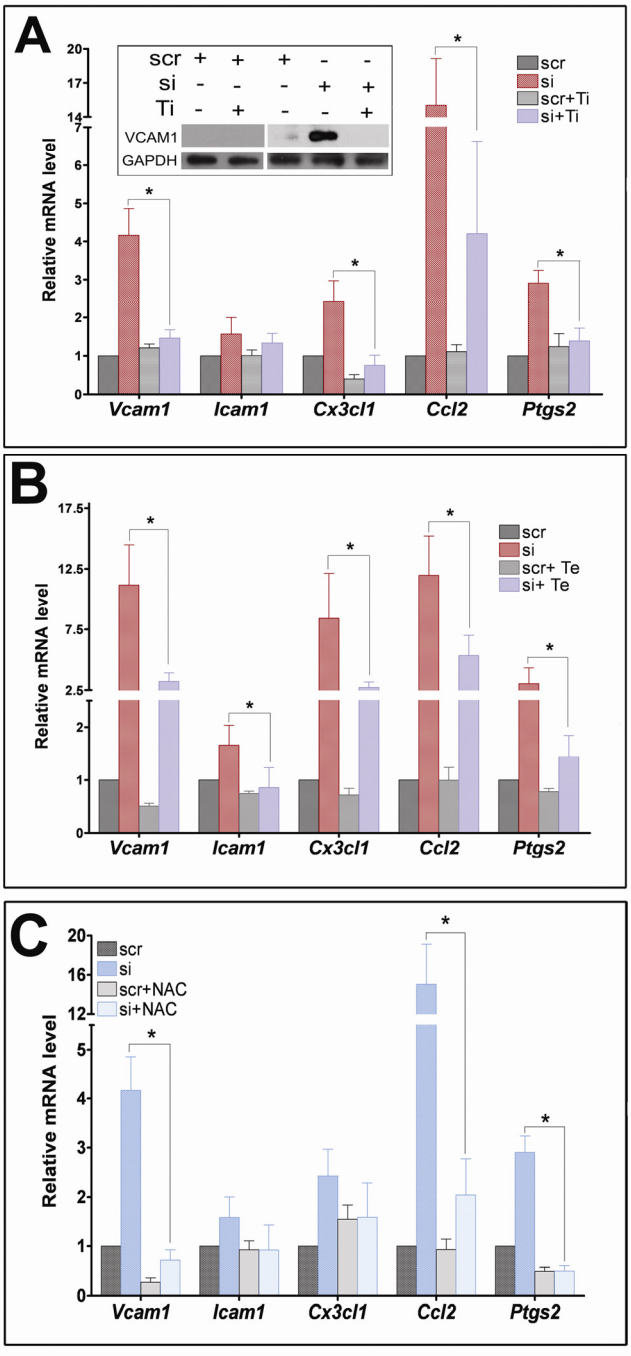

Figure 24. Elevated ROS production after *Sm22* disruption induced activation of pro-inflammatory genes. PAC1 cells transfected with scrambled RNA (scr) or *Sm22* siRNA (si) in the absence or presence of Tiron **(A)** or Tempol **(B)** or NAC **(C).** The blocking effect on pro-inflammatory gene induction after *Sm22* knockdown using rtRT-PCR and WB (inserted panel in A). Values were means ± SE. The asterisk, *, indicates $p < 0.05$. Abbreviations: scr, scrambled RNA; si, *Sm22* siRNA; Ti, Tiron; Te, Tempol. Data were from three independent experiments.

3.6. Boosted ROS production after *Sm22* knockdown induced *Sox9* expression

To inspect if the elevated ROS contributes to *Sox9* induction after *Sm22* knockdown, we abolished ROS increase using Tiron (Fig. 25, si+Ti group vs. si group). For easy comparison, we show in the figure boosted ROS production (DHE and DCFDA) after *Sm22* knockdown (Fig. 25, si group vs. scr group). After interference by Tiron upon *Sm22* knockdown, transcriptional activation of *Sox9* was significantly suppressed (Fig. 25, *Sox9* columns, si+Ti group vs. si group). Accordingly, increased expression of Sox9 protein was also suppressed by Tiron as shown by WB analyses (Fig. 25, inserted panel).

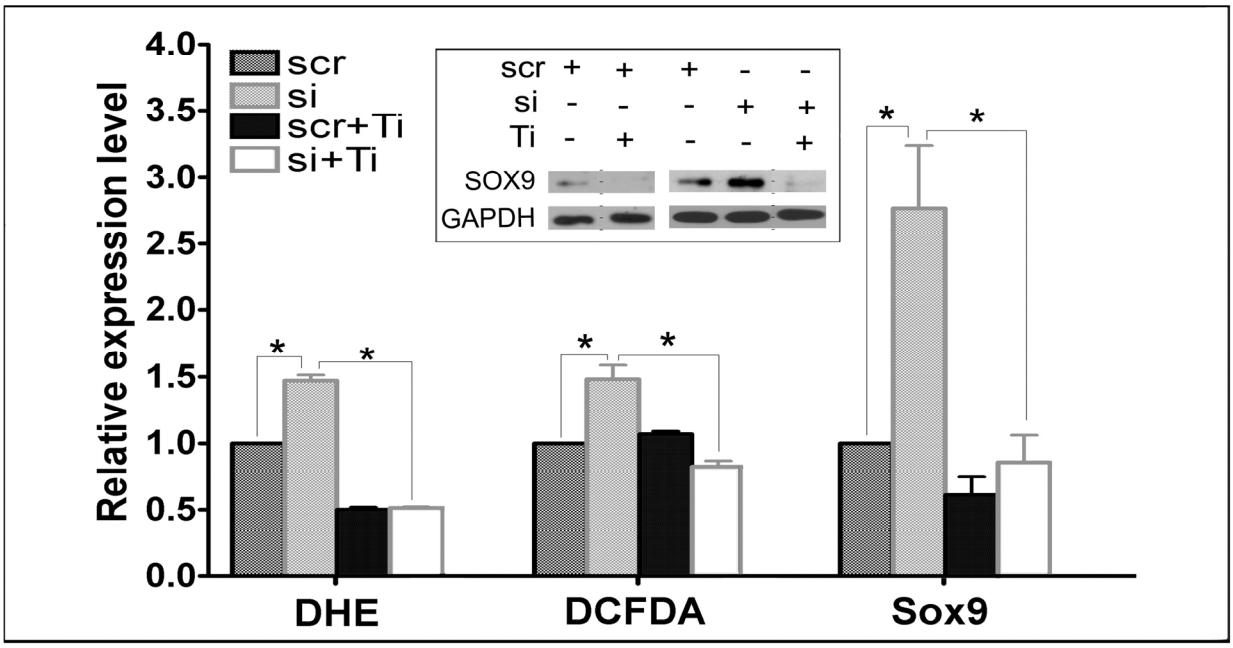

Figure 25. Elevated ROS production induced *Sox9* expression after *Sm22* knockdown. PAC1 cells transfected with scrambled RNA (scr) or *Sm22* siRNA (si) in the absence or presence of Tiron. ROS levels were evaluated by DHE and DCFDA. *Sox9* expression was investigated using rtRT-PCR (*Sox9* bars) and WB (inserted panel). Values are means ± SE from three independent experiments. The asterisk, *, indicates $p < 0.05$.

3.7. ROS produced by both mitochondria and NADPH oxidase might be facilitated by disorganized cytoskeleton in the absence of *Sm22*

In order to locate the sources of the elevated ROS after *Sm22* disruption, we scanned mRNA expression of known ROS production related genes including SOD system, NADPH oxidase system, dual oxidase, catalase and glutathione peroxidase [87]. *Sod2* mRNA in PAC1 after *Sm22* knockdown increased about 2.5 times by rtRT-PCR (Fig. 26A); the Sod2 increase was confirmed by WB (Fig. 26B) and IF (Fig. 26C). In accordance, *Sod2* mRNA induction by injury was also higher in $Sm22^{-/-}$ mice compared to their $Sm22^{+/+}$ littermates (Fig. 26A); however, this difference was not statistically significant between primary VSMCs from $Sm22^{+/+}$ and $Sm22^{-/-}$ mice (Fig. 26A). Since *Sod2* is a known NF-κB target [88], NF-κB activation may plausibly induce Sod2 expression. Indeed, the upregulation of *Sod2* after *Sm22* knockdown was repressed by Bay-11-7082 (a NF-κB pathway inhibitor) (Fig. 26B). It is known that SOD2 is a mitochondrial matrix protein and scavenges mitochondrial superoxide, the increase of *Sod2* suggested boosted mitochondrial superoxide production as a feedback. Further observation on mitochondria morphology and distribution revealed mitochondria aggregation and fusion into megamitochondria (Fig. 27) which is associated with ROS production [89].

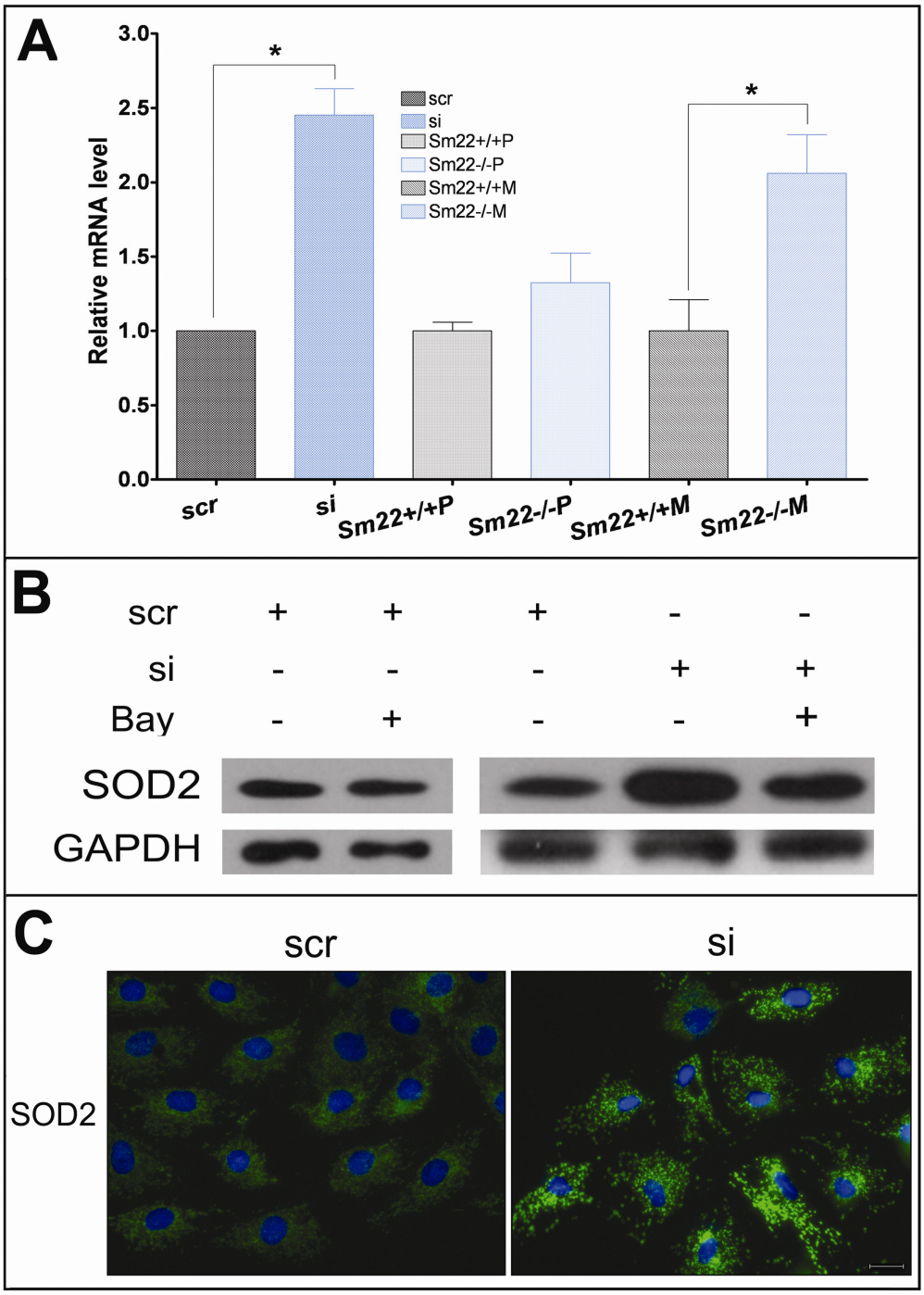

Figure 26. Induction of *Sod2* after *Sm22* disruption. (A) Expression of *Sod2* mRNA in PAC1 cells transfected with scrambled RNA (scr) or *Sm22* siRNA (si), primary VSMCs (P) and injured mouse carotid arteries (M) was investigated using rtRT-PCR. Values are means ± SE. The asterisk, *, indicates $p < 0.05$. **(B)** *Sm22* knockdown induced Sod2 protein expression, and this induction was repressed by Bay-11-7082 (Bay, a NF-κB inhibitor) as shown in WB**. (C)** Induction of Sod2 after *Sm22* knockdown was shown in IF.

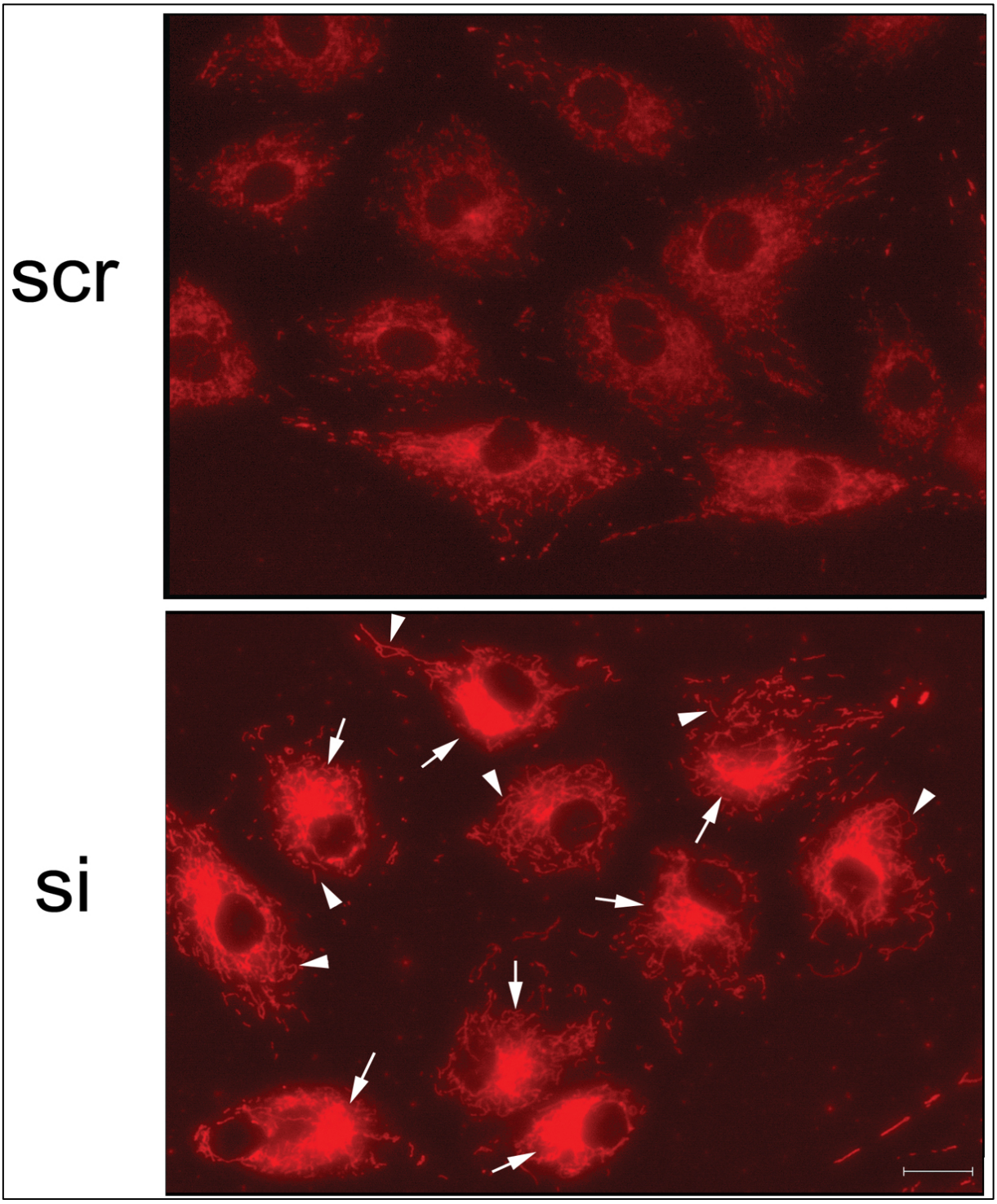

Figure 27. Altered mitochondria organization after *Sm22* disruption. Mitotracker Red was used to visualize mitochondria. Mitochondria aggregation and megamitochondria after *Sm22* knockdown in PAC1 cells are indicated by arrows and arrow heads respectively. Abbreviations: scr, scrambled RNA; si, *Sm22* siRNA.

Moreover, we observed that *Sm22* knockdown induced cell periphery translocation of p47phox (Fig. 28A), an indication of NADPH oxidase activation [90]. Diphenyleneiodonium (DPI), an inhibitor of both NADPH oxidase and mitochondrial complex I, significantly blocked the upregulation of pro-inflammatory genes and *Sox9* after *Sm22* knockdown (Fig. 28B). Therefore, mitochondria and NADPH oxidase may both contribute to the elevated ROS.

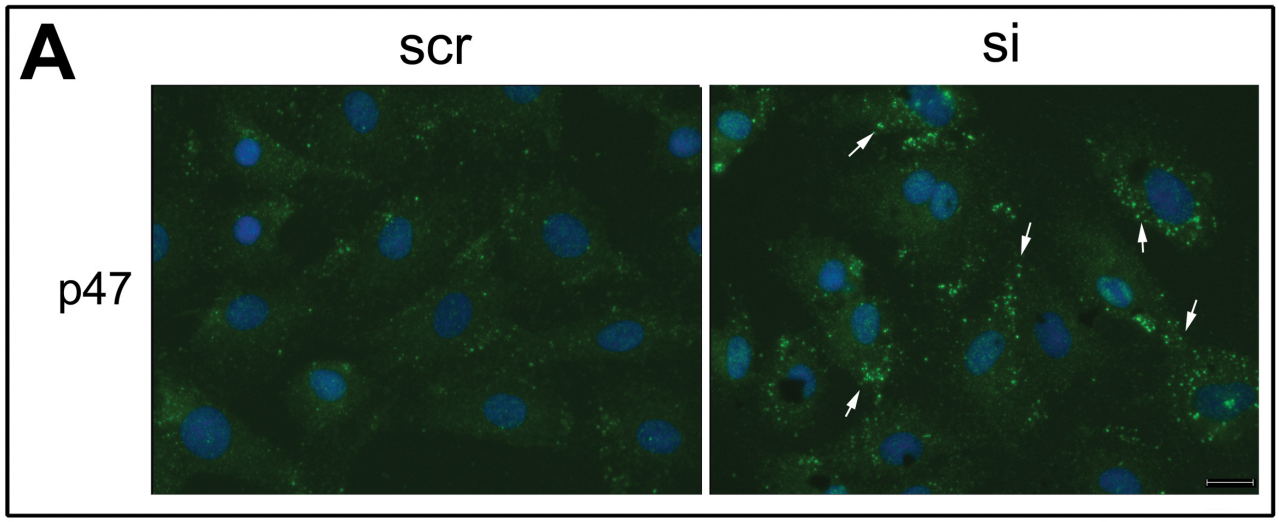

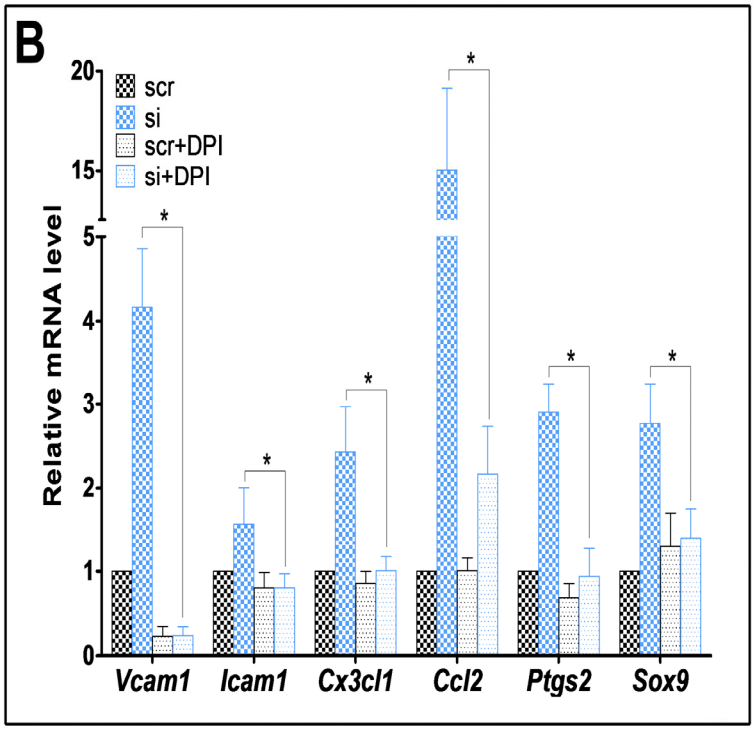

Figure 28. Activation of NADPH oxidase after *Sm22* disruption. (A) Cell peripheral assembly of p47phox after *Sm22* knockdown was investigated with a p47phox antibody and indicated by arrows. (**B**) Suppression of induction of pro-inflammatory genes and *Sox9* by DPI (an NADPH oxidase inhibitor) was evaluated using rtRT-PCR. Values are means ± SE. The asterisk,*, indicates $p < 0.05$. Abbreviations: scr, scrambled RNA; si, *Sm22* siRNA;

Since SM22 is an actin associated protein and NADPH oxidase activation might be affected by change in actin cytoskeleton organization [90], we examined the actin cytoskeleton and observed significantly less actin stress fiber in PAC1 cells after *Sm22* knockdown (Fig. 15C). Microtubules and actin cytoskeleton cooperate functionally during a variety of cellular processes and regulate mitochondria distribution[91]; therefore, we examined whether *Sm22* disruption affect the microtubule cytoskeleton. We found that microtubules were unevenly distributed in the *Sm22* knockdown cells and displayed local aggregation (Fig. 29). These results suggest that cytoskeleton remodeling induced by disruption of *Sm22* in VSMCs might activate multiple ROS production machineries.

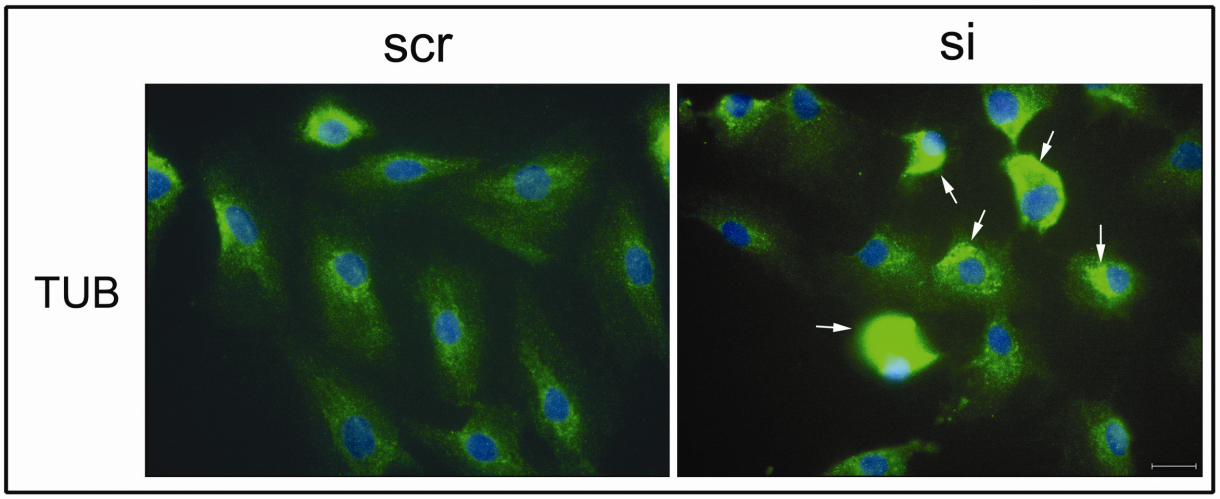

Figure 29. Altered microtubule organization after *Sm22* disruption. Microtubule structure was investigated using IF with a tubulin antibody (TUB), and the aggregation of tubulin after *Sm22* knockdown in PAC1 cells is indicated by arrows. Abbreviations: scr, scrambled RNA; si, *Sm22* siRNA.

4. Discussion

4.1. ROS mediated NF-κB activation as a shared molecular switch between inflammation and chondrogenesis after *Sm22* disruption

NF-κB was initially identified in leukocytes. Activation of NF-κB pathways is well documented during arterial inflammation and just recently discovered during chondrogenesis [82-84]. All aforementioned pro-inflammatory genes [42-44] and *Sox9* [84] are direct targets of NF-κB. NF-κB pathways can be classified into canonical, non-canonical and atypical based on the different NF-κB dimers formed during activation [85]. Most studies thus far have focused on the activation of the canonical pathway. Surprisingly, the striking nuclear localization of NFKB2 rather than RELA in injured *Sm22*$^{-/-}$ carotid arteries and primary *Sm22*$^{-/-}$ VSMCs indicated that non-canonical NF-κB pathways activation is predominant in our situation. However, this does not seem to fully agree with the fact that both canonical and non-canonical NF-κB pathways were activated in PAC1 cells after *Sm22* knockdown. There are several possible explanations for this discrepancy. One is that the injured carotid arteries were examined 2 weeks after injury, that is, outside the time window of acute inflammation, when the RELA-associated canonical pathway is activated in response to arterial injury [58, 92]. However, this cannot explain why the canonical pathway was activated in the *Sm22* knockdown PAC1 cells, but not in the *Sm22*$^{-/-}$ primary VSMCs under the same culture condition. This discrepancy may be due to different differentiation states of primary VSMCs compared to the PAC1 VSMC cell line and response variations among different systems. PAC1 cells after *Sm22* knockdown may more closely resemble an acute inflammation model, since our experiments were performed three days after transfection. In view of this, it would not surprise us to observe activation of NFKB2, the non-canonic pathway, in the acute phase of carotid injury. This possibility could be examined in

future studies. Although it is possible that some of the NF-κB signals in injured arteries were from the infiltrated inflammatory cells, the *in vitro* NF-κB activation in VSMCs after *Sm22* disruption lends support to the possibility of *in vivo* NF-κB activation in VSMCs after carotid injury.

NF-κB is a redox-sensitive transcription factor [86, 93], and ROS is one key source for NF-κB activation in VSMCs in arterial diseases [42, 44, 93]. On the other hand, increased ROS production under hypoxia [94] during osteochondral organogenesis activates ROS sensitive transcription machinery including HIF1A and contributes to transactivation of *Sox9* [75, 95]. Although ROS production is associated with the hypoxia during embryogenic chondrogenesis, ROS is also generated under numerous non-hypoxic conditions [95, 96] and the hypoxia-independent ROS in stressed VSMCs [87, 97, 98] may contribute to arterial calcification. Taken together, it is reasonable to propose that ROS might stand upstream of NF-κB activation after *Sm22* knockdown in PAC1 cells and participate in the up-regulation of pro-inflammatory genes and *Sox9*. As expected, increased ROS level was disclosed in primary *Sm22*$^{-/-}$ VSMCs and in PAC1 after *Sm22* knockdown indicating high oxidative stress in VSMCs with *Sm22* disruption. Different ROS scavengers, Tiron, Tempol or NAC consistently blocked NF-κB activation and pro-inflammatory genes induction. This provides further evidence indicating that increased production of ROS may initiate NF-κB activation in PAC1 cells after *Sm22* disruption. We tried to identify increased ROS production in injured carotid arteries *in vivo* using both DHE and DCFDA on frozen sections. Disappointingly, high background from elastin and collagen thwarted further analysis. Although DHE and DCFDA-based assays have been used to detect ROS from live cells, ROS may not be preserved in our frozen sections. Nevertheless, we

observed higher expression of *Sod2* in the injured *Sm22*$^{-/-}$ carotid arteries. Activated NF-κB perhaps induces *Sod2* expression in anticipation of redox signaling. Therefore, increased expression of *Sod2* may reflect a higher redox state in the injured carotid arteries of *Sm22*$^{-/-}$ mice.

4.2. Sources of ROS production and association with cytoskeleton alteration

Mitochondria and NADPH oxidase are two important sources of ROS in VSMCs [99, 100]. The megamitochondria formation and mitochondria aggregation after *Sm22* knockdown indicated mitochondria dysfunction associated with mitochondrial ROS production [89]; the upregulated *Sod2* may reflect such a dysfunction and serve as a rescuing mechanism via the ROS-NF-κB feedback (Fig. 30). NADPH oxidase, a major ROS source from VSMC membranes [99], was also activated after *Sm22* knockdown. These observations suggest that disruption of *Sm22* in stressed VSMCs may activate multiple ROS production mechanisms that might work together to foster a high redox environment.

How does the disruption of an actin-binding protein lead to simultaneous activation of NADPH oxidase and dysfunction of mitochondria? Activation of NADPH oxidase requires the membrane assembly of cytosolic p47phox, p67phox, p40phox and Rac2 [90, 99]. It was reported that the actin cytoskeleton and associated proteins may affect this process [90]. The correlation between NADPH oxidase activation and diminished stress fiber formation in PAC1 cells after *Sm22* knockdown might reflect the role of the actin cytoskeleton in maintaining VSMCs phenotype. Furthermore, the actin cytoskeleton cooperates with microtubules [91] in regulating organelle distribution including mitochondria [91, 101]. The mitochondria aggregation and formation of megamitochondria may be due to the compromised actin cytoskeleton after *Sm22* knockdown

or to be an outcome of subsequent disorganized microtubules. The changes in the fine structure of cytoskeleton and mitochondria after *Sm22* disruption will be investigated in the future using electron microscopy.

4.3. Arterial inflammation and arterial chondrogenesis: coupled or sequential?

Accumulating studies indicate that inflammation participates in arterial osteochondrogenesis in a variety of arterial diseases [78]. Indeed, our current study revealed prominent inflammation and enhanced medial chondrogenesis in injured carotid arteries from *Sm22*$^{-/-}$ mice. It is reasonable to argue that the enhanced chondrogenesis is caused by the exogenous cytokines from the infiltrated inflammatory cells such as macrophages. On the other hand, we can not exclude the possibility that loss of *Sm22* autonomously couples chondrogenic conversion of VSMCs with inflammatory responses. This notion is supported by the following evidence. In *Sm22* disrupted VSMCs, we observed the simultaneous activation of pro-inflammatory NF-κB, Sox9 induction and the repression of myocardin. Since NF-κB can induce *Sox9* expression [84] and repress myocardin myogenic activity [102], NF-κB may be pivotal in coupling chondrogenesis with inflammation in arterial diseases where *Sm22* is down-regulated. Thus, it is noteworthy that this coupling of chondrogenesis and inflammation could be independent of inflammatory cells as reported before [52]. Therefore, disruption of *Sm22* in VSMCs might contribute to arterial osteochondrogenesis through at least two avenues, either directly by activating chondrogenic differentiation or indirectly by inducing pro-osteochondrogenic events as a result of VSMC inflammation.

4.4. A working model for phenotypic modulation of VSMCs and arterial pathogenesis after *Sm22* disruption

Based on our *in vivo* and *in vitro* results, we propose that disruption of *Sm22* expression in stressed VSMCs results in actin cytoskeleton and microtubules remodeling, thereby leading to a high redox state via mitochondria malfunction and NADPH oxidase activation. In turn, increased ROS production activates the NF-κB pathways required for establishing both pro-inflammatory and chondrogenic/anti-myogenic environment (Fig. 30).

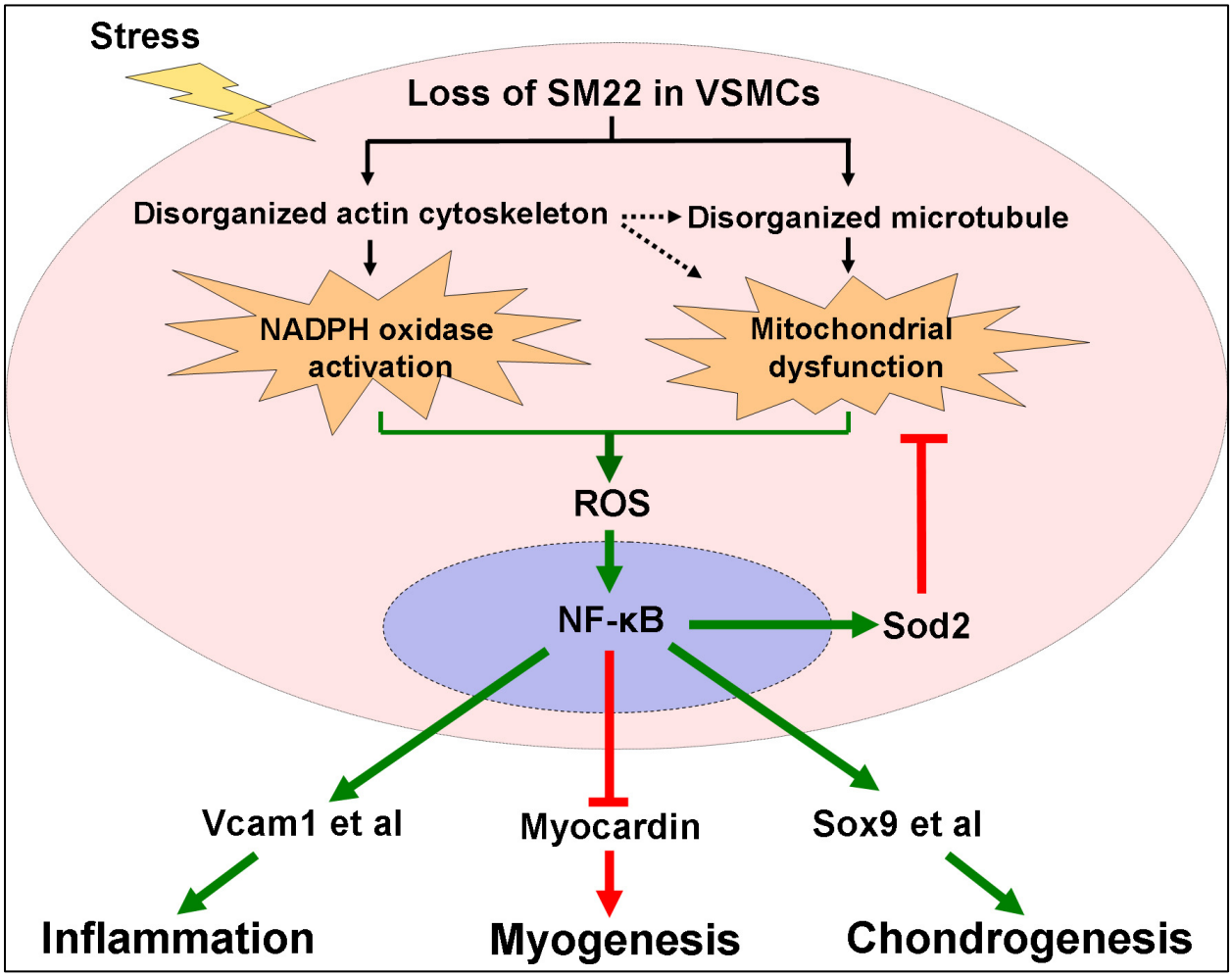

Figure 30. A working model illustrating phenotypic modulation of VSMCs and arterial pathogenesis after *Sm22* disruption.

4.5 Remarks on further research

Questions of several layers remain to be answered. It is interesting to reveal that non-canonical NF-κB pathway plays a pivotal role after *Sm22* disruption; however, the specific NF-κB complexes and the bridging pathways through which ROS activate NF-κB are yet to be characterized. Moreover, transcription factors function as modules, and NF-κB activation only samples the shifting patterns of global transcriptional network after *Sm22* disruption. The dynamic map transcriptional regulatory machinery needs to be drawn in future research. To better understand how Sm22 exerts its effects on cytoskeletal organization and other molecular functions, domain mapping of Sm22 is an indispensable part of future research plan. Similarly important is the fact that *Sm22*$^{-/-}$ mice maintain arterial homeostasis equally well compared to their wild type littermates without pathogenic stimuli, which poses a possibility that VSMCs from these mice might have distinct stimulus sensing machinery (either more sensitive or more potent) that remain inert in physiological conditions and only responds to arterial injury signals such as serum exposure. Thus, investigation on membrane receptors including GPCRs in these mice may hold key to another exciting discovery.

Increasing evidence supports the notion that actin cytoskeleton remodeling plays important roles in VSMC phenotypic modulation [103]. The present study on the consequences of abolishing Sm22, an actin-binding protein, offers a glimpse on how the cytoskeletal proteins could actively affect arterial pathogenesis. Therefore, maintaining VSMC cytoskeleton gene expression in VSMCs may serve as a therapeutic strategy to treat arterial diseases. One un-addressed question is whether other VSMC cytoskeletal proteins also have similar anti-inflammatory and anti-chondrogenic roles or these functions are unique to Sm22. Therefore,

paralleled research on other cytoskeletal proteins is anticipated. Given that carotid artery denudation is a simplified model for vascular injury, it is important to validate Sm22's role as an anti-inflammatory agent in animal disease models such as diet-induced atherosclerosis mouse model. On the other hand, SM22 expression is downregulated in a variety of cancers [104]. The finding that loss of *Sm22* creates a pro-inflammatory environment may also shed lights on the role of downregulation of SM22 in carcinogenesis. Thus, maintaining SM22 expression might also serve as a therapeutic strategy to repress the dysregulated inflammatory responses in cancers.

Particular Statement: the research results and text in this dissertation have been published [105, 106].

APPENDIX

Appendix A: Abbreviations

ACAN, aggrecan;
ACTA2, smooth muscle α actin;
ALP, alkaline phosphatase
BGLAP, bone gamma-carboxyglutamic acid-containing protein, osteocalcin;
CCL2, monocyte chemotactic protein 1;
CD3, cluster of differentiation 3;
CKD, chronic kidney disease;
COL2A1, type II collagen α 1;
Cre, Cre recombinase;
CX3CL1, chemokine (C-X3-C motif) ligand 1;
CXCL12, chemokine (C-X-C motif) ligand 12
BMP2, bone morphogenic protein 2;
DAB, diaminobenzidine;
DAPI, 4',6-diamidino-2-phenylindole;
DCFDA, dichloro fluorescein diacetate;
DHE, dihydroethidium;
DPI, diphenylene iodonium
ECM, extracellular matrix;
EMSA, electrophoresis migration shift assay;
FBS, fetal bovine serum;
G/F – actin, globular actin /filamentous actin;
GAPDH, glyceraldehyde 3-phosphate dehydrogenase;
H&E, hematoxylin and eosin stain;
HIF1A, hypoxia-inducible factor 1, alpha subunit;
ICAM1, intercellular adhesion molecule 1;
IF, immunofluorescence;
IHC, immunohistochemistry;
IKB, I-kappa-B;
IKK, IκB kinase;
MGP, matrix gla protein;
MYH11, smooth muscle myosin heavy chain;
MYOCD, myocardin;
NAC, N-Acetylcysteine;
NADPH, reduced form of nicotinamide adenine dinucleotide phosphate;
NF-κB, nuclear factor kappa-light-chain-enhancer of activated B cells;
NFKB1, p50;
NFKB2, p52;
OCT, optimal cutting temperature compound;
p40phox, neutrophil cytosol factor 4;
p47phox, neutrophil cytosol factor 1;
p67phox, neutrophil cytosol factor 2;
PAC1, a pulmonary arterial SMC cell line;

RAC2, Ras-related C3 botulinum toxin substrate 2
rtRT-PCR, real-time RT-PCR;
RUNX2, Runt-related transcription factor 2
PTGS2, prostaglandin-endoperoxide synthase 2;
RELA, p65;
ROS, reactive oxygen species;
siRNA, small interfering RNA;
Sm22$^{-/-}$, *Sm22* knockout;
Sm22$^{+/+}$, *Sm22* wild type;
SMA, smooth muscle α actin;
SMC, smooth muscle cell;
snRNA, small nuclear RNA;
SOD2, superoxide dismutase 2;
SOX9, SRY-box containing gene 9;
SPP1, osteopontin;
SRY, sex determining region Y;
VCAM1, vascular cell adhesion molecule 1;
VSMC, vascular smooth muscle cell;
WB, western blotting.

REFERENCES

1. Worth, N.F., Rolfe, B.E., Song, J., and Campbell, G.R. 2001. Vascular smooth muscle cell phenotypic modulation in culture is associated with reorganisation of contractile and cytoskeletal proteins. *Cell Motil Cytoskeleton* 49:130-145.
2. Kawai-Kowase, K., and Owens, G.K. 2007. Multiple repressor pathways contribute to phenotypic switching of vascular smooth muscle cells. *Am J Physiol Cell Physiol* 292:C59-69.
3. Iyemere, V.P., Proudfoot, D., Weissberg, P.L., and Shanahan, C.M. 2006. Vascular smooth muscle cell phenotypic plasticity and the regulation of vascular calcification. *J Intern Med* 260:192-210.
4. Owens, G.K. 2007. Molecular control of vascular smooth muscle cell differentiation and phenotypic plasticity. *Novartis Found Symp* 283:174-191; discussion 191-173, 238-141.
5. Hao, H., Gabbiani, G., and Bochaton-Piallat, M.L. 2003. Arterial smooth muscle cell heterogeneity: implications for atherosclerosis and restenosis development. *Arterioscler Thromb Vasc Biol* 23:1510-1520.
6. Hastings, N.E., Simmers, M.B., McDonald, O.G., Wamhoff, B.R., and Blackman, B.R. 2007. Atherosclerosis-prone hemodynamics differentially regulates endothelial and smooth muscle cell phenotypes and promotes pro-inflammatory priming. *Am J Physiol Cell Physiol* 293:C1824-1833.
7. Johnson, R.C., Leopold, J.A., and Loscalzo, J. 2006. Vascular calcification: pathobiological mechanisms and clinical implications. *Circ Res* 99:1044-1059.
8. Demer, L.L., and Tintut, Y. 2008. Vascular calcification: pathobiology of a multifaceted disease. *Circulation* 117:2938-2948.

9. Orr, A.W., Hastings, N.E., Blackman, B.R., and Wamhoff, B.R. Complex regulation and function of the inflammatory smooth muscle cell phenotype in atherosclerosis. *J Vasc Res* 47:168-180.

10. Steitz, S.A., Speer, M.Y., Curinga, G., Yang, H.Y., Haynes, P., Aebersold, R., Schinke, T., Karsenty, G., and Giachelli, C.M. 2001. Smooth muscle cell phenotypic transition associated with calcification: upregulation of Cbfa1 and downregulation of smooth muscle lineage markers. *Circ Res* 89:1147-1154.

11. Lagna, G., Ku, M.M., Nguyen, P.H., Neuman, N.A., Davis, B.N., and Hata, A. 2007. Control of phenotypic plasticity of smooth muscle cells by bone morphogenetic protein signaling through the myocardin-related transcription factors. *J Biol Chem* 282:37244-37255.

12. Miyoshi, T., Tian, J., Matsumoto, A.H., and Shi, W. 2006. Differential response of vascular smooth muscle cells to oxidized LDL in mouse strains with different atherosclerosis susceptibility. *Atherosclerosis* 189:99-105.

13. Doran, A.C., Meller, N., and McNamara, C.A. 2008. Role of smooth muscle cells in the initiation and early progression of atherosclerosis. *Arterioscler Thromb Vasc Biol* 28:812-819.

14. Tanikawa, T., Okada, Y., Tanikawa, R., and Tanaka, Y. 2009. Advanced glycation end products induce calcification of vascular smooth muscle cells through RAGE/p38 MAPK. *J Vasc Res* 46:572-580.

15. Yoon, S.J., Yoon, Y.W., Lee, B.K., Kwon, H.M., Hwang, K.C., Kim, M., Chang, W., Hong, B.K., Lee, Y.H., Park, S.J., et al. 2009. Potential role of HMG CoA reductase inhibitor on oxidative stress induced by advanced glycation endproducts in vascular smooth muscle cells of diabetic vasculopathy. *Exp Mol Med* 41:802-811.

16. Ailawadi, G., Moehle, C.W., Pei, H., Walton, S.P., Yang, Z., Kron, I.L., Lau, C.L., and Owens, G.K. 2009. Smooth muscle phenotypic modulation is an early event in aortic aneurysms. *J Thorac Cardiovasc Surg* 138:1392-1399.

17. Zheng, J.P., Ju, D., Shen, J., Yang, M., and Li, L. 2010. Disruption of actin cytoskeleton mediates loss of tensile stress induced early phenotypic modulation of vascular smooth muscle cells in organ culture. *Exp Mol Pathol* 88:52-57.

18. Lindner, V., Fingerle, J., and Reidy, M.A. 1993. Mouse model of arterial injury. *Circ Res* 73:792-796.

19. Lees-Miller, J.P., Heeley, D.H., and Smillie, L.B. 1987. An abundant and novel protein of 22 kDa (SM22) is widely distributed in smooth muscles. Purification from bovine aorta. *Biochem J* 244:705-709.

20. Shapland, C., Hsuan, J.J., Totty, N.F., and Lawson, D. 1993. Purification and properties of transgelin: a transformation and shape change sensitive actin-gelling protein. *J Cell Biol* 121:1065-1073.

21. Lawson, D., Harrison, M., and Shapland, C. 1997. Fibroblast transgelin and smooth muscle SM22alpha are the same protein, the expression of which is down-regulated in many cell lines. *Cell Motil Cytoskeleton* 38:250-257.

22. Fu, Y., Liu, H.W., Forsythe, S.M., Kogut, P., McConville, J.F., Halayko, A.J., Camoretti-Mercado, B., and Solway, J. 2000. Mutagenesis analysis of human SM22: characterization of actin binding. *J Appl Physiol* 89:1985-1990.

23. Gimona, M., Kaverina, I., Resch, G.P., Vignal, E., and Burgstaller, G. 2003. Calponin repeats regulate actin filament stability and formation of podosomes in smooth muscle cells. *Mol Biol Cell* 14:2482-2491.

24. Li, L., Miano, J.M., Cserjesi, P., and Olson, E.N. 1996. SM22 alpha, a marker of adult smooth muscle, is expressed in multiple myogenic lineages during embryogenesis. *Circ Res* 78:188-195.

25. Li, L., Miano, J.M., Mercer, B., and Olson, E.N. 1996. Expression of the SM22alpha promoter in transgenic mice provides evidence for distinct transcriptional regulatory programs in vascular and visceral smooth muscle cells. *J Cell Biol* 132:849-859.

26. Zhang, J.C., Kim, S., Helmke, B.P., Yu, W.W., Du, K.L., Lu, M.M., Strobeck, M., Yu, Q., and Parmacek, M.S. 2001. Analysis of SM22alpha-deficient mice reveals unanticipated insights into smooth muscle cell differentiation and function. *Mol Cell Biol* 21:1336-1344.

27. Zeidan, A., Sward, K., Nordstrom, I., Ekblad, E., Zhang, J.C., Parmacek, M.S., and Hellstrand, P. 2004. Ablation of SM22alpha decreases contractility and actin contents of mouse vascular smooth muscle. *FEBS Lett* 562:141-146.

28. Je, H.D., and Sohn, U.D. 2007. SM22alpha is required for agonist-induced regulation of contractility: evidence from SM22alpha knockout mice. *Mol Cells* 23:175-181.

29. Dong, L.H., Wen, J.K., Liu, G., McNutt, M.A., Miao, S.B., Gao, R., Zheng, B., Zhang, H., and Han, M. Blockade of the Ras-extracellular signal-regulated kinase 1/2 pathway is involved in smooth muscle 22 alpha-mediated suppression of vascular smooth muscle cell proliferation and neointima hyperplasia. *Arterioscler Thromb Vasc Biol* 30:683-691.

30. Zhang, Z.W., Yang, Z.M., Zheng, Y.C., and Chen, Z.D. Transgelin induces apoptosis of human prostate LNCaP cells through its interaction with p53. *Asian J Androl* 12:186-195.

31. Shields, J.M., Rogers-Graham, K., and Der, C.J. 2002. Loss of transgelin in breast and colon tumors and in RIE-1 cells by Ras deregulation of gene expression through Raf-independent pathways. *J Biol Chem* 277:9790-9799.

32. Yang, Z., Chang, Y.J., Miyamoto, H., Ni, J., Niu, Y., Chen, Z., Chen, Y.L., Yao, J.L., di Sant'agnese, P.A., and Chang, C. 2007. Transgelin Functions as a Suppressor via Inhibition of ARA54-Enhanced Androgen Receptor Transactivation and Prostate Cancer Cell Growth. *Mol Endocrinol* 21:343-358.

33. Zhao, L., Wang, H., Deng, Y.J., Wang, S., Liu, C., Jin, H., and Ding, Y.Q. 2009. Transgelin as a suppressor is associated with poor prognosis in colorectal carcinoma patients. *Mod Pathol*.

34. Shanahan, C.M., Cary, N.R., Metcalfe, J.C., and Weissberg, P.L. 1994. High expression of genes for calcification-regulating proteins in human atherosclerotic plaques. *J Clin Invest* 93:2393-2402.

35. Lenk, G.M., Tromp, G., Weinsheimer, S., Gatalica, Z., Berguer, R., and Kuivaniemi, H. 2007. Whole genome expression profiling reveals a significant role for immune function in human abdominal aortic aneurysms. *BMC Genomics* 8:237.

36. Wamhoff, B.R., Hoofnagle, M.H., Burns, A., Sinha, S., McDonald, O.G., and Owens, G.K. 2004. A G/C element mediates repression of the SM22alpha promoter within phenotypically modulated smooth muscle cells in experimental atherosclerosis. *Circ Res* 95:981-988.

37. Feil, S., Hofmann, F., and Feil, R. 2004. SM22alpha modulates vascular smooth muscle cell phenotype during atherogenesis. *Circ Res* 94:863-865.

38. Yang, M., Jiang, H., and Li, L. 2010. Sm22alpha transcription occurs at the early onset of the cardiovascular system and the intron 1 is dispensable for its transcription in smooth muscle cells during mouse development. *Int J Physiol Pathophysiol Pharmacol* 2:12-19.

39. Rothman, A., Kulik, T.J., Taubman, M.B., Berk, B.C., Smith, C.W., and Nadal-Ginard, B. 1992. Development and characterization of a cloned rat pulmonary arterial smooth muscle

cell line that maintains differentiated properties through multiple subcultures. *Circulation* 86:1977-1986.

40. Libby, P. 2002. Inflammation in atherosclerosis. *Nature* 420:868-874.

41. Paoletti, R., Gotto, A.M., Jr., and Hajjar, D.P. 2004. Inflammation in atherosclerosis and implications for therapy. *Circulation* 109:III20-26.

42. Kutuk, O., and Basaga, H. 2003. Inflammation meets oxidation: NF-kappaB as a mediator of initial lesion development in atherosclerosis. *Trends Mol Med* 9:549-557.

43. Hansson, G.K. 2005. Inflammation, atherosclerosis, and coronary artery disease. *N Engl J Med* 352:1685-1695.

44. Savoia, C., and Schiffrin, E.L. 2007. Vascular inflammation in hypertension and diabetes: molecular mechanisms and therapeutic interventions. *Clin Sci (Lond)* 112:375-384.

45. Vaziri, N.D., and Rodriguez-Iturbe, B. 2006. Mechanisms of disease: oxidative stress and inflammation in the pathogenesis of hypertension. *Nat Clin Pract Nephrol* 2:582-593.

46. Kuivaniemi, H., Platsoucas, C.D., and Tilson, M.D., 3rd. 2008. Aortic aneurysms: an immune disease with a strong genetic component. *Circulation* 117:242-252.

47. Rifkin, D.E., and Sarnak, M.J. 2009. Does inflammation fuel the fire in CKD? *Am J Kidney Dis* 53:572-575.

48. Ray, J.L., Leach, R., Herbert, J.M., and Benson, M. 2001. Isolation of vascular smooth muscle cells from a single murine aorta. *Methods Cell Sci* 23:185-188.

49. Zernecke, A., Shagdarsuren, E., and Weber, C. 2008. Chemokines in atherosclerosis: an update. *Arterioscler Thromb Vasc Biol* 28:1897-1908.

50. Linton, M.F., and Fazio, S. 2004. Cyclooxygenase-2 and inflammation in atherosclerosis. *Curr Opin Pharmacol* 4:116-123.

51. Holtwick, R., Gotthardt, M., Skryabin, B., Steinmetz, M., Potthast, R., Zetsche, B., Hammer, R.E., Herz, J., and Kuhn, M. 2002. Smooth muscle-selective deletion of guanylyl cyclase-A prevents the acute but not chronic effects of ANP on blood pressure. *Proc Natl Acad Sci U S A* 99:7142-7147.

52. Speer, M.Y., Yang, H.Y., Brabb, T., Leaf, E., Look, A., Lin, W.L., Frutkin, A., Dichek, D., and Giachelli, C.M. 2009. Smooth muscle cells give rise to osteochondrogenic precursors and chondrocytes in calcifying arteries. *Circ Res* 104:733-741.

53. Zhang, W.D., Bai, H.Z., Sawa, Y., Yamakawa, T., Kadoba, K., Taniguchi, K., Masuda, J., Ogata, J., Shirakura, R., and Matsuda, H. 1999. Association of smooth muscle cell phenotypic modulation with extracellular matrix alterations during neointima formation in rabbit vein grafts. *J Vasc Surg* 30:169-183.

54. Nagai, R., Kowase, K., and Kurabayashi, M. 2000. Transcriptional regulation of smooth muscle phenotypic modulation. *Ann N Y Acad Sci* 902:214-222; discussion 222-213.

55. Rossi, G.P., Cavallin, M., Belloni, A.S., Mazzocchi, G., Nussdorfer, G.G., Pessina, A.C., and Sartore, S. 2002. Aortic smooth muscle cell phenotypic modulation and fibrillar collagen deposition in angiotensin II-dependent hypertension. *Cardiovasc Res* 55:178-189.

56. Sullivan, G.W., Sarembock, I.J., and Linden, J. 2000. The role of inflammation in vascular diseases. *J Leukoc Biol* 67:591-602.

57. Intengan, H.D., and Schiffrin, E.L. 2001. Vascular remodeling in hypertension: roles of apoptosis, inflammation, and fibrosis. *Hypertension* 38:581-587.

58. Roque, M., Fallon, J.T., Badimon, J.J., Zhang, W.X., Taubman, M.B., and Reis, E.D. 2000. Mouse model of femoral artery denudation injury associated with the rapid accumulation of

adhesion molecules on the luminal surface and recruitment of neutrophils. *Arterioscler Thromb Vasc Biol* 20:335-342.

59. Zaidi, S.H., You, X.M., Ciura, S., O'Blenes, S., Husain, M., and Rabinovitch, M. 2000. Suppressed smooth muscle proliferation and inflammatory cell invasion after arterial injury in elafin-overexpressing mice. *J Clin Invest* 105:1687-1695.

60. Okamoto, E., Couse, T., De Leon, H., Vinten-Johansen, J., Goodman, R.B., Scott, N.A., and Wilcox, J.N. 2001. Perivascular inflammation after balloon angioplasty of porcine coronary arteries. *Circulation* 104:2228-2235.

61. Zernecke, A., Bidzhekov, K., Ozuyaman, B., Fraemohs, L., Liehn, E.A., Luscher-Firzlaff, J.M., Luscher, B., Schrader, J., and Weber, C. 2006. CD73/ecto-5'-nucleotidase protects against vascular inflammation and neointima formation. *Circulation* 113:2120-2127.

62. Osaka, M., Hagita, S., Haraguchi, M., Kajimura, M., Suematsu, M., and Yoshida, M. 2007. Real-time imaging of mechanically injured femoral artery in mice reveals a biphasic pattern of leukocyte accumulation. *Am J Physiol Heart Circ Physiol* 292:H1876-1882.

63. Faggin, E., Puato, M., Zardo, L., Franch, R., Millino, C., Sarinella, F., Pauletto, P., Sartore, S., and Chiavegato, A. 1999. Smooth muscle-specific SM22 protein is expressed in the adventitial cells of balloon-injured rabbit carotid artery. *Arterioscler Thromb Vasc Biol* 19:1393-1404.

64. Cooley, B.C. 2007. Mouse strain differential neointimal response in vein grafts and wire-injured arteries. *Circ J* 71:1649-1652.

65. Harmon, K.J., Couper, L.L., and Lindner, V. 2000. Strain-dependent vascular remodeling phenotypes in inbred mice. *Am J Pathol* 156:1741-1748.

66. Sindermann, J.R., Kobbert, C., Skaletz-Rorowski, A., Breithardt, G., Plenz, G., and March, K.L. 2006. Vascular injury response in mice is dependent on genetic background. *Am J Physiol Heart Circ Physiol* 290:H1307-1310.

67. Korshunov, V.A., and Berk, B.C. 2004. Strain-dependent vascular remodeling: the "Glagov phenomenon" is genetically determined. *Circulation* 110:220-226.

68. Speer, M.Y., McKee, M.D., Guldberg, R.E., Liaw, L., Yang, H.Y., Tung, E., Karsenty, G., and Giachelli, C.M. 2002. Inactivation of the osteopontin gene enhances vascular calcification of matrix Gla protein-deficient mice: evidence for osteopontin as an inducible inhibitor of vascular calcification in vivo. *J Exp Med* 196:1047-1055.

69. Bobryshev, Y.V. 2005. Transdifferentiation of smooth muscle cells into chondrocytes in atherosclerotic arteries in situ: implications for diffuse intimal calcification. *J Pathol* 205:641-650.

70. Giachelli, C.M., and Steitz, S. 2000. Osteopontin: a versatile regulator of inflammation and biomineralization. *Matrix Biol* 19:615-622.

71. Goldring, M.B., Tsuchimochi, K., and Ijiri, K. 2006. The control of chondrogenesis. *J Cell Biochem* 97:33-44.

72. Akiyama, H., Chaboissier, M.C., Martin, J.F., Schedl, A., and de Crombrugghe, B. 2002. The transcription factor Sox9 has essential roles in successive steps of the chondrocyte differentiation pathway and is required for expression of Sox5 and Sox6. *Genes Dev* 16:2813-2828.

73. Lim, Y.B., Kang, S.S., An, W.G., Lee, Y.S., Chun, J.S., and Sonn, J.K. 2003. Chondrogenesis induced by actin cytoskeleton disruption is regulated via protein kinase C-dependent p38 mitogen-activated protein kinase signaling. *J Cell Biochem* 88:713-718.

74. Han, M., Dong, L.H., Zheng, B., Shi, J.H., Wen, J.K., and Cheng, Y. 2009. Smooth muscle 22 alpha maintains the differentiated phenotype of vascular smooth muscle cells by inducing filamentous actin bundling. *Life Sci* 84:394-401.

75. Amarilio, R., Viukov, S.V., Sharir, A., Eshkar-Oren, I., Johnson, R.S., and Zelzer, E. 2007. HIF1alpha regulation of Sox9 is necessary to maintain differentiation of hypoxic prechondrogenic cells during early skeletogenesis. *Development* 134:3917-3928.

76. Wang, D., Chang, P.S., Wang, Z., Sutherland, L., Richardson, J.A., Small, E., Krieg, P.A., and Olson, E.N. 2001. Activation of cardiac gene expression by myocardin, a transcriptional cofactor for serum response factor. *Cell* 105:851-862.

77. Chen, J., Kitchen, C.M., Streb, J.W., and Miano, J.M. 2002. Myocardin: a component of a molecular switch for smooth muscle differentiation. *J Mol Cell Cardiol* 34:1345-1356.

78. Shao, J.S., Cheng, S.L., Sadhu, J., and Towler, D.A. 2010. Inflammation and the osteogenic regulation of vascular calcification: a review and perspective. *Hypertension* 55:579-592.

79. Murakami, S., Lefebvre, V., and de Crombrugghe, B. 2000. Potent inhibition of the master chondrogenic factor Sox9 gene by interleukin-1 and tumor necrosis factor-alpha. *J Biol Chem* 275:3687-3692.

80. Sitcheran, R., Cogswell, P.C., and Baldwin, A.S., Jr. 2003. NF-kappaB mediates inhibition of mesenchymal cell differentiation through a posttranscriptional gene silencing mechanism. *Genes Dev* 17:2368-2373.

81. Roman-Blas, J.A., Stokes, D.G., and Jimenez, S.A. 2007. Modulation of TGF-beta signaling by proinflammatory cytokines in articular chondrocytes. *Osteoarthritis Cartilage* 15:1367-1377.

82. Yates, K.E. 2006. Identification of cis and trans-acting transcriptional regulators in chondroinduced fibroblasts from the pre-phenotypic gene expression profile. *Gene* 377:77-87.

83. Park, M., Yong, Y., Choi, S.W., Kim, J.H., Lee, J.E., and Kim, D.W. 2007. Constitutive RelA activation mediated by Nkx3.2 controls chondrocyte viability. *Nat Cell Biol* 9:287-298.

84. Ushita, M., Saito, T., Ikeda, T., Yano, F., Higashikawa, A., Ogata, N., Chung, U., Nakamura, K., and Kawaguchi, H. 2009. Transcriptional induction of SOX9 by NF-kappaB family member RelA in chondrogenic cells. *Osteoarthritis Cartilage*.

85. Ghosh, S., and Hayden, M.S. 2008. New regulators of NF-kappaB in inflammation. *Nat Rev Immunol* 8:837-848.

86. Gloire, G., Legrand-Poels, S., and Piette, J. 2006. NF-kappaB activation by reactive oxygen species: fifteen years later. *Biochem Pharmacol* 72:1493-1505.

87. Mueller, C.F., Laude, K., McNally, J.S., and Harrison, D.G. 2005. ATVB in focus: redox mechanisms in blood vessels. *Arterioscler Thromb Vasc Biol* 25:274-278.

88. Xu, Y., Kiningham, K.K., Devalaraja, M.N., Yeh, C.C., Majima, H., Kasarskis, E.J., and St Clair, D.K. 1999. An intronic NF-kappaB element is essential for induction of the human manganese superoxide dismutase gene by tumor necrosis factor-alpha and interleukin-1beta. *DNA Cell Biol* 18:709-722.

89. Wakabayashi, T. 2002. Megamitochondria formation - physiology and pathology. *J Cell Mol Med* 6:497-538.

90. Touyz, R.M., Yao, G., Quinn, M.T., Pagano, P.J., and Schiffrin, E.L. 2005. p47phox associates with the cytoskeleton through cortactin in human vascular smooth muscle cells: role in NAD(P)H oxidase regulation by angiotensin II. *Arterioscler Thromb Vasc Biol* 25:512-518.

91. Goode, B.L., Drubin, D.G., and Barnes, G. 2000. Functional cooperation between the microtubule and actin cytoskeletons. *Curr Opin Cell Biol* 12:63-71.

92. Bu, D.X., Erl, W., de Martin, R., Hansson, G.K., and Yan, Z.Q. 2005. IKKbeta-dependent NF-kappaB pathway controls vascular inflammation and intimal hyperplasia. *FASEB J* 19:1293-1295.

93. Napoli, C., de Nigris, F., and Palinski, W. 2001. Multiple role of reactive oxygen species in the arterial wall. *J Cell Biochem* 82:674-682.

94. Guzy, R.D., and Schumacker, P.T. 2006. Oxygen sensing by mitochondria at complex III: the paradox of increased reactive oxygen species during hypoxia. *Exp Physiol* 91:807-819.

95. Kietzmann, T., and Gorlach, A. 2005. Reactive oxygen species in the control of hypoxia-inducible factor-mediated gene expression. *Semin Cell Dev Biol* 16:474-486.

96. Haddad, J.J., and Land, S.C. 2001. A non-hypoxic, ROS-sensitive pathway mediates TNF-alpha-dependent regulation of HIF-1alpha. *FEBS Lett* 505:269-274.

97. Byon, C.H., Javed, A., Dai, Q., Kappes, J.C., Clemens, T.L., Darley-Usmar, V.M., McDonald, J.M., and Chen, Y. 2008. Oxidative stress induces vascular calcification through modulation of the osteogenic transcription factor Runx2 by AKT signaling. *J Biol Chem* 283:15319-15327.

98. Shao, J.S., Aly, Z.A., Lai, C.F., Cheng, S.L., Cai, J., Huang, E., Behrmann, A., and Towler, D.A. 2007. Vascular Bmp Msx2 Wnt signaling and oxidative stress in arterial calcification. *Ann N Y Acad Sci* 1117:40-50.

99. Sorescu, D., Somers, M.J., Lassegue, B., Grant, S., Harrison, D.G., and Griendling, K.K. 2001. Electron spin resonance characterization of the NAD(P)H oxidase in vascular smooth muscle cells. *Free Radic Biol Med* 30:603-612.

100. Wosniak, J., Jr., Santos, C.X., Kowaltowski, A.J., and Laurindo, F.R. 2009. Cross-talk between mitochondria and NADPH oxidase: effects of mild mitochondrial dysfunction on angiotensin II-mediated increase in Nox isoform expression and activity in vascular smooth muscle cells. *Antioxid Redox Signal* 11:1265-1278.

101. Boldogh, I.R., and Pon, L.A. 2006. Interactions of mitochondria with the actin cytoskeleton. *Biochim Biophys Acta* 1763:450-462.

102. Tang, R.H., Zheng, X.L., Callis, T.E., Stansfield, W.E., He, J., Baldwin, A.S., Wang, D.Z., and Selzman, C.H. 2008. Myocardin inhibits cellular proliferation by inhibiting NF-{kappa}B(p65)-dependent cell cycle progression. *Proc Natl Acad Sci U S A*.

103. Xin, M., Small, E.M., Sutherland, L.B., Qi, X., McAnally, J., Plato, C.F., Richardson, J.A., Bassel-Duby, R., and Olson, E.N. 2009. MicroRNAs miR-143 and miR-145 modulate cytoskeletal dynamics and responsiveness of smooth muscle cells to injury. *Genes Dev* 23:2166-2178.

104. Assinder, S.J., Stanton, J.A., and Prasad, P.D. 2009. Transgelin: an actin-binding protein and tumour suppressor. *Int J Biochem Cell Biol* 41:482-486.

105. Shen, J., Yang, M., Ju, D., Jiang, H., Zheng, J.P., Xu, Z., and Li, L. 2010. Disruption of SM22 promotes inflammation after artery injury via nuclear factor kappaB activation. *Circ Res* 106:1351-1362.

106. Shen, J., Yang, M., Jiang, H., Ju, D., Zheng, J.P., Xu, Z., Liao, T.D., and Li, L. 2011. Arterial injury promotes medial chondrogenesis in Sm22 knockout mice. *Cardiovasc Res* 90:28-37.

ABSTRACT

IDENTIFYING SM22 AS A KEY PLAYER IN ARTERIAL DISEASES

by

JIANBIN SHEN

August 2012

Advisor: Dr. Li, Li

Major: Molecular Biology and Genetics

Degree: Doctor of Philosophy

Background: Expression of vascular smooth muscle cell (VSMC) cytoskeleton markers including SM22 is down-regulated in arterial diseases including atherosclerosis where inflammation and osteochondrogenesis are present. However, the role of this downregulation in arterial pathogenesis is unknown.

Hypothesis: Downregulation of SM22 may actively contribute to arterial pathogenesis. **Methods**: Five *Sm22* knockout ($Sm22^{-/-}$) mice and their wild type littermates were subjected to carotid artery denudation, an artery injury model. Analyses were conducted on carotid arteries 2 weeks after injury. Primary VSMCs were isolated from mouse aortas and investigated individually at passage 2 to 4. *Sm22* knockdown was performed in triplicate using siRNA in a VSMC line, PAC1, followed by downstream experiments 3 days after transfection.

Results: $Sm22^{-/-}$ mice developed both enhanced arterial inflammatory response and prominent medial chondrogenesis along with remarkable NF-κB activation compared to their wild-type littermates. The inflammation was evidenced by excessive artery swelling, macrophage infiltration and high induction of pro-inflammatory molecules including Vcam1,

Icam1, Cx3cl1, Ptgs2 and Ccl2. The medial chondrogenesis was characterized by augmented expression of type II collagen, aggrecan, osteopontin, Bmp2 and the key osteochondrogenic transcription factors Sox9. In accordance with the *in vivo* findings, expression of the aforementioned pro-inflammatory genes and Sox9 was up-regulated in *Sm22*$^{-/-}$ primary VSMCs and after *Sm22* knockdown in PAC1 cells. Interestingly, *Sm22* knockdown also led to NF-κB activation, and inhibition of NF-κB pathway reversed the up-regulation of both pro-inflammatory genes and *Sox9*. As an initiator of NF-κB activation, reactive oxygen species (ROS) production was boosted in *Sm22*$^{-/-}$ primary VSMCs and after *Sm22* knockdown. ROS scavengers effectively blocked NF-κB activation and induction of both pro-inflammatory genes and *Sox9* after *Sm22* knockdown. Further, the altered cell morphology and increased actin dynamics after *Sm22* knockdown might contribute to the elevated ROS.

Conclusions: These findings suggest that loss of *Sm22* in VSMCs coupled injury induced arterial inflammation with chondrogenesis in part via ROS induced NF-κB activation and that Sm22 plays both anti-inflammatory and anti-osteochondrogenic roles in arterial diseases partly by maintaining actin cytoskeleton integrity.

AUTOBIOGRAPHICAL STATEMENT

JIANBIN SHEN

ACADEMIC DEGREES:

B.M. 1998 Xinxiang Medical College, Xinxiang, PRC, *Summa cum laude.*
M.M. 2001 Shanghai Second Medical University, Shanghai, PRC.

PROFESSIONAL EXPERIENCE:

2001.8-2005.7 Resident, Internal Medicine, Xinhua Hospital, Shanghai Second Medical University, Shanghai, PRC.
2005.8-present Graduate Research Assistant, Center for Molecular Medicine and Genetics, Wayne State University.

HONORS AND MEMBERSHIPS:

Thomas C. Rumble University Fellowship, Wayne State University, 2007-2008.
Poster 1st place, National Symposium on Inflammation and Disease Progression, Wayne State University, 2008.
Travel Award for Outstanding Young Investigators, American Heart Association, 2009.
Member of American Society of Hematology.
Member of American Heart Association.

PUBLICATIONS:

1. Lillvis J, Erdman R, Schworer C, Golden A, Derr K, Gatalica Z, Cox L, **Shen J**, Vander Heide R, Lenk G, Hlavaty L, Li L, Elmore J, Franklin D, Gray J, Garvin R, Carey D, Lancaster W, Tromp G, Kuivaniemi H. Regional expression of HOXA4 along the aorta and its potential role in human abdominal aortic aneurysms. *BMC Physiology*. 2011, 11:9.
2. **Shen J**, Yang M, Jiang H, Ju D, Zheng JP, Xu Z, Liao TD, Li L. Arterial injury promotes medial chondrogenesis in Sm22 knockout mice. *Cardiovasc Res*. 2011, 90(1):28-37.
3. Zheng JP, Ju D, Jiang H, **Shen J**, Yang M, Li L. Resveratrol induces p53 and suppresses myocardin-mediated vascular smooth muscle cell differentiation. *Toxicol Lett*. 2010, 199(2):115-22.
4. **Shen J**, Yang M, Ju D, Jiang H, Zheng JP, Xu Z, Li L. Disruption of SM22 promotes inflammation after artery injury via nuclear factor kappaB activation. *Circ Res*. 2010, 106(8):1351-62.
5. Zheng JP, Ju D, **Shen J**, Yang M, Li L. Disruption of actin cytoskeleton mediates loss of tensile stress induced early phenotypic modulation of vascular smooth muscle cells in organ culture. *Exp Mol Pathol*. 2010, 88(1):52-7.
6. **Shen J**, Yang M, Ju D, Jiang H, Zheng J, Li L. Loss of SM22 Couples Arterial Inflammation With Osteochondrogenesis in a Murine Artery Injury Model. *Circulation*. 2009, 120:S1028.
7. **Shen JB**, Tang JY, Pan C, Chen J, Xue HL, Wang YP. Telomerase activity and clinical characteristics of acute leukemia in children. *Academic Journal of Shanghai Second Medical University*, 2004, 24(5):340-342.
8. Wong X, Deng XH, Ma JQ, **Shen JB**, Yu JM, Liang H. Effect of different T cell ratios between graft and receptor on GVHD during transplantation. *Academic Journal of Shanghai Second Medical University*, 2004, 24(2):94-96.
9. **Shen JB**, Tang JY, Zhao JC, Pan C, Chen J, Zhou X, Wang YP. Telomerase activity and its correlation with proliferative potential of bone marrow in aplastic anemia in children. *Acta Haematol*, 2002, 107(4):208-212.
10. **Shen JB**, Tang JY, Zhao JC, Pan C, Chen J, Zhou X, Wang YP. Initial research on telomerase activity in aplastic anemia. *Zhonghua Xue Ye Xue Za Zhi*, 2001, 22(10):543-545.
11. **Shen JB**, Tang JY. Telomere, telomerase and pediatric malignant tumors. *Journal of Leukemia*, 2000, 9(1):55-57.
12. **Shen JB**, Tang JY. INK4, INK4 genes and hematological malignancies. *Zhonghua Xue Ye Xue Za Zhi*, 2000, 21(5):274-276.